Spring 1996

Gamma-Ray Optical Studies of ^{73}Ge and ^{57}Fe

Walter Carlton McDermott III
Old Dominion University

Recommended Citation

McDermott, Walter C.. "Gamma-Ray Optical Studies of ^{73}Ge and ^{57}Fe" (1996). Doctor of Philosophy (PhD), Dissertation, Physics, Old Dominion University, DOI: 10.25777/dn8q-8683
https://digitalcommons.odu.edu/physics_etds/115

GAMMA-RAY OPTICAL STUDIES OF ^{73}Ge AND ^{57}Fe

by

Walter Carlton McDermott III
B.S. May 1988, Old Dominion University
M.S. May 1991, Old Dominion University

A dissertation submitted to the Faculty of Old Dominion University
in Partital Fulfilment of the Requirement for the Degree of

DOCTOR OF PHILOSOPHY
PHYSICS

OLD DOMINION UNIVERSITY
May, 1996

Approved:

Gilbert R. Hoy (Director)

ABSTRACT

GAMMA RAY OPTICS USING ^{57}Fe AND ^{73}Ge

Walter C. McDermott III
Old Dominion University, 1996
Director: Dr. Gilbert R. Hoy

The research described herein is among the first attempts to test one of the more popular theories for development of a gamma-ray laser. This work is a "marriage" between the Borrmann effect, which is a consequence of the dynamical theory of x-ray diffraction, and time-filtering, which comes from time-domain Mössbauer spectroscopy.

Our experiments involved the search for a nuclear Borrmann effect and the subsequent time-filtering effect using ^{57}Fe and ^{73}Ge. In both cases, no nuclear Borrmann effect was observed; however, the methodology and criteria necessary for such an observation with any isotope were documented. The procedures necessary for testing the crystal samples for the ability to support a Borrmann effect, both prior to and after the introduction of the parent nuclei, were derived for both a table-top x-ray system and a synchrotron radiation facility. For the table-top system, energy dispersive photon detectors were used to map the crystals in a computer-controlled goniometer system. At the synchrotron facility, the technique of x-ray topography was used to determine crystal quality. Additionally, a process was developed in which radioactive ^{73}As was introduced into natural germanium single crystals via electro-deposition and subsequent annealing for the nuclear Borrmann effect studies.

The experimental setup and circuitry required for observation of the time-filtering effect were also developed and tested. The processing electronics used in the delayed coincidence circuit were optimized and the resulting configuration documented. Time filtering experiments were performed on ^{57}Fe and ^{73}Ge using both powder and crystalline samples. During these investigations, a new method for studying the time-filtering effect was investigated using the internal conversion channel. This led to the realization that the currently accepted theory explaining time-filtering is incomplete, and requires further study and experimentation.

Director of Advisory Committee: Dr. Gilbert R. Hoy

ACKNOWLEDGMENTS

I would like to express my sincere gratitude and thanks to my advisor, Dr. Gilbert R. Hoy. I will always be indebted to him for his guidance and patience in the process of preparing and performing the work that is reported in this dissertation. I will greatly miss our discussions from which I have learned so much.

I would also like to thank the members of my dissertation committee: Dr. Desmond Cook, Dr. Gary Copeland, Dr. Mark Havey, and Dr. John Adam. I am greatful for the enormous effort that was put forth by each of them during the reading of this dissertation and the comments that they contributed.

A special thank-you goes to Mr. Bruce Hanna and his family for all of the moral and "lab" support that they have given me. I do not know how I would have been able to complete this degree without their contributions and friendship.

I also would like to thank Mr. Walt Hooks and his family for the friendship that they have shown.

I am also deeply greatful to the staff of the Science Shop, Mr. Thurmond Gardner, Mr. Bobby Powell, and Mr. Robert Kiszar, for there precision machining and swiftness in which they delivered the parts that I needed to perform this research. I will not forget all of the techniques of machining and electronics design that I have learned from them.

My thanks are also due to Dr. Peter Siddons and Dr. Jerome Hasting of the National Synchrotron Light Source at Brookhaven National Laboratory and Dr. Michael Dudley of The State University of New York at Stoney Brook for providing samples for

this research and the excellent opportunity to learn about synchrotron radiation.

I would also like to thank Old Dominion University and the Department of Physics for awarding me the Special Doctoral Research Assistantship and the GAANN Fellowship.

Finally, I would like to thank my wife Pam for all of her support through this ordeal. As proofreader, typist, critic, cheerleader, friend, and wife, no one could ask for anyone better.

This work was partially supported by the Innovative Science and Technology/Strategic Defense Initiative Office and administered by the Naval Research Laboratory.

TABLE OF CONTENTS

Page

ACKNOWLEDGMENTS ii

LIST OF TABLES vi

LIST OF FIGURES vii

Chapter 1. Gamma-Ray Optics 1
- 1.1 Introduction 1
- 1.2 The Mössbauer Effect 3
- 1.3 Modification to the Hannon and Trammel Theory 6
- 1.4 Organization of the Dissertation 7

Chapter 2. Dynamical Theory and the Borrmann Effect 9
- 2.1 Characteristics of Kinematical and Dynamical Diffraction 9
- 2.2 Simultaneous Diffraction 11
- 2.3 Determining Reflection Conditions 14
- 2.4 The Two Beam Borrmann Mode 18
- 2.5 The Two Beam Borrmann Effect: Wavefield Approach 22
- 2.6 Multibeam Borrmann Modes 28
- 2.7 The Internal Source and Multibeam Borrmann Modes 29

Chapter 3. The Search for the Nuclear Borrmann Effect 31
- 3.1 Introduction 32
- 3.2 Fe Single Crystals 32
- 3.3 Ge Single Crystals: Sample Preparation 38
  - 3.3.1 Origins of the Ge Single Crystals 38
  - 3.3.2 The Cutting Process 39
  - 3.3.3 Alignment 44
  - 3.3.4 Testing for the Borrmann Effect - X-Ray Source 45

3.4 ^{73}As Doped Ge Single Crystal Source Preparation 47
3.5 ^{73}Ge Decay 52
3.6 Observation of Nuclear Borrmann Effect 53
3.7 Concluding Remarks 58

Chapter 4. Time Filtering 60
4.1 Introduction 60
4.2 Theoretical Considerations 61
4.3 Mathematical Description 61
4.4 Example Curves 65

Chapter 5. Experimental Time Filtering 70
5.1 Introduction 70
5.2 Experimental Setup 74
5.3 Fitting and Analysis Procedure 79
5.4 Gamma Ray Time Filtering for ^{73}Ge 81
5.5 X Ray Time Filtering for ^{73}Ge 86
5.6 Iron Time Filtering: The Gamma Ray Case 90
5.7 Iron Time Filtering: The X Ray Case 95

Chapter 6. Summary, Conclusions, and Future Directions 105
6.1 The Nuclear Borrmann Effect 105
6.2 Time-Filtering Effect 106
6.3 General Remarks 107

References 108

Appendices 111

Vita 131

LIST OF TABLES

Page

Table 5.1 ^{73}Ge Gamma-Ray Fit Parameters 86

Table 5.2 ^{73}Ge X-Ray Fit Parameters 87

Table 5.3 ^{57}Fe Gamma-Ray Fit Parameters 95

LIST OF FIGURES

Page

Figure 2.1 Intensity plot for the forward diffracted and diffracted beams for a) a kinematical crystal, and b) a dynamical crystal 12

Figure 2.2 Ewald's Sphere of Reflection intersecting a plane in receiprocal space . . 14

Figure 2.3 Ewald's Sphere of Reflection showing simultaneous diffraction 16

Figure 2.4 Construction of a Bragg reflection showing the orientation of the electric and magnetic fields associated with each wavevector 23

Figure 2.5 Standing Wave Figure 27

Figure 3.1 Pulse-height spectrum showing the transmitted ^{57}Fe radiation 33

Figure 3.2 Laue photograph 35

Figure 3.3 Topography photograph 37

Figure 3.4 Schematic representation of the procedure for measuring a rocking curve 40

Figure 3.5 Schematic representation of the eularian cradle 42

Figure 3.6 Barrel holder used to orient and cut the Ge single crystals 43

Figure 3.7 Scan about the χ angle to search for Borrmann transmissions 46

Figure 3.8 Borrmann scan of the Ge (111) crystal showing the three-fold symmetry axis 48

Figure 3.9 Schematic of the electroplating cell used to apply radioactive ^{73}As onto the Ge single crystal 49

Page

Figure 3.10 Laue scan of the transmitted 53 keV radiation for a Ge (111) crystal 54

Figure 3.11 Borrmann scan of the 13.26 keV gamma ray 56

Figure 4.1 Time-filtering curve for $\beta=1$ and $\Delta\omega=0$ 66

Figure 4.2 Time-filtering curve for $\beta=10$ and $\Delta\omega=0$ 67

Figure 4.3 Time-filtering curve for $\beta=10$ and $\Delta\omega=7$ 69

Figure 5.1 Schematic diagram for the ^{57}Co-^{57}Fe decay 72

Figure 5.2 Schematic diagram for the ^{73}As-^{73}Ge decay 73

Figure 5.3 Pulse-height spectrum of ^{73}Ge 75

Figure 5.4 Pulse-height spectrum of ^{73}Ge (Enlarged) 76

Figure 5.5 Schematic of the coincidence setup 77

Figure 5.6 Background rate with High Stop Rate 82

Figure 5.7 Time-Filtering Curve for ^{73}Ge Gamma Ray 84

Figure 5.8 Plot of Residuals from the ^{73}Ge Gamma Ray Fit 85

Figure 5.9 Time-Filtering Curve for ^{73}Ge X Ray 88

Figure 5.10 Plot of Residuals from the ^{73}Ge X Ray Fit 89

Figure 5.11 Time-Filtering Curve for ^{57}Fe Gamma Ray Using Two NaI(Ti) Detectors 91

Figure 5.12 Plot of Residuals from the ^{57}Fe Gamma Ray Fit 92

Figure 5.13 Time-Filtering Curve for ^{57}Fe Gamma Ray Using a Ge Detector 93

Figure 5.14 Plot of Residuals from the ^{57}Fe Gamma Ray Fit (Ge Detector) 94

Figure 5.15 ^{57}Fe Time-Filtering Curve Using 6.4 keV X Ray (Two NaI Detectors) . . 96

Figure 5.16 ^{57}Fe Time-Filtering Curve Using 6.4 keV X Ray (Ge Detector) 98

Figure 5.17 Pulse-height Spectrum of Filtered ^{57}Fe Radiation 99

Page
Figure 5.18 57Fe Lifetime from ~8 keV Background 101

Figure 5.19 Plot of 57Fe Time Filtering Using the 6.4 keV Xray, no prompt 103

Figure A.1 A Fresnel zone in a horizontal plane 112

Figure A.2 A Fresnel zone in the vertical plane 114

Figure A.3 Schematic representation of the diffracted and forward diffracted wavefields inside the crystal 117

Chapter One

Gamma-Ray Optics

1.1 Introduction

For many years, researchers have questioned the possibility of constructing a gamma-ray laser (graser). Much theoretical work exists on the subject which is outlined in the paper by Baldwin et al[1], however very little experimental work has been done to test the theory. This research is a preliminary test that is based on one theoretical work that has been introduced by Hannon, Trammel and coworkers[2-5] of Rice University. The relevant experimental details of the Hannon and Trammel theory are addressed in the papers and doctoral thesis of Hutton[6-8] and are discussed below.

The Hannon and Trammel theory uses crystalline optics and the Mössbauer effect to provide a system that is capable of producing narrow beams of gamma radiation and also stimulate emission of gamma rays from excited nuclei. The basic premise consists of the implantation of excited nuclei whose transitions are of multipolarity M1 or higher, in a nuclear-resonant perfect single-crystal environment. This configuration allows the decaying nuclei to feed eigenmodes of the radiation field inside the crystal that suppress photoelectric absorption. Additionally, these eigenmodes provide a mechanism that allows the emitting nuclei to couple to other excited nuclei in the crystal and possibly stimulate them to radiate.

In order to have enough nuclei for this coupling to occur, the crystal must be sufficiently thick. Ordinarily this could pose a problem if electronic attenuation is considered, since the radiation would be expected to simply get absorbed within the crystal. However, as this is a single crystal, a phenomenon know as the Borrmann effect[9] becomes an important consideration. The Borrmann effect, required when dealing with highly perfect single crystals, allows radiation to travel through crystals that, from an ordinary attenuation stand point, would be considered too thick. This is accomplished by having the electric field of the radiation be near zero at the atomic sites. At the same time the electric field is at a minimum, the magnetic field and electric-field gradient are near a maximum. This is due to the Borrmann mode being comprised of a traveling wave in one direction (say the z direction) and a standing wave in the directions perpendicular to the traveling wave (the x and y direction). In a standing electromagnetic wave, the magnetic field and electric field are $\pi/2$ out of phase[10]. Therefore, when one is a maximum, the other will be a near zero. Using this phase relationship, the Hannon and Trammel theory predicts that a nuclear radiator of multipolarity M1 or higher, which has a maximum magnetic or electric field gradient at the nucleus, placed at a lattice site inside a perfect single crystal, could feed a Borrmann mode and the radiation can get out of the crystal relatively unattenuated electronically since these type of radiators will have a near zero electric field at the atomic site.

Stimulated emission can be achieved in the Borrmann channel since the nuclei along the direction of the Borrmann channel are strongly coupled. This coupling is due to the nuclear radiator having a near maximum magnetic field or electric field gradient at the nucleus. This allows other excited nuclei to "see" each other. As one nucleus decays, it may influence others to decay, thus causing a net "gain" in the photon field. If however the gamma emitting nucleus were the only excited nucleus in the resonant crystal (i.e. all other nuclei were in the ground state) then the gamma ray would not be able to exit the crystal due to nuclear absorption and subsequent internal conversion.

This theory relies on the Mössbauer effect for the absorption and emission of the gamma radiation. This is because any loss of energy to the photon through recoil will be enough to move the centroid of the gamma ray energy line off resonance (or detuned) with respect to other nuclei. If this would happen, then the photon would not be able to interact with other excited state nuclei in the crystal. This would give the system zero gain as the photon propagated through the medium resulting in no lasing. Therefore, the losses in energy must be reduced to a minimum. This dependence on the recoilless emission and absorption of gamma radiation requires a brief introduction to the Mössbauer effect.

1.2 The Mössbauer Effect

In 1957, while working on his doctoral thesis research studying resonance fluorescence using the 129 keV first excited state energy level in ^{191}I, Rudolph L. Mössbauer discovered the effect which eventually won him the Noble Prize in Physics[11] in 1961 and now bears his name. The now well-known Mössbauer Effect[8] is the recoilless emission and absorption of gamma radiation. Since the nucleus effectively does not recoil, the energy width of the emission and absorption lines approach the lower limit governed by the Heisenberg Time-Energy Uncertainty Principle. This is due to the ground state having an infinite lifetime and hence no uncertainty in the energy of this level[13].

$$\Gamma\tau = \frac{h}{2\pi} \tag{1.1}$$

In Eq. 1.1, Γ is the energy width of the state, τ is the mean lifetime of the excited state, and h is Planck's constant.

To illustrate the properties and describe the background of the Mössbauer effect, it is instructive to consider the process of nuclear resonance fluorescence. Nuclear resonance fluorescence occurs when a nucleus makes a transition from an excited state to the ground state by emitting a gamma ray. This gamma ray is then used to excite a nucleus of the same type from the ground state to the excited state which in turn re-radiates this gamma ray not necessarily in the original direction.

The first experiments designed to detect nuclear resonance fluorescence were attempted in 1929 by Kuhn[14]. These experiments were unsuccessful due to nuclear recoil shifting the energy of the emitted gamma ray such that it was no longer on resonance, and thermal Doppler broadening effects which broadened the spectral energy distribution of gamma ray. At the time, nuclear recoil was understood to cause the energy of the emission or absorption linewidths to be shifted[15]. However, it was theorized that by thermally broadening the linewidths of the gamma rays, some overlap of the lines would occur, resulting in some resonance phenomenon[16].

In order to obtain a significant probability of nuclear resonance fluorescence, the absorption and emission energy distributions must strongly overlap[17]. If either the emission line or absorption line is displace with respect to energy, the probability of a resonance being observed is decreased. Additionally, as Mössbauer discovered, if the linewidths are thermally broadened, the amount of the observed resonance also decreases due to changes in the recoilless fraction. From these principles, in the ideal case, resonance will be strongest when the two line widths overlap exactly and have the same linewidth.

Consider a free nucleus that makes a transition from an excited state to the ground state by emission of a gamma ray. By conservation of momentum, the nucleus will recoil with an energy given by

$$E_R = \frac{E_\gamma^2}{2Mc^2} \tag{1.2}$$

where E_R is the recoil energy, E_γ is the transition energy, M is the mass of the atom, and c is the speed of light. In order for a gamma ray to induce an excitation from the ground state to the excited state in a free nucleus of the same type, it must provide the transition energy plus the recoil energy. If the gamma ray was originally emitted with recoil, it would be deficient by $2E_R$ with respect to the transition energy[18]. This would effectively reduce the absorption probability.

Now consider a nucleus bound in a solid -- specifically a crystal lattice. When the nucleus emits a gamma ray, the nucleus recoils. Since the nucleus is in an atom that is on a crystal lattice, the whole atom recoils also. If the "spring constant" of the coupling of the atoms is strong, then a macroscopic part of the crystal participates in the recoil by producing phonons in the lattice. Since there are typically 10^{15} atoms in a crystal, the recoil energy is negligibly small. This is easily seen by noting that the recoil energy in Eq. 1.3 is inversely proportional to the mass, which in this case can be considered the mass of the crystal. This large mass term makes the recoil energy small. From another point of view, the recoil energy goes into producing phonons in the crystal lattice. Since phonons are quantized, there exists a finite probability that the nucleus will emit without recoil[19]. In this case, the gamma ray is emitted with the "full" energy of the transition.

There are other factors that can cause a "detuning" in energy between the source and absorber. These include an isomer (or chemical) shift, and relative thermal motion of the nuclei. The thermal motion shows up only as a second order Doppler shift[20]. This motion, if large enough, can cause a significant shift in the resonance energy between the source and absorber. The isomer shift occurs when the emitting nucleus and the absorbing nucleus are in two different environments[21]. For example, if ^{57}Co is placed in a Pd matrix and the absorber is ^{57}Fe in a natural Fe matrix, each nucleus (both the source and absorber) will "see" different local magnetic and/or electric fields. These fields can produce a shift in the nuclear levels such that the two nuclei are no longer exactly on resonance.

1.3 Modification to the Hannon and Trammel Theory

This thesis is based on the Hannon and Trammel theory with some subtle modifications. These modifications rely on a consequence of the Mössbauer effect called time filtering in order for the gamma-ray to exit the single crystal medium.

The Hannon and Trammel theory predicts that a gamma-ray emitted from a nucleus that is embedded deep inside a nuclear resonant single crystal will not be able to exit the nuclear-resonant single crystal because of the nuclear absorption and subsequent internal conversion. One way to circumvent this loss problem and is the basis of this thesis, is to suppress the internal conversion channel or enhance the radiative channel. This enhancement or speed-up of the radiative channel is a natural result of time-domain Mössbauer spectroscopy[22].

As the photon propagates through the resonant medium, it is absorbed and reradiated into the forward direction. The absorption occurs at the center of the line which "eats out the center" of the line. This broadens the linewidth. Invoking the Heisenberg time-energy uncertainty principle again, as the spectral energy linewidth broadens, the associated lifetime decreases. We interpret this "speed-up" in the lifetime as an enhancement of the radiative channel.

1.4 Organization of the Dissertation

Our experiments in gamma-ray optics include studies of the Borrmann effect and time-domain Mössbauer spectroscopy (time filtering). The isotopes selected for study were ^{57}Fe, due to its large and well-known Mössbauer effect; and ^{73}Ge, due to the highly perfect single crystals for which Ge is known. Theoretical explanations and experimental work for the Borrmann effect are given in Chapters Two and Three, respectively. Theoretical descriptions and experimental work for time-domain Mössbauer spectroscopy (time filtering) are given in Chapters Four and Five. Conclusions are given in Chapter Six.

Chapter Two

Dynamical Theory and the Borrmann Effect

2.1 Characteristics of Kinematical and Dynamical Diffraction

The Borrmann effect, first discovered in 1960 by G. Borrmann[23], is the anomalous transmission of x-radiation through perfect single crystals. This effect is predicted by the dynamical theory of x-ray diffraction[24], which assumes highly perfect single crystals. In the so called two-beam Borrmann mode, the incident and diffracted waves inside the crystal are considered to be one wavefield instead of two separate and distinct wavefields, and multiple scattering is allowed between these two components of the wavefield[25]. As the waves propagate through the crystal, certain eigenmodes of the radiation field have effectively a zero electric field amplitude at each lattice site. This will lead to a near zero coupling of the electric field to the atoms occupying these lattice sites. The result is suppressed photoelectric absorption, allowing this mode of the radiation to travel through crystals that, from ordinary mass-attenuation considerations, would be deemed too thick.

There are two possible theories for calculating the intensity associated with any diffraction process, depending on the relative thickness and perfection of the crystal being used: the kinematical theory, for smaller thicknesses and less perfect crystals, and the dynamical theory, for thicker and perfect single crystals. The differences between these two theories can be readily observed by examining the intensity profiles of both the forward diffracted (incident) and diffracted (reflected) beams for a Laue transmission experiment.

The Laue transmission consists of simple Bragg reflections where the incident radiation enters one face of a crystal and exits from a different surface. In this so-called Laue setting, the radiation scatters off of planes that are (usually) perpendicular to the entrance surface. In contrast, in the Bragg setting, the incident beam enters and exits the crystal from the same face, with the planes (usually) are parallel to the entrance surface. It is possible to have the planes that are being used for the scattering at some other angle relative to the crystal face, however, the type of reflection (either Laue or Bragg) is still classified by the entrance and exit surfaces. In either type of reflection, the scattering is governed by Bragg's law, which states that

$$n\lambda = 2d\sin\theta \qquad (2.1)$$

where n is an integer, λ is the wavelength of the incident radiation, d is the lattice spacing, and θ is the angle the incident radiation makes with the scattering planes.

The well-known kinematical theory is used when dealing with crystals whose thicknesses are small such that the normal absorption coefficient is on the order of unity

$\mu t=1$ (where μ is the mass attenuation coefficient and t is the thickness of the sample). The kinematical theory applies if the crystal has many imperfections within the lattice. This theory treats each volume element of the crystal independently. As the incident wave travels into the crystal, each "layer" reflects a small percentage of the incident wave. In addition, each incident wave is allowed to scatter only once. The diffracted wave in this case is a summation of the individual waves scattered by each plane. To illustrate, if a monochromatic x-ray beam is incident upon a "kinematical" crystal, some of the intensity from the forward diffracted beam is re-channeled into the diffracted beam as the Bragg condition is satisfied, decreasing the intensity of the forward diffracted beam. (Fig. 2.1a)

If the crystal thickness is much larger ($\mu t \sim 10$) and has a lattice that is highly perfect, the dynamical theory of x-ray diffraction must be used, as the kinematical theory will not properly predict the measured intensity. The dynamical theory allows for multiple scattering within the crystal. Thus, the total wavefield inside the crystal must be considered since the forward diffracted and diffracted waves are allowed to interact. As the diffracted beam travels through the crystal, it will reflect multiple times back into the direction of the forward diffracted beam. Rather than "stealing" intensity, the diffracted beams enhance the forward diffracted beam. Using the illustration above, as the Bragg condition is satisfied for a "dynamical" crystal, the wavefields inside the crystal undergo multiple reflections. As a result, the intensity of the forward diffracted beam increases (Fig. 2.1b).

2.2 Simultaneous Diffraction

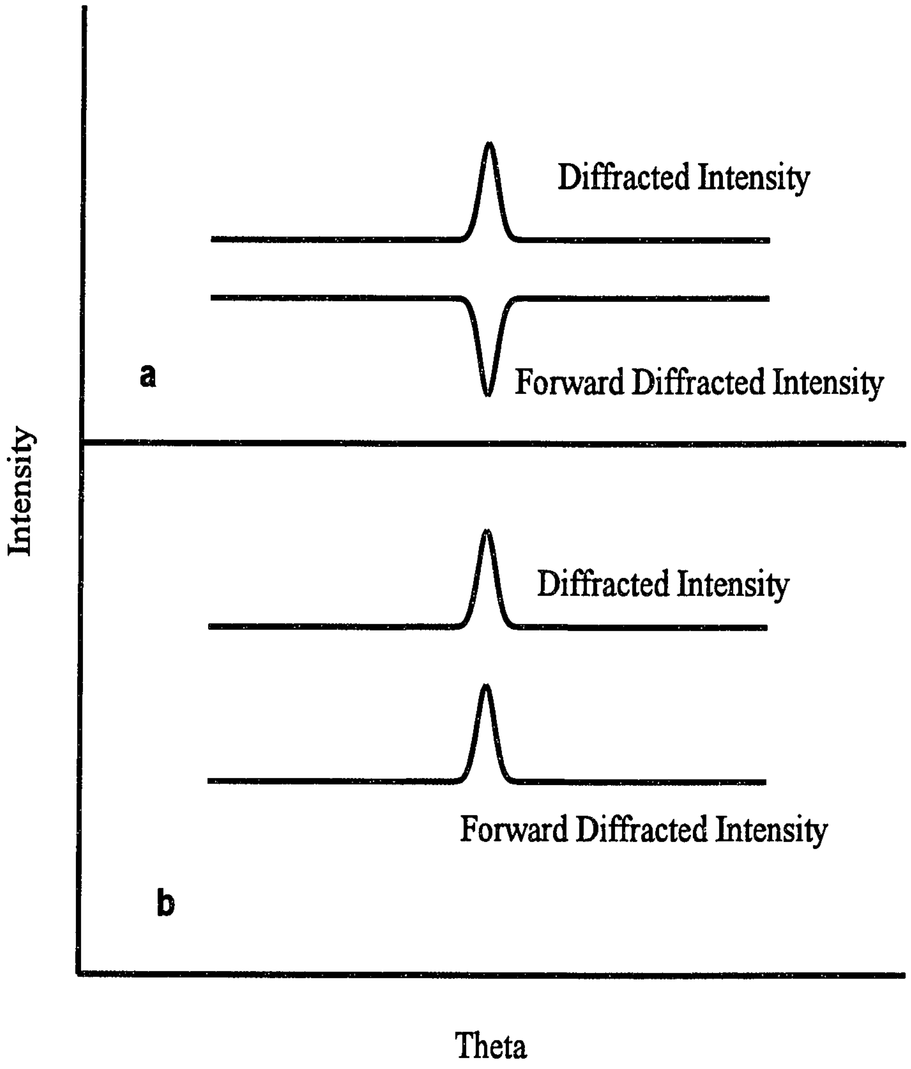

Fig. 2.1 Intensity plot for the forward diffracted and diffracted beams for a) a kinematical crystal, and b) a dynamical crystal.

The possibility exists that the incident beam may simultaneously diffract from multiple reciprocal lattice vectors, if the crystal has the proper symmetry. A helpful way to visualize this is to use the construction developed by Ewald[26]. This construction considers the intersection of a sphere, whose radius is defined by the wave vector of the radiation inside the crystal, with a plane in reciprocal space (Fig 2.2). If two reciprocal lattice points lie on the surface of the "sphere of reflection", the incident radiation can be reflected from one of the reciprocal lattice points to the other by means of the reciprocal lattice vector connecting the two points. This is simply a geometrical construction of Bragg's law. To prove that this is Bragg's law, an examination of the components making up the incident and diffracted waves is required.

First, by adding the components that are along the direction of the reciprocal lattice vector, an expression relating the wavevectors to the reciprocal lattice vector *H* is obtained.

$$k_1 \sin\theta + k_2 \sin\theta = H \qquad (2.2)$$

However, the wavevectors k_1 and k_2 are equal to the radius of the sphere of reflection, k. Therefore,

$$2k\sin\theta = H \qquad (2.3)$$

By definition, $k = 2\pi/\lambda$ and $|H| = 2\pi/d$. Substituting these into Eq. 2.3, the familiar Bragg's law is obtained.

$$\lambda = 2d\sin\theta \qquad (2.4)$$

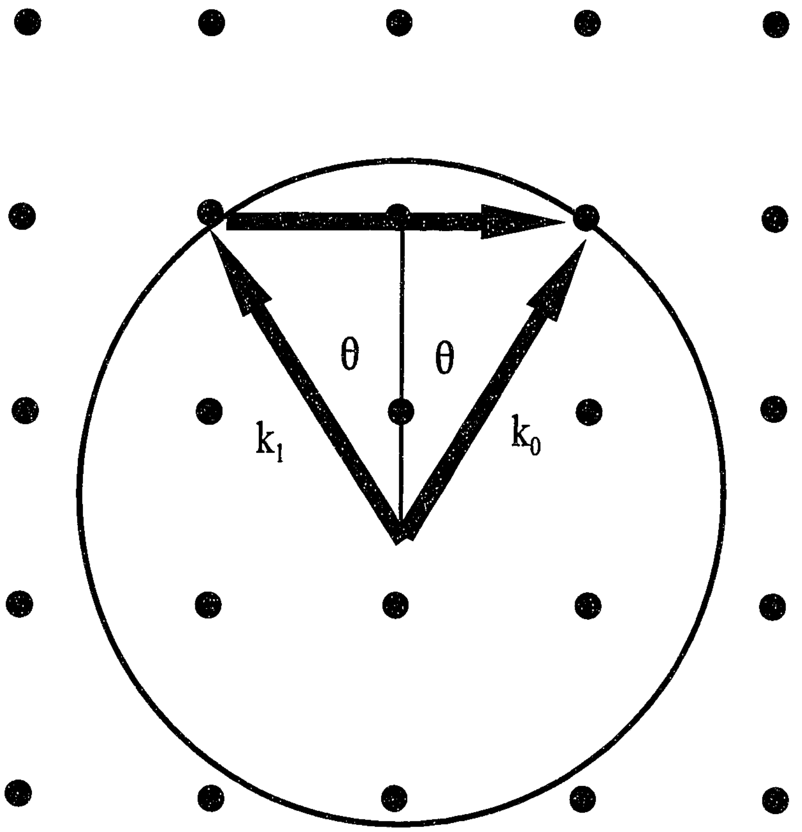

Fig. 2.2 Ewald's Sphere of Reflection intersecting a plane in reciprocal space.

If the sphere of reflection intersects more than two reciprocal lattice points, the radiation can be scattered from one of the reciprocal lattice points to any or all of the other reciprocal lattice points, provided that 1) the reciprocal lattice points lie on the sphere of reflection and 2) the reciprocal lattice vector that connects the two points corresponds to an allowed reflection (Fig. 2.3).

After this initial scattering, it is possible for the waves to scatter from the new reciprocal lattice point to a completely different reciprocal lattice point (not back to the initial point). As these waves scatter from point to point, the wavefield inside the crystal becomes a superposition of all of these possible allowed reflections, resulting in a multi-beam diffraction. In order for this to occur for an external source, the incident radiation direction and the crystal orientation must be in complete alignment to satisfy the Bragg condition for multiple sets of planes within the crystal. For an internal source, this problem is minimized, since the source radiates in approximately all possible directions.

2.3 Determining Reflection Conditions

Reflection conditions need to be calculated in order to determine whether a given set of planes within a specific crystal will produce a Bragg peak. If a Bragg peak is produced, the reflection is considered an "allowed" reflection. This is determined by calculating the structure factor for the specific crystal being studied.

The structure factor describes the reflecting power for a unit cell in a crystal. Calculation of the structure factor involves summing the contributions to the scattered

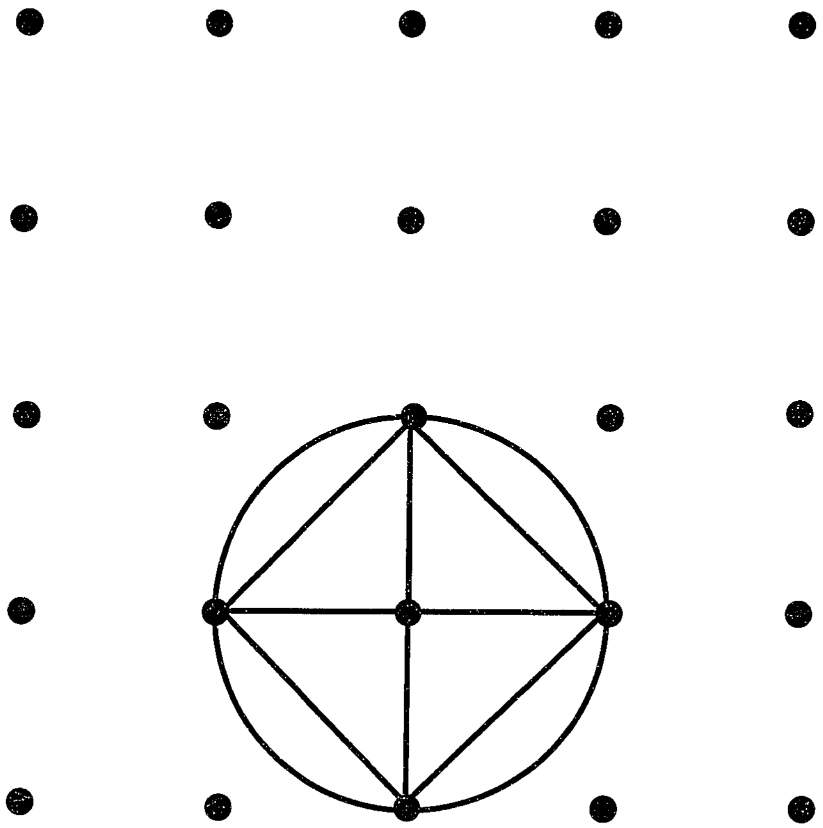

Fig. 2.3 Ewald's Sphere of Reflection showing simultaneous diffraction. Since the sphere intersects with four reciprocal lattice points, there will be a four beam diffraction.

radiation which come from all of the atoms in the unit cell. This summing takes into account the phase shift associated with having a distribution of atoms over a volume instead of having the atoms all concentrated at a single point[27]. In equational form, the structure factor is written as

$$F=\sum_{i=1}^{N} f_i e^{2\pi i\vec{H}\cdot\vec{r}_i} \tag{2.5}$$

where f_i is the atomic scattering factor of the ith atom, $\bar{H} = h\hat{x} + k\hat{y} + l\hat{z}$ is the reciprocal lattice vector corresponding to the reflection being considered (h, k, l are the Miller indices), and $\bar{r}_i$ is the location of the ith atom in the unit cell. If the crystal is comprised of more than one type of atom, the atomic scattering factor for that atom is used in the summation. The atomic scattering factor is allowed to have an imaginary component to allow for absorption, thus giving the structure factor an additional imaginary contribution. These "corrections" to the atomic scattering factor are known as the Hönl corrections[28].

As an example of the determination of the reflection conditions, natural Fe is considered. Fe is a body-centered cubic (bcc) crystal, meaning the unit cell has an Fe atom at each corner of a cube and an additional atom located at the center of the cube. Summation over the total number of atoms actually inside the unit cell is two. The atoms on the corners of the cube each contribute 1/8 of an atom to the sum, as this is the amount that is located inside the cell. Since there are 8 corners in a cube, the sum yields one total atom for this portion.

Choosing an origin at one of the corners of the cube, the location of the two atoms are $r_1=(0, 0, 0)$ and $r_2=(½, ½, ½)$. Using these values, the structure factor becomes

$$F=f(1+e^{2\pi i(\frac{h}{2}+\frac{k}{2}+\frac{l}{2})}) \tag{2.6}$$

Examination of the structure factor shows non-zero values when h+k+l=2n, where n is an integer. If the sum of h+k+l is odd, the exponential factor will be -1 and the structure factor will vanish, resulting in a zero reflected intensity. When h+k+l is even, the structure factor would give F = 2f. This would be considered an allowed reflection.

2.4 The Two Beam Borrmann Mode

As stated earlier, one of the interesting consequences of the dynamical theory of x-ray diffraction is the existence of the Borrmann effect. There are two theoretical approaches for describing and showing the properties of the Borrmann effect that may be taken when using the dynamical theory. The first is an elegant treatment originally developed by Laue[29] which involves solving Maxwell's equation in a periodic medium. The second, developed by Darwin[30], is a more straightforward approach from a diffraction standpoint, and will be outlined here as decribed by Warren[31] in terms of a simple two-beam case. A complete development of a simple two-beam case is given in Appendix A.

The Darwin approach begins by calculating the electric field of a wave that is scattered from a single plane. The first consideration is the differential electric field produced by scattering from some differential surface element in the plane. This is integrated over the surface of the plane such that the path-length of the radiation (from its point of origin to a point in the plane and on to a point some distance from the plane) is no greater than $\lambda/2$. The use of this constraint defines the integration surface as a classical Fresnel zone.

Next, the possibility for multiple scattering must be included. This involves determining a recursion relationship for both the forward diffracted and diffracted waves. The recursion relationship for a forward diffracted wave at a given position in the crystal can be written mathematically as a superposition of 1) the forward diffracted wave from the previous plane, plus 2) the component from the diffracted wave of the current plane, each with the proper phase factors included. The recursion relationship for the diffracted wave is written much the same way; a superposition of 1) the diffracted wave from the previous plane, plus 2) the component of the forward diffracted wave of the current plane. Again, each component has a phase factor which must be included.

Now that both recursion relationships are known, one can be substituted into the other to derive an expression in terms of only the forward diffracted wave, or of only the diffracted wave. The general power series solution is assumed for both equations. Upon substitution, the solutions for the forward diffracted wave and the diffracted wave are obtained.

When the Bragg condition is satisfied exactly, the equations for the forward diffracted and diffracted wave reduce to:

$$T_r=\frac{T_0}{2}e^{-i\phi r}\left[e^{i(g_0+g)r}+e^{i(g_0-g)r}\right] \qquad (2.7)$$

and

$$S_{r-1}e^{-i\phi}=\frac{T_0}{2}e^{-i\phi r}[e^{i(g_0+g)r}-e^{i(g_0-g)r}] \qquad (2.8)$$

respectively, where T_r is the forward diffracted wave after the r^th^ plane, S_{r-1} is the diffracted wave after the r-1 plane, ϕ is the phase of the wave, g is the scattering power of the reflection for the diffracted beam, g_0 is the scattering power of the reflection for the forward diffracted beam, and r is the number of planes the radiation has traversed.

To allow for absorption, the scattering factors g and g_0 are complex quantities:

$$g=g^{\prime}+ig^{\prime\prime} \qquad g_0=g_0^{\prime}+ig_0^{\prime\prime} \qquad (2.9)$$

These complex scattering factors are substituted into Eq. 2.7 and Eq. 2.8. If the possible polarization states within the crystal are considered, there will be four wave fields present. All but one will be attenuated out (absorbed after passing through many planes of atoms) for large values of r. The surviving wavefield for the forward diffracted and diffracted waves is the Borrmann mode. The equations for the Borrmann mode electric field amplitudes are written as

$$T_r=\frac{T_0}{2}e^{-i\phi r}e^{i(g_0^{\prime}-g^{\prime})r} \qquad (2.10)$$

and

$$S_{r-1}e^{i\phi} = -\frac{T_0}{2}e^{-i\phi r}e^{i(g_0'-g')r} \qquad (2.11)$$

Notice that both wavefields do not decrease with increasing r. Therefore, these waves will pass through very thick crystals with no attenuation.

The intensity of the Borrmann mode can finally be calculated by the taking absolute value squared of the electric field component in each wave. Mathematically, this is written as

$$|I_T| = \frac{|T_0|^2}{4} \ , \quad |I_S| = \frac{|T_0|^2}{4} \qquad (2.12)$$

where I_T and I_S are the intensities of the forward diffracted and diffracted beams of the Borrmann mode, respectively.

An unpolarized input x-ray beam can be expressed as a superposition of two perpendicular linearly polarized waves of equal intensity. These polarization states are commonly referred to as σ and π polarizations. The σ polarization is defined as the direction perpendicular to the plane of reflection (defined by the incident and reflected wave vectors). The π polarization is defined as the direction perpendicular to the wave vector yet lying in the plane of reflection (See Fig. 2.4).

Therefore, for a given intensity, half is σ polarized and half is π polarized. For the Borrmann mode, only the σ component is present. This results in intensities in the two beam Borrmann mode that will be one eighth the input intensity.

$$I_T=\frac{I_\sigma}{4} \quad , \quad I_S=\frac{I_\sigma}{4} \tag{2.13}$$

where $I_\sigma = I_0/2$.

2.5 The Two Beam Borrmann Effect: Wavefield Approach

The Darwin development treats the wavefields inside the crystal as being independent of one another. In reality, these two wavefield are actually one single wave in which each component is continually modifying the other. Assuming the waves can be considered plane waves, and the amplitudes of the electric fields are equal for the incident and diffracted waves, the superposition of these two (from Fig. 2.4) can be written as

$$\vec{E}=(E_0 e^{-i(\omega t-\vec{k}_0\cdot\vec{r})}-E_0 e^{-i(\omega t-\vec{k}_1\cdot\vec{r})})\hat{x} \tag{2.14}$$

where from Fig. 2.4

$$\vec{k}_0=k_y\hat{y}+k_z\hat{z} \tag{2.15a}$$

and

$$k_1=-k_y\hat{y}+k_z\hat{z} \tag{2.15b}$$

Substituting in for k_0 and k_1, this reduces to

$$\vec{E}=(2i)E_0 e^{-i\omega t} e^{i(k_z z)}\sin(k_y y)\hat{x} \tag{2.16}$$

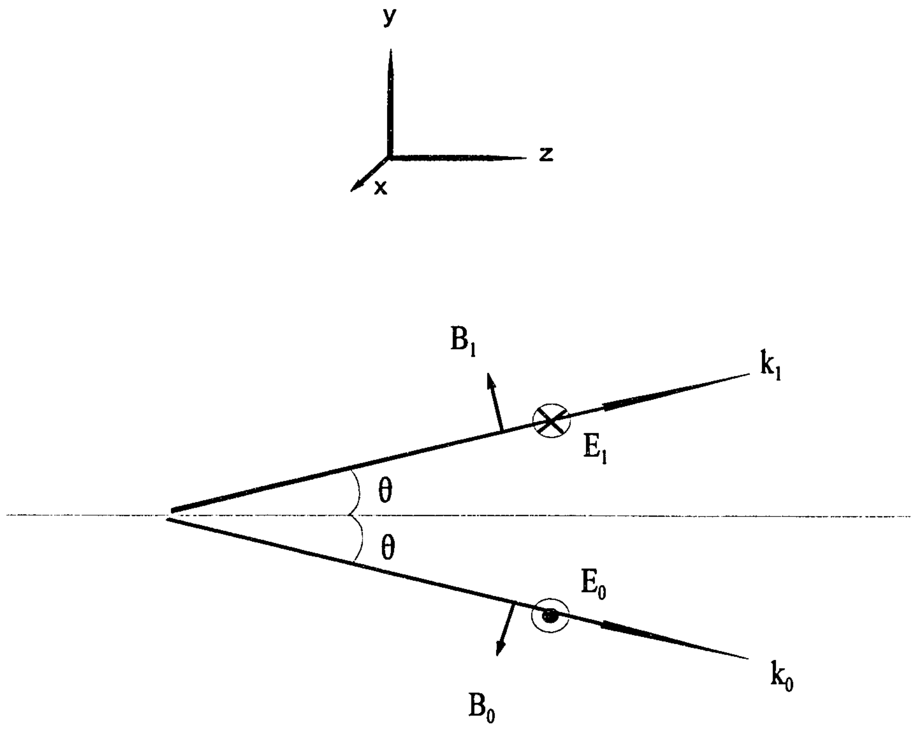

Fig 2.4 Construction of a Bragg reflection showing the orientation of the electric and magnetic fields associated with each wavevector.

and

$$\vec{E}=E_0 e^{-i\omega t} e^{i(k_z z)}[e^{i(k_y y)}-e^{-i(k_y y)}]\hat{x} \tag{2.17}$$

The value of $k_y y$ will be an integer multiple of 2π at any of the lattice sites, since the scattered radiation originates from the atoms located at the lattice sites. It follows from the above equation that there will be a **zero electric field amplitude at the atomic sites** which is again a consequence of the Borrmann effect. Because the electric field is zero it will not couple very strongly to produce photoelectric absorption. This allows the radiation to traverse through a very thick crystal. In practice the electric field is not truly zero but near zero. This is due to the fact that thermal motion of the atoms has not yet been considered in this calculation. To be complete, it is possible to include such thermal vibrations if a Debye-Waller factor e^{-2M} is introduced into the equations. This factor describes the mean-squared-displacement of the atoms as a function of temperature.

The magnetic field amplitude inside the crystal may be written in much the same way the electric field was written. However, since the magnetic field is transverse to the electric field, it will have components in the y and z directions.

$$\vec{B}=\frac{B_0}{2} e^{-i\omega t} e^{i\vec{k}_0\cdot\vec{r}}(\cos\theta\hat{y}-\sin\theta\hat{z}) + B_0 e^{-i\omega t} e^{i\vec{k}_1\cdot\vec{r}}(-\cos\theta\hat{y}-\sin\theta\hat{z}) \tag{2.18}$$

Substituting in for k_0 and k_1 and simplifying,

$$\vec{B}=B_0 e^{-i\omega t} e^{ik_z z}[i\sin(k_y y)\cos\theta\hat{y} - \cos(k_y y)\sin\theta\hat{z}] \tag{2.19}$$

We may now calculate the time average of the Poynting vector.

$$\vec{S}=\frac{1}{2}\vec{E}\times\vec{H}^{*} \tag{2.20}$$

$$\vec{S}=\frac{1}{2}E_0B_0\sin^2(k_yy)\cos\theta\,\hat{z}+(i)E_0B_0\sin(k_yy)\cos(k_yy)\sin\theta\,\hat{y} \tag{2.21}$$

From the Poynting vector for the Borrmann mode, we see that **there is a real net energy flow only along the z direction**. This corresponds to the radiation traveling along a path directly through the crystal before it is "split" into the forward diffracted and diffracted beams upon emerging from the crystal. The experiment to observe this direct beam is easily performed by placing a film plate behind a crystal undergoing dynamical diffraction. The film records three intensity spots. Two of the spots correspond to the diffracted and forward diffracted beams. The third spot is a direct hard component of the beam. The thickness of the crystal can then be calculated by measuring the distance from the direct beam and the diffracted beam. This is an indication that the beam travels directly through the crystal and splits into the two beams.

The component of the Poynting vector for the y direction is an imaginary quantity interpreted as a standing wave in this direction. This standing wave is another property of the Borrmann mode that may be exploited. In a standing electromagnetic wave, the electric field is π/2 out of phase with the magnetic field.[32] Utilizing this detail, if the electric field for a Borrmann mode is near zero at the atomic sites, the magnetic field is near a maximum at these sites (Fig. 2.5).

In the case of an external x-ray source, if the incident wave produces an electric field whose maximum occurs at a lattice site inside the crystal, this wave would excite an anti-Borrmann mode and would be attenuated strongly by photoelectric absorption. By reciprocity, if a radiator is placed at an atomic site and radiates by electric dipole (E1) emission, a large electric field would be produced at each site. Again, the radiation would not be able to propagate out of the crystal.

However, if an **internal** radiator at a lattice site radiated **magnetically** (i.e. M1 radiation), the magnetic field would be at a maximum at each lattice site and the electric field would be at a minimum. Such a case would excite a Borrmann mode and hence would allow the radiation to traverse through the crystal. For example, if excited ^{57}Fe were doped into a Ge single crystal, it might be possible to excite a Borrmann mode since the first excited state in ^{57}Fe is a magnetic dipole (M1) radiator.

Now consider the crystal as being comprised of a material which is nuclear resonant with M1 radiation, and assume the source of the radiation originates from within the crystal. In this situation, it might be possible for the radiation to escape due to a suppression of photoelectric absorption. However, since the medium is now nuclear resonant, the radiation has another competing absorbing factor and thus may not exit from the crystal. For example, if the crystal were an ^{57}Fe crystal containing excited ^{57}Fe radiators, the radiation theoretically would not be able to leave the crystal due to attenuation through nuclear absorption and subsequent internal conversion. In spite of this, if the radiation were able to propagate through the crystal, this would be the first observation of a nuclear Borrmann mode. This

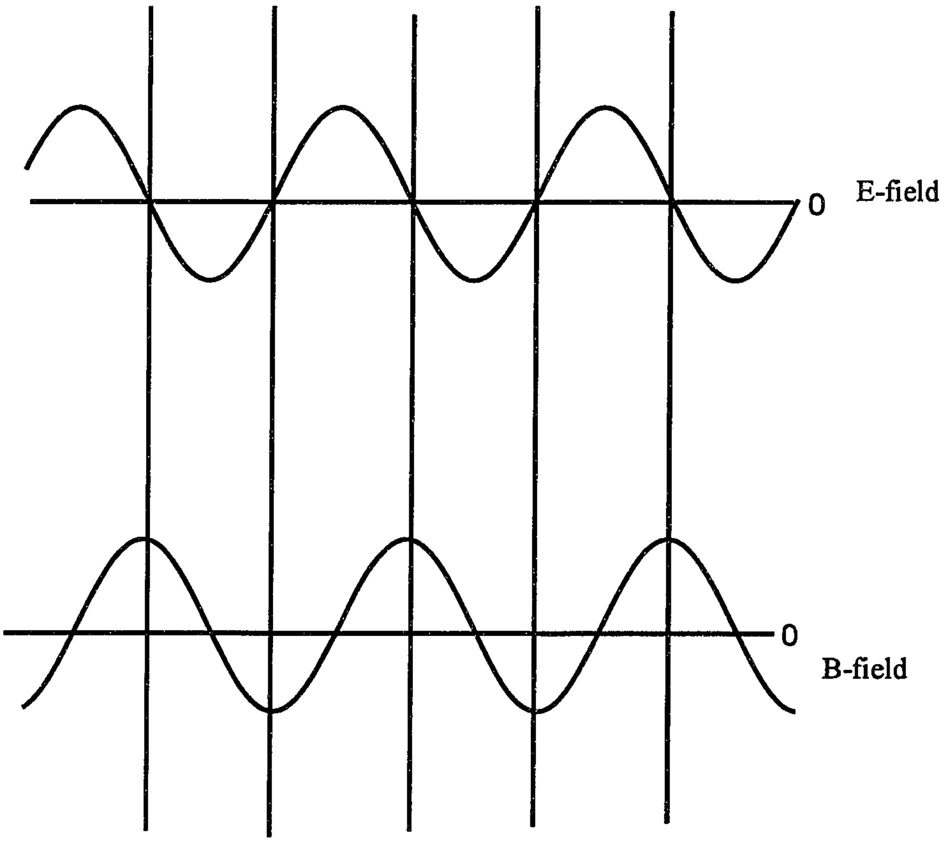

Fig. 2.5 The standing wave in the crystal produces an electric field that is near zero at the atomic sites, and magnetic field that is large at the atomic sites. The vertical lines represent the planes of atoms. If the radiation is resonant with the nuclei, the radiation will couple strongly to the nuclei if the transition is magnetic dipole (M1).

observation would also signify that an enhancement of the radiative channel is occurring within the crystal.

2.6 Multibeam Borrmann Modes

A multibeam Borrmann mode can exist if 1) the crystal is set up for simultaneous diffraction with the incident beam oriented in such a way as to excite two different reflections and 2) the crystal is capable of supporting a Borrmann mode. Generally speaking, the multibeam Borrmann mode can be considered a collection of two-beam modes that are allowed to "mix". As a rule, the intensity of a multibeam mode will be larger than a two-beam mode by a scaling factor proportional to the number of beams. This is due to the number of photons that are actually channeled into a Borrmann mode, which is in turn governed by the angular width of the Bragg reflection. This angular width is called the Darwin width of the reflection. Typically the Darwin width is on the order of a few arcseconds. This width defines the acceptance of the radiation being channeled into this mode. The larger the acceptance of the channel, (and the more channels), the larger the flux of photons that will be available for use in the diffraction process.

The Darwin width of a Bragg reflection is calculated from the following:[33]

$$s=2.12*(\frac{e^2}{mc^2})\frac{N\lambda^2|F|}{\pi\sin 2\theta}(\frac{1+|\cos 2\theta|}{2}) \tag{2.22}$$

where N is the number of atoms per volume, λ is the wavelength of the radiation, $|F|$ is the absolute value of the structure factor, and θ is the Bragg angle of the reflection being considered.

As an example, consider a Ge single crystal with a (111) orientation. The lattice parameter in Ge is 5.658 Å. The atomic scattering factor for Ge at 13.26 keV is approximately 27. This gives a structure factor of $\cong 153$. The number of atoms per cm^3 is $4.4x10^{22}$. Inserting these values into Eq. 2.22 gives a Darwin width of approximately 7.8 arcsec. If there are 1000 photons per second incident on the crystal from an <u>external</u> source with a divergence of 0.1°, the number that would actually be channeled into the Borrmann mode would be approximately 10.

2.7 The Internal Source and Multibeam Borrmann Modes

If attention is turned again to the internal source problem, the situation arises where the source is radiating into 4π steradians and therefore should excite all possible reflections that lie on the Ewald sphere which, with the proper symmetry, should produce a multibeam Borrmann mode. The complication to this process is that, practically, there must be enough activity such that an appreciable amount of radiation has the possibility to be channeled into one of these Bragg reflections. A one millicurie source placed inside a crystal will produce $3.7x10^7$ photons (actually disintegrations) per second into 4π steradians. If the area of a Bragg reflection is considered (Darwin width times vertical divergence), it is easily shown that only a small amount of flux actually contributes to the diffracted intensity. This means that a relatively large amount of activity must be introduced into the crystal, especially if there are any other loss factors present, such as photo-ionization or internal conversion, in order to produce a reasonable counting rate at the detector.

Chapter Three

The Search for the Nuclear Borrmann Effect

3.1 Introduction

The experimental work concerning the nuclear Borrmann effect involved the use of two different isotopes, ^{57}Fe and ^{73}Ge. Most of the experiments were done using ^{73}Ge due to the highly perfect single crystals for which germanium is known. In order to observe a nuclear Borrmann effect, there were three criteria that had to be met. These were 1) highly perfect single crystals (required from a dynamical diffraction aspect), 2) an isotope with a Mössbauer effect at room temperature (to minimize complications with cooling the sample that may have resulted in damage to the crystal lattice), and 3) a readily available radioactive parent with a usable half-life. Some, if not all, of these conditions are present in both of the isotopes selected.

3.2 Iron Single Crystals

The experimental effort began with a study of natural Fe crystals doped with ^{57}Co. Even though natural Fe crystals are generally known to be of poor crystallographic quality, this isotope has a very large Mössbauer effect at room temperature. Two Fe single crystals that were cut from a (100) oriented boule of natural iron were purchased from Monocrystals Corp. These crystals were 1 mm and 0.5 mm thick. Orientation of the crystals was confirmed through Laue back scattering photographs taken at the National Synchrotron Light Source (NSLS) at Brookhaven National Laboratory (BNL).

Both crystals were doped with 1 mCi of ^{57}Co in a 1/8th inch spot on one side of the crystal. This was done by Isotope Products Corp. The doping procedure involved drying liquid CoCl onto the crystal surface. The crystals were then annealed in flowing hydrogen at 800°C for one half hour. After cooling to room temperature, the active spot was coated with a thin plastic film to prevent the activity from flaking off.

A pulse-height spectrum was collected for the radiation coming from the un-doped side of the ^{57}Co doped Fe single crystal. The results are shown in Fig. 3.1. The spectrum clearly shows a peak corresponding to the 14.4 keV gamma-ray coming from the ^{57}Fe decay. This suspicious peak was found to be caused by contamination of the undoped side of the crystal. To prove contamination existed, the undoped side of the crystal was etched four separate times in a 5% nitric acid and 95% alcohol solution to remove any activity that may have been on the surface. After each etching process, a pulse-height spectrum was collected. The 14.4 keV peak diminished with each etching. This was a clear indication that a small amount of activity was now inadvertently on the wrong side of the crystal. The etching

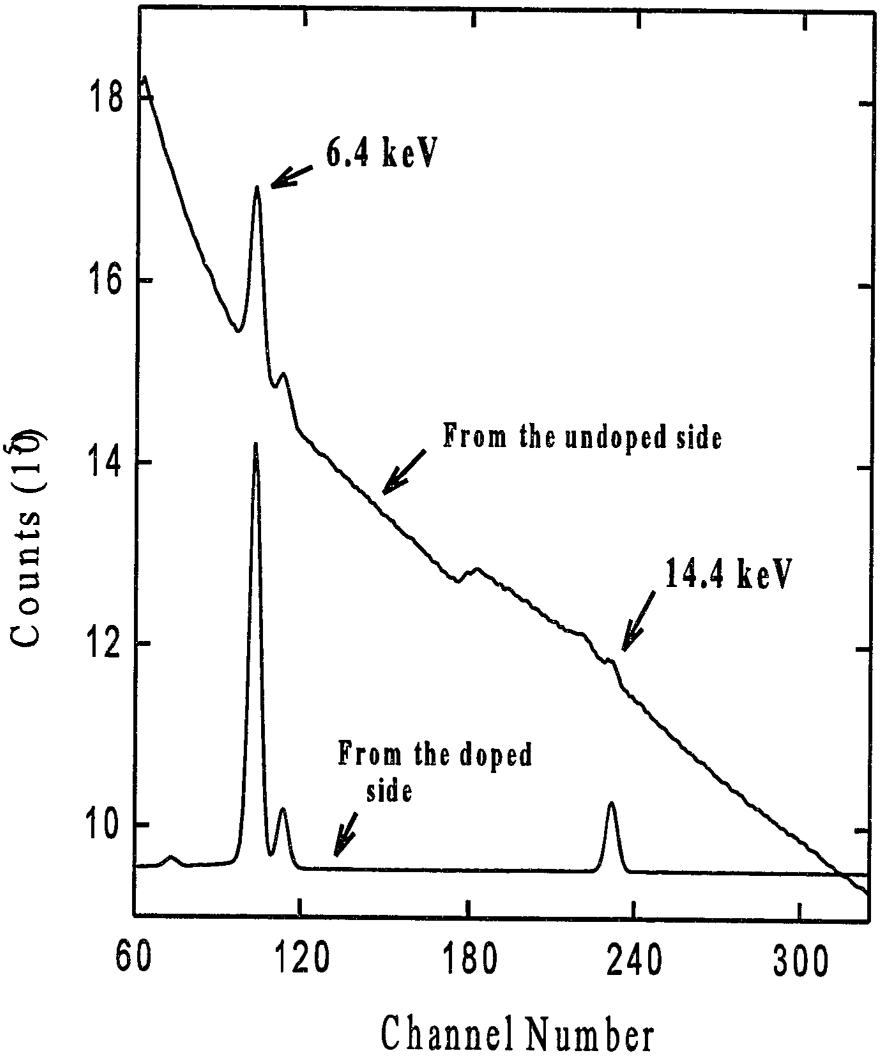

Fig. 3.1 Pulse-height spectrum showing the transmitted ^{57}Fe radiation. A pulse-height spectrum from a standard ^{57}Co source is superimposed on the graph to help show the locations of the peaks.

process was then continued until there was no significant change in the pulse-height spectrum (i.e. the 14.4 keV peak had disappeared). After cleaning the undoped side of the Fe single crystals, some preliminary scans to search for the Borrmann effect were performed. These experiments produced inconclusive results.

Since the iron single crystals were purchased and doped through commercial vendors, little preliminary testing was done to determine the crystals' ability to support a Borrmann effect. In addition, the equipment necessary to test the crystals was not readily accessible in the laboratory at that time. Therefore, an attempt was made to test the crystals using synchrotron radiation at the NSLS at BNL.

So-called "white" synchrotron radiation was used as the input signal to generate Laue diffraction photographs. As the radiation traveled through the crystal, it diffracted according to Bragg's Law. In addition, a hard component (high energy) of the incident beam passed straight through the crystal and produced an intensity maximum exposure point on the film (Fig.3.2). The Laue diffraction spots were measured along the plane of the film relative to this maximum exposure point. With the diffraction spot measurements and the known crystal-to-film distance, it was possible to calculate the diffraction angle associated with the Laue spots. This angle was then used with the accepted lattice spacing for Fe crystals to calculate the energy of the photons that produced the Laue spots. Some of the diffracted spots produced corresponded to some multiple of near 14.4 keV radiation. This was interesting because, the nuclear Borrmann effect in ^{57}Fe uses the 14.4 keV gamma ray from the decay of the first excited state. However, in the Laue pictures there was no distinction between actual 14.4 keV photons and higher harmonics of 14.4 keV photons. It was

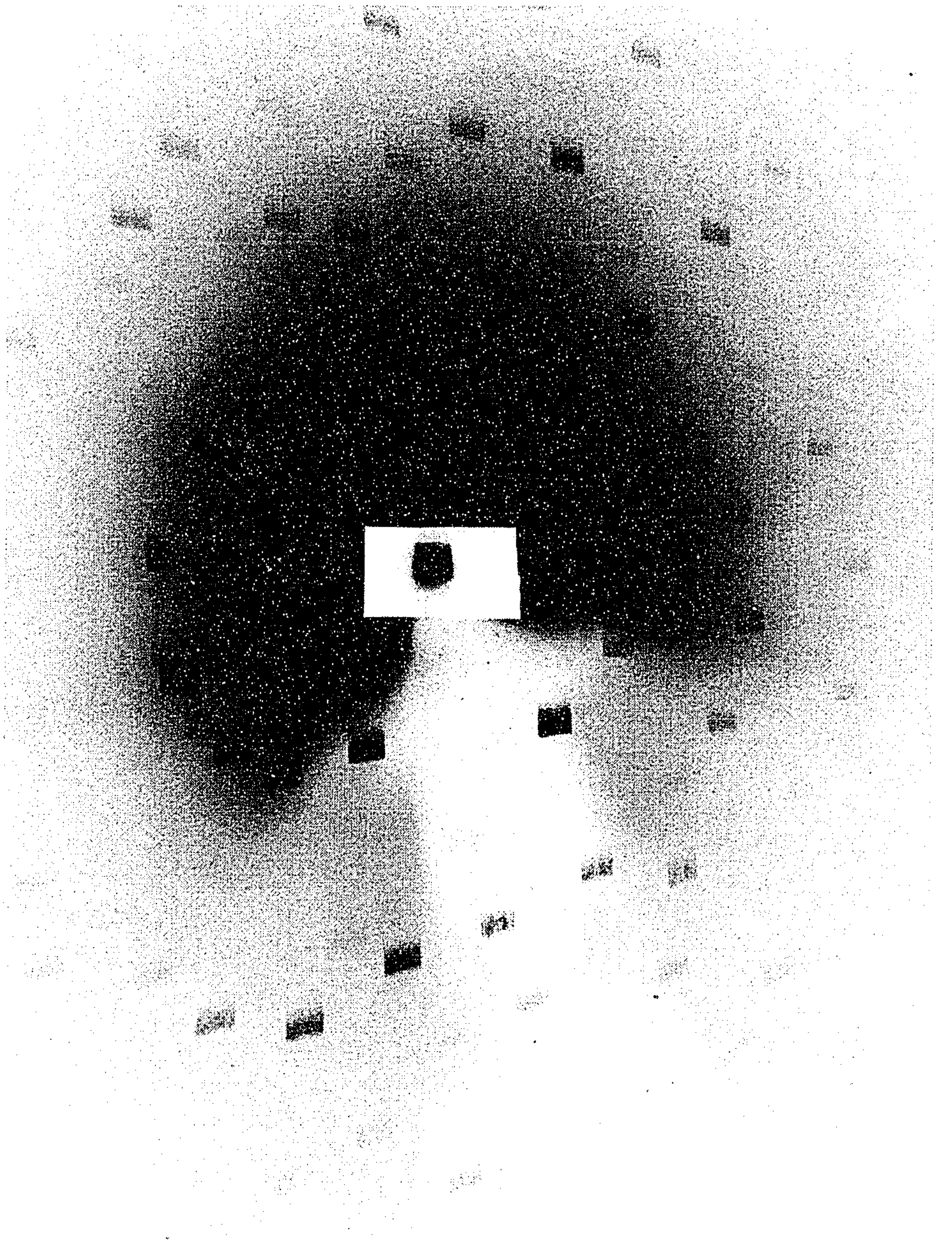

Fig 3.2 Laue transmission photograph. The crystal being used is one of the ^{57}Co doped Fe single crystals.

impractical to determine the exact composition of the Laue diffracted beams because the detectors capable of resolving these photo peaks are incapable of handling the high photon flux present in the diffracted beams.

Even though specific photon energies could not be determined, some inferences may be made regarding the source of the Laue spots. First, iron crystals are generally known to be of poor quality[34]. If this supposition proved to be true, it would imply that higher harmonics were responsible for producing the Laue spots. This implication is based on the relationship between photon energy and photoelectric absorption. Higher energy photons effectively make the material optically thinner and are therefore less likely to get absorbed. Conversely, lower energy photons are more likely to be absorbed within the material because the photoelectric cross section is higher. With higher energy photons, the crystal is still capable of diffracting the radiation, however the crystal is treated in a kinematical sense rather than a dynamical sense.

Secondly, x-ray film is more sensitive to lower energy photons. If the Laue spots had been produced by 14.4 keV radiation, the exposure time should have been relatively short. Instead, approximately 15 minutes was required to produce any exposure on the film. The requisite long exposure time again suggests that the Laue spots were produced by higher energy photons.

Some elementary x-ray topography was also performed on these crystals. This technique passes x radiation through the crystal at a Bragg angle. The Laue spot then recorded on a film plate is scrutinized as to size and content. If the Laue spot is studied carefully under a microscope, dislocations in the lattice can be seen inside the spot (Fig. 3.3).

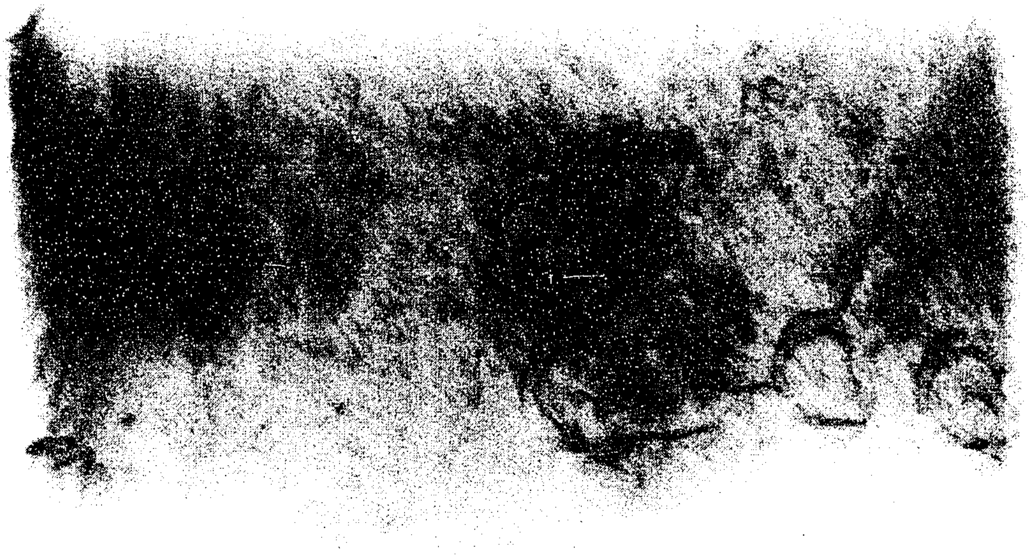

Fig. 3.3 X-ray topography photograph. The "circular" objects in the photograph are dislocations within the lattice structure of the crystal.

Also, if the horizontal and vertical size of the incident beam is known, then the Laue spot should preserve this size if the lattice is "perfect". On the basis of the results of these experimental tests, the Fe crystals were judged to be of poor quality and not worth further study.

The first results obtained with these Fe single crystals (primarily dealing with "time-filtering" studies addressed in the next section) produced some criticism about the lack of knowledge concerning the exact condition of the samples before and after the doping process. Therefore, it was deemed necessary to perform the doping and subsequent testing of the samples in our laboratory, as opposed to having an outside source perform the doping and testing. Since this research required the use of single crystals of high crystallographic perfection (difficult to obtain in Fe), a switch to Ge seemed to be an obvious choice. Additionally, Ge does have a small but observable Mössbauer effect at room temperature, a radioactive parent with a useable half life, and was readily obtainable.

3.3 Ge Single Crystal: Sample Preparation

3.3.1 Origins of the Ge Single Crystals

The Ge single crystals were obtained from several different sources. Two were purchased from Atomerge Inc., one with a (100) orientation (crystal #Ge1) and the other with a (111) orientation (unlabeled). Two others were obtained from National Institute of Standards and Technology (crystals #Ge4 and #Ge5) courtesy of Dr. Richard Deslattes and

Dr. Ernest Kessler. Both of these crystals were (111) orientation. The remainder (crystals #Ge2 and #Ge3) were cut from a boule (100) supplied by Dr. Peter Siddons from the National Synchrotron Light Source at Brookhaven National Laboratory (BNL).

3.3.2 The Cutting Process

Prior to cutting any crystal to a desired orientation, the exact orientation of the crystal must first be known. This is usually done through electronic means instead of Laue back scattering photographs, because the electronic measurements have the potential to be much more accurate. To orient any crystal through electronic means requires performing a series of rocking curves. A rocking curve is a measurement of diffracted intensity as a function of incident angle. The crystal is usually mounted in a holder with the detector located at an angle $2\theta_B$ (twice the Bragg angle), measured with respect to the incident beam direction. The crystal is then rotated through the Bragg angle, about an axis perpendicular to the plane defined by the detector and incident radiation (Fig. 3.4).

For orientation purposes, the crystal samples were mounted in a four-circle goniometer consisting of an Eulerian cradle mounted on a two-circle stage. The entire system was computer controlled through stepper motors, which allowed precision movement and high reproducibility with respect to the angle measurements. The Eulerian cradle allowed a two-axis movement about the axes χ and ϕ. The χ axis is the rotation of the crystal mount about the outside circle of the eulerian cradle. The ϕ axis is a rotation of the crystal mount structure about itself within the cradle circle. The two-circle stage allowed

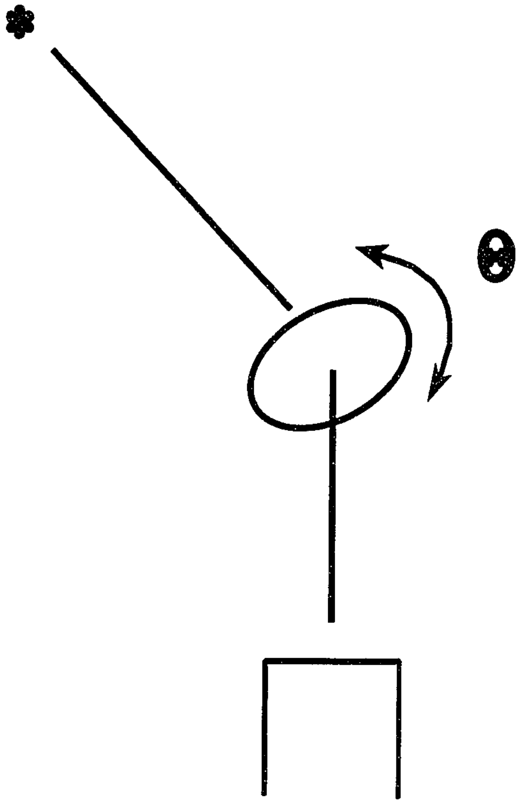

Fig 3.4 Schematic representation of the procedure for measuring a rocking curve. The detector is held fixed while the crystal is rotated about an axis perpendicular to the plane defined by the incident beam and the diffracted beam.

a rotation of the Eulerian cradle and provided an arm for which a detector could be mounted and rotated independently of the cradle axis. (Fig. 3.5).

The Ge boule supplied by BNL was oriented and cut using a device known as a barrel mount[35]. The barrel mount consists of a crystal mount which can pivot in two directions perpendicular to each other, corresponding to a horizontal (χ = 0°, 180°) and vertical (χ = 90°, 270°) adjustment. This allows for dynamic orientation of the crystal face while in the path of the x-ray beam. The barrel holder was held in place in the x-ray goniometer by means of a V-block (Fig. 3.6).

A rocking curve was taken for χ = 0° and the center of the Bragg peak was measured. The barrel holder was then rotated 180° and another rocking curve was taken to find the Bragg peak for this position. The difference between these two Bragg peak positions was calculated, and the crystal was placed at an angle centered between the two. The horizontal adjustment on the barrel holder was then used to adjust the orientation of the crystal such that it produced a Bragg peak at this centered, pre-determined angle. This first step aligned the crystal with respect to the barrel axis in the horizontal plane. In order to align the crystal in the vertical plane, the barrel holder was rotated 90° and the procedure repeated at settings of 90° and 270°. When these two steps were completed, it was possible to rotate the barrel holder about the barrel axis 360° without straying from the Bragg peak. The final result of this procedure was the alignment of the crystallographic axis of the crystal face with the barrel holder axis. With this alignment accomplished, the barrel holder could be transplanted to a diamond saw.

To cut the crystal, an identical V-block was mounted on a diamond saw such that the

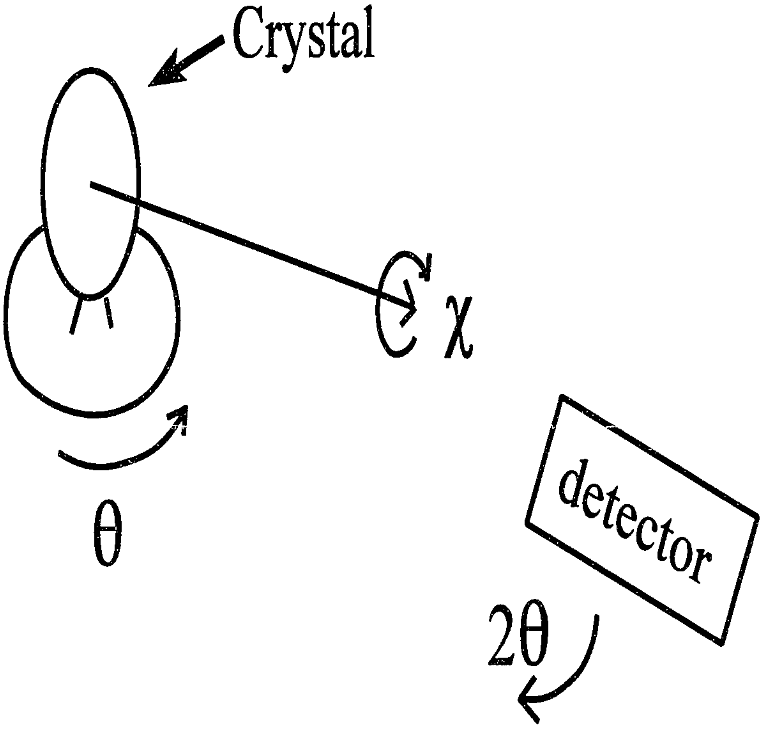

Fig. 3.5 Block diagram defining the angles used on the goniometer. The θ axis corresponds to a rotation about the crystal mount. The χ axis is a rotation about the axis of the crystal face, and 2θ is the angle of the detector.

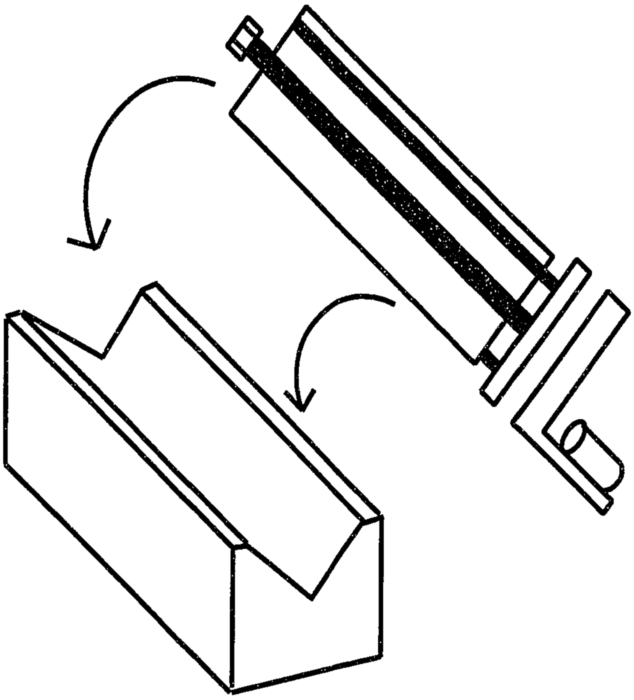

Fig. 3.6 Barrel holder used to orient and cut the Ge single crystals. The barrel holder fits into a V-block that helps keep it stationary during cutting and orientation.

axis of the V-block was perpendicular to the saw blade. The barrel holder was then transplanted from the goniometer V-block to the diamond saw V-block. The resulting cut produced two wafers that were approximately 1 mm thick and oriented with a face axis of (100) (crystals #Ge2 and #Ge3).

To rid the crystal faces of surface damage from the saw blade, 600 grit sandpaper was used to even the affected surfaces. To further smooth the crystals, they were then rubbed with a 1 μm polishing board. The next step was to chemically etch the crystals with a solution of 5% hydrofluoric acid in 95% nitric acid. This etching process was controlled by placing the etching container in a water bath. Continuous agitation was required to minimize any etch pits on the crystal surface. The etching process removed material at a rate of approximately 1 μm per 10 minutes.

3.3.3 Alignment

The single crystals were aligned in the goniometer much the same way they were aligned for cutting. Putty was used to hold the wafer was held in place on the goniometer head. The advantage of using putty, over other mechanical means, was the absence of any strain on the crystal lattice. For the horizontal alignment, Bragg reflections from the face of the crystal were measured for χ angles of 0° and 180°. The difference between the two Bragg peaks was compensated for by adding or subtracting half of the difference angle in the ϕ axis. Once this was completed, the crystal was aligned horizontally with respect to the axis of the goniometer.

To align the crystal axis with the goniometer axis in the vertical direction, ideally one would wish to use the χ angles 90° and 270°. However, this was not possible due to interference of the goniometer structure with the detector. Therefore, rocking curves for χ = +/- 15° were measured to complete the vertical alignment. This alternative is acceptable because any difference in the Bragg peak positions would be due to the vertical component only, since the horizontal component had already been adjusted. The difference in the Bragg peaks can be adjusted by rotating the "tip" angle adjustment on the goniometer head.

As a final test of alignment, the crystal was held at the proper Bragg angle and rotated about the χ axis. Once the Bragg peak was observed as the crystal was rotated, the crystallographic axis could be considered aligned with the goniometer axis.

3.3.4 Testing for Borrmann Effect - External X-Ray Source

Once the crystal was aligned in the goniometer, it was possible to test the capability of the crystal to support a Borrmann mode. The testing procedure began with the positioning of the crystal and the detector at the proper θ and 2θ angle, respectively, for Laue diffraction. The crystal was then rotated about the χ axis and the diffracted radiation intensity measured as a function of angle (Fig. 3.7). If the crystal were perfect enough to support a Borrmann mode, an increase in the intensity would occur when the diffraction planes were rotated into proper alignment. For crystal #Ge5, using Mo K_α x-rays at 17 keV for a (220) reflection, the Bragg angle is 10.25°. Since this crystal had a three-fold symmetry axis about the (111) axis, it should have produced six peaks as the crystal was

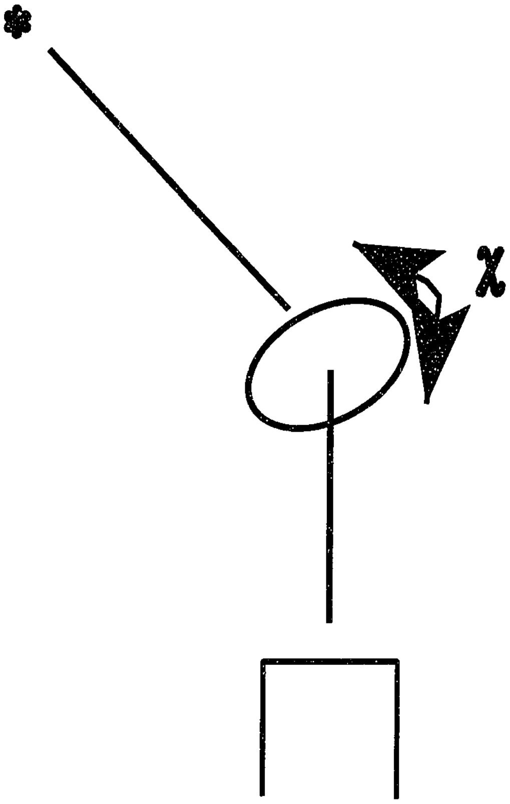

Fig. 3.7 Scan about the χ angle to search for Borrmann transmissions. The crystal is oriented in the Laue geometry and rotated about the face axis. As the planes become aligned, the Bragg condition is satisfied, and an intensity peak is recorded in the detector.

rotated 360° about the χ axis. The experimental results are shown in Fig. 3.8. This crystal was approximately 0.55 mm thick, which corresponds to an absorption coefficient of $\mu t=15$ (for 17 keV radiation). Therefore, calculating the decrease in intensity due to electronic absorption,

$$\frac{I}{I_0}=e^{-\mu t}=3\times10^{-7}$$

little to no radiation should have been able to propagate through the crystal. However, as the experimental results clearly show peaks in the χ scan, the Borrmann mode was observed in crystal #Ge5. Similar results were obtained with each of the other Ge crystals tested. Thus, we can say that all of our samples were perfect enough to support the Borrmann effect.

3.4 ^{73}As Doped Ge Single Crystal Source Preparation

Prior to this work, ^{73}As had not been electroplated onto a Ge crystal. Experimentation was done to determine such a possibility. Nickel was first electroplated onto Ge as a proof of principle experiment to show that elements could be electroplated onto Ge surfaces. Next, natural As was used and was also successful. Since natural As could be electroplated onto a Ge surface, there was high confidence that the radioactive As would electroplate equally as well.

The optimal thickness for observation of the Borrmann mode in the Ge crystals for the 13.26 keV gamma ray was calculated to be 0.5 mm. Since most of our crystals were on

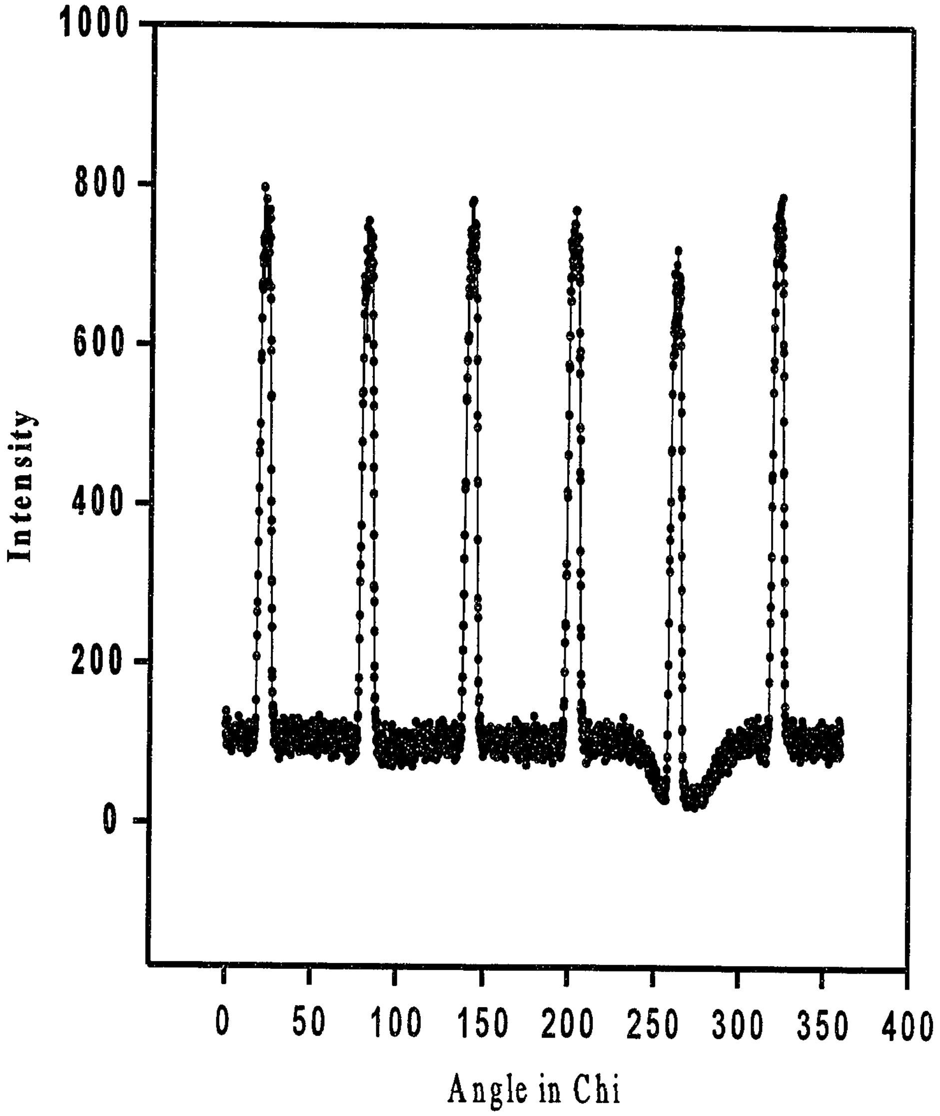

Fig. 3.8 Borrmann scan of the Ge (111) crystal showing the three-fold symmetry axis.

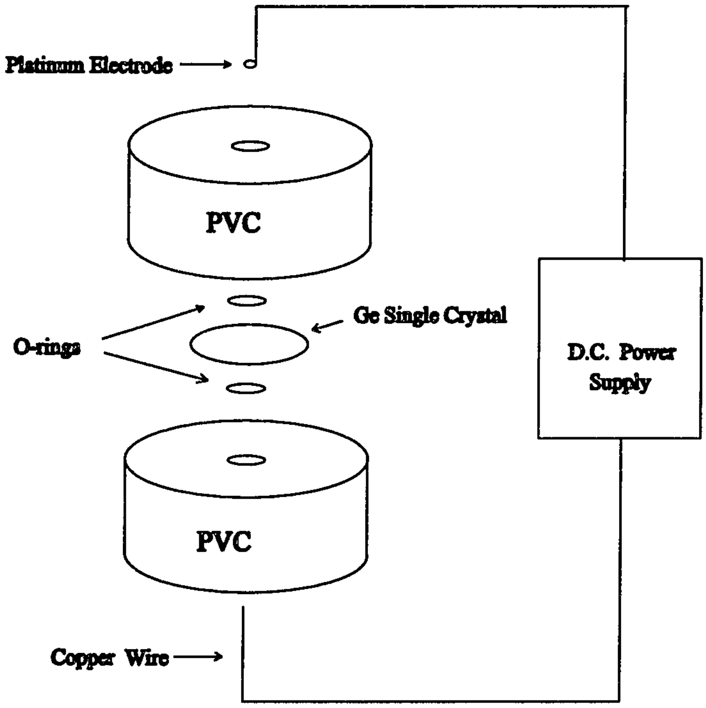

Fig. 3.9 Schematic of the electroplating cell used to apply radioactive ^{73}As onto the Ge single crystal.

the order of 1 mm, thinning was required. This thinning was accomplished by etching the crystal in 10% HF in 90% HNO_3 for 20 minutes intervals. After the etching was completed such that the crystals were of the predetermined thickness, they were placed in an electroplating cell constructed from Polyvinyl Chloride (PVC). The cell consisted of two pieces of PVC round stock with a groove milled about the center of each piece to hold an O-ring. The crystal was placed between the two O-rings and the two sides of the electroplating cell were clamped together. The O-rings served two purposes: the first was to apply even pressure on the crystal to minimize lattice strain during the electroplating process, and the second was to constrain the As solution to a small area on the crystal. A copper electrode was passed through a hole in the bottom piece of the plating cell and placed in contact with the Ge crystal. Another electrode made of platinum, was placed into the plating solution. A schematic representation of the plating cell is displayed in Fig. 3.9.

The As was purchased from Los Alamos National Laboratory and came in a 0.1 M HCl solution. Before plating, the pH of the As solution was adjusted to approximately 10 by adding stock NH_4OH to the As. Once the solution was transferred to the plating cell, a DC power supply was attached to the electrodes and the voltage adjusted until 1 A/cm^2 of current was flowing (for our applications and a plating area of 1/8 inch, the current was 75 mA). The first attempt showed it was necessary to agitate the solution, since bubbles would form between the electrode and the Ge surface and effectively break the current path. This was done by removing the plating solution with a syringe, returning the solution to the stock solution, and then refilling the plating cell with the stock solution. This procedure was repeated until the desired activity was plated onto the Ge crystal. Another effective solution was to taper the opening of the hole in which the solution was placed, allowing the gas bubbles to escape around the sides of the electrode rather than becoming trapped under the electrode.

The next step was to anneal the As into the Ge crystal. Our first few doped crystals were placed in stainless steel boats with a recess milled in it to accommodate the crystals and leave the surfaces flush with the top of the boats. Next, a stainless steel cover was placed over the Ge crystals masking all of the crystal area except for the As spot. The boats were then placed in a tube furnace and annealed for 1 hour at 100° C in a flowing Hydrogen-Argon atmosphere. The temperature was then slowly ramped up to 800°C at a rate of about 7°C/min. The crystals were held at this temperature for 48 hours and then slowly cooled.

After the annealing process, the source spot on the crystal was covered with a protective coating of an acrylic enamel to keep the activity from flaking off. The crystal was also etched on the "undoped side" to remove any activity that may have found its way to that side during the annealing process. One undesirable outcome of this particular annealing procedure was that just as much activity evaporated off of the surface as was driven into the crystal. A much better approach was to effectively seal the activity inside the crystal. This was accomplished by depositing a thin film of natural Ge over the electroplated radioactive spot and then annealing according to the procedures outlined above to relieve any strains that may have formed in the lattice.

The Ge thin film was deposited on the doped side of the crystal via vapor deposition in an evacuation chamber. The chamber consisted of a bell jar attached to a diffusion and roughing pump system. The natural Ge powder was placed in a tungsten boat with the radioactively doped crystal suspended above the boat. Once a vacuum of less than $5x10^{-6}$ torr had been achieved, the Ge powder was heated to the melting point by passing ~ 10 amp through the tungsten boat. The deposition rate was not measured, as the goal was to simply place a covering over the active spot as opposed to controlling the absolute thickness of the covering. Once the activity on the Ge crystal was completely covered, the crystal was removed from the vacuum deposition chamber, placed in the goniometer, and once again tested for the Borrmann effect.

3.5 ^{73}Ge Decay

The As-Ge decay not only produces the photon necessary for a nuclear Borrmann effect, but also produces other photons that could be instrumental in confirming the alignment of the crystal with respect to the goniometer system. First, As decays to Ge by electron capture. This leaves the Ge in the second excited state along with the release of a germanium x-ray from an electron filling in the hole left by the electron capture. The second excited state decays by emission of a 53 keV gamma ray to the first excited state. This state subsequently decays through emission of a 13.26 keV gamma ray or by internal conversion. Internal conversion occurs when the excited nucleus transfers its energy directly to a core electron and ejects the electron from the atom. The result is an electron with some kinetic energy plus an x-ray formed when the resulting hole is filled by an electron. While only the 13.26 keV gamma ray will lead to a nuclear Borrmann effect, the other photons, specifically the 53 keV photon, verify alignment when detected. Since the 53 keV gamma ray is high enough in energy that the crystal can be approximated by kinematical diffraction, many of the complications of the dynamical theory will not be present.

3.6 Observation of Nuclear Borrmann Effect

A proof of principle experiment was performed, attempting to observe the Laue diffracted 53 keV gamma ray, in order to verify the alignment of the Ge single crystal. Since this photon has a relatively high energy, a Bragg peak in Laue geometry would not necessarily be considered a Borrmann mode. However, a positive result, such as a Bragg peak, would indicate that the crystal was capable of producing a diffraction process with an internal source. To test for this, a rocking curve was measured and the results are shown in Fig. 3.10.

This procedure involved setting the crystal at a fixed angle and rotating the detector about the crystal through an angular range of 0° to 45°. One would expect to see an increase in transmitted intensity as the detector passed through the Bragg peak. No such increase in intensity was observed.

One interesting result of the rocking curve was a decrease in intensity corresponding to an increase in angle. The decrease in intensity corresponded to an increase in the amount of material through which the radiation had to travel as the angle increased, causing a larger absorption coefficient. This suggested that the radiation reaching the detector had to traverse through the crystal. While a diffracted peak was not observed, the rocking curve results implied that the majority of the activity on the Ge crystal was concentrated on one side; i.e.,

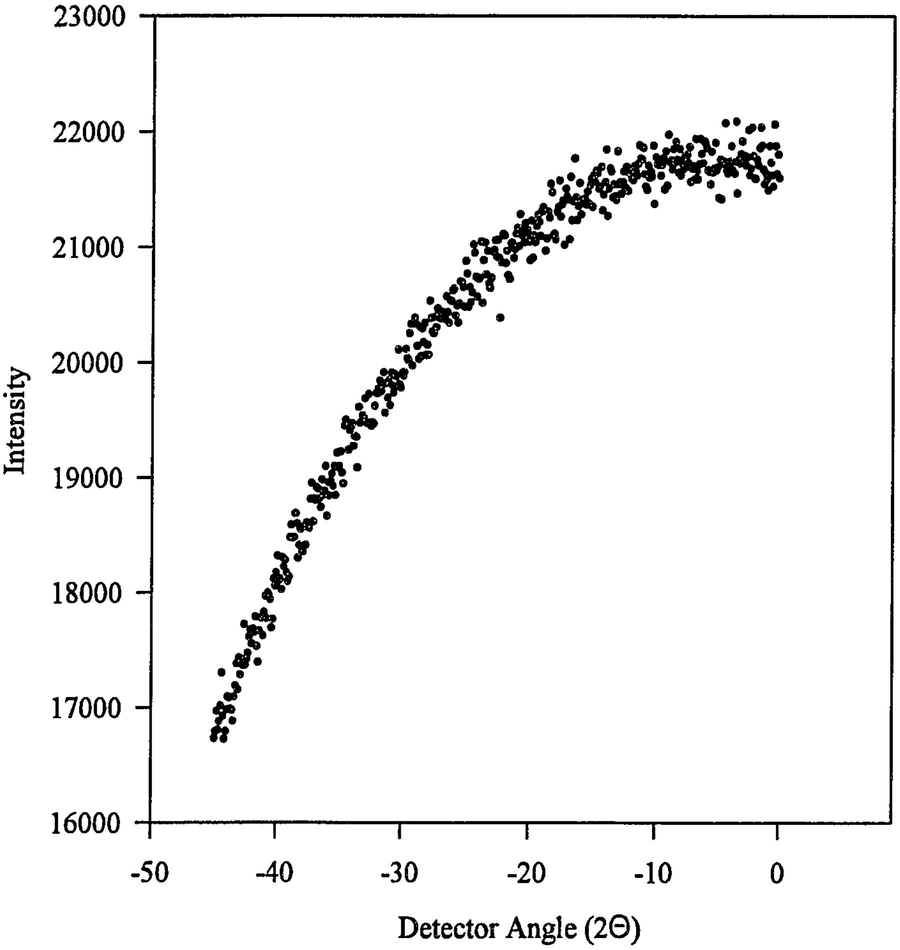

Fig. 3.10 Laue scan of the transmitted 53 keV radiation for a Ge (111) crystal. A Bragg peak is expected at 3.35°. No peak is present, however the shape suggests the radiation had to traverse the crystal since at larger angles the radiation had more material to travel through.

no contamination on the undoped side. If the undoped side was contaminated, the radiation would have produced a flat background.

Another possible photon to study was the 10 keV x-ray produced from the internal conversion process in the Ge decay. These experiments were not expected to produce any discernible results, because the internal conversion process is not the sole source of Ge x-rays. As stated earlier, there are also x-rays produced from the electron capture and from photo ionization. Subsequent rocking curves confirmed this suspicion.

The actual nuclear Borrmann effect in Ge comes from the only gamma ray present in the decay capable of supporting the effect, the 13.26 keV gamma ray. Similar rocking curves to the ones described above were performed in an effort to observe the 13.26 keV emission. Due to the high internal conversion coefficient, the count rates were extremely small, on the order of 0.1 counts per second. In order to obtain statistically significant data, long observation times were required. The results of the summed rocking curves are shown in Fig. 3.11.

There is no obvious peak in the scan shown. Some possible explanations are: 1) poor signal to noise, 2) insufficient activity, and 3) insufficient diffusion of the activity into the crystal. The poor signal to noise problem could be eliminated by discriminating on the detected radiation through polarization. This was not done due to insufficient equipment to perform these measurements.

As for the problem of insufficient activity, the typical count rates achieved during the Borrmann scans were on the order of 1/10th of a count per second. This dismal rate could be increased simply by putting more activity into the crystal. Most of the crystals prepared

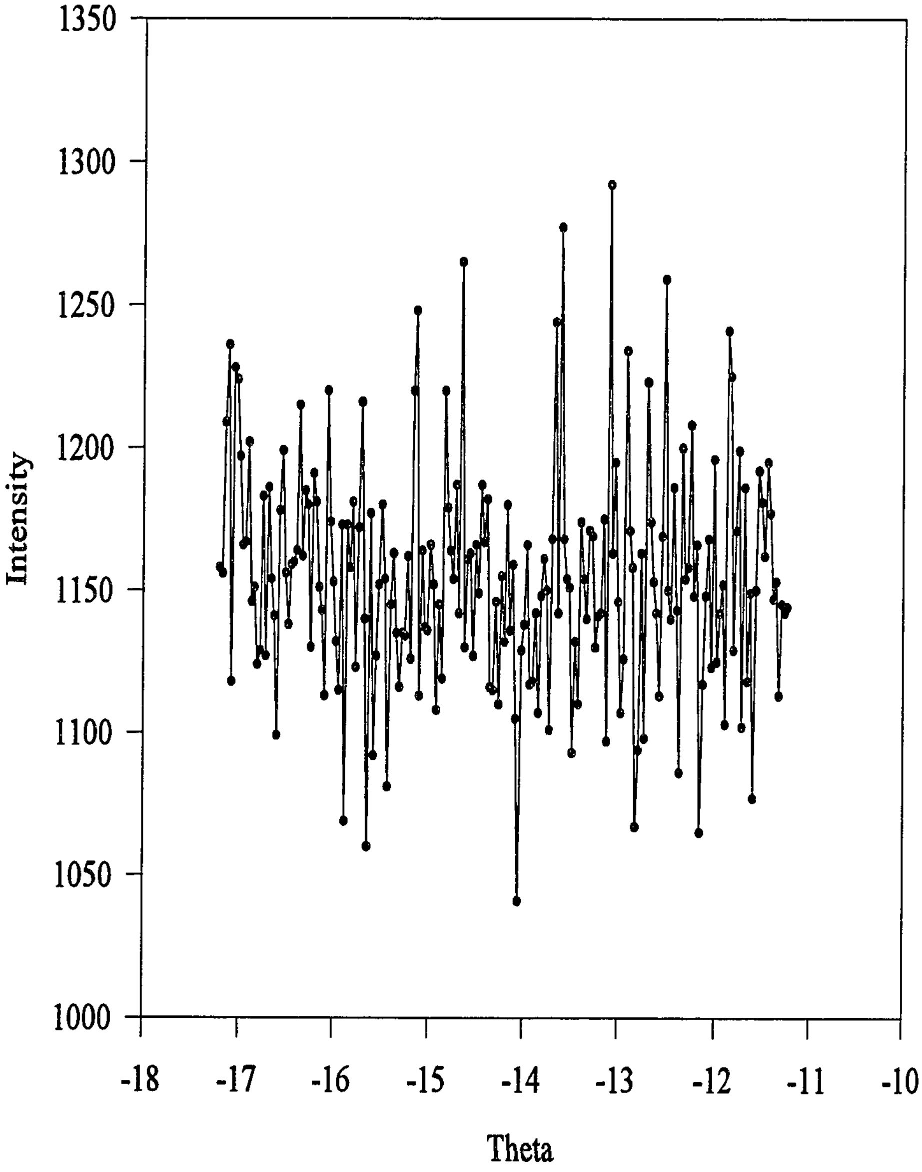

Fig. 3.11 Borrmann scan of the 13.26 keV gamma ray. A peak should occur at 13.52°. No peak is present which may be due to the small signal to noise ratio.

in our laboratory were plated with about 1 mCi. This was due to the limited quantities that were accessible. If the activity were increased, the signal to noise ratio would increase.

To verify the diffusion of activity into the crystal, a standard Mössbauer experiment was performed using the doped crystal with an enriched Ge absorber. After one month of collecting data, no Mössbauer effect was observed. Normally, this would lead to the conclusion that the activity had not sufficiently diffused into the crystal. However, the Mössbauer effect in Ge is very difficult to observe. Extreme care must be taken to ensure that the source and absorber are magnetically shielded and all external vibrations have been eliminated. The size of the Mössbauer effect in Ge is approximately 4% using an enriched absorber[36]. Comparing ^{73}Ge to ^{57}Fe, Ge has a resonance cross-section approximately three orders of magnitude smaller than Fe. Due to the long lifetime of the first excited state in ^{73}Ge, a very narrow resonance line width is produced. The earth's magnetic field is strong enough to de-tune the source and absorber by one line width, thus magnetic shielding is required. Additionally, with such a small resonance line-width, minute relative vibrations can easily cause the source and absorber to shift off resonance.

Mu metal was used around the Mössbauer drive to attempt to negate the earth's magnetic field. The Mössbauer transducer was also mounted on a 6,000 lb. granite slab to eliminate vibrations. To calibrate the transducer and to test the stability at a very low velocity, a Mössbauer spectrum was taken using a ^{57}Co in Pd source and an enriched ^{57} Fe foil. Since the Mössbauer parameters are well known for this combination, the velocity of the drive could be easily calibrated.

Next, a single-line ^{57}Co in Rh source and an enriched ^{57}Fe in Rh absorber was used.

The drive velocity was held at the same setting (approximately ten millimeters per second) and a Mössbauer spectrum recorded. From this measurement, the pertinent parameters for the source and absorber were obtained; namely the isomer shift between the source and the absorber, the width of the resonance line, and the thickness of the absorber.

Finally, the drive velocity was lowered until the width of the ^{57}Fe in Rh line spanned the entire velocity range. This width, having been determined through the experiments described above, allowed a re-calibration of the drive at these lower velocities. With the lower drive velocities established and proven to be relatively stable, it was possible to run the transducer at the speeds necessary to observe the Mössbauer effect in ^{73}Ge. The smallest velocity obtainable was approximately ±100 μm/sec. The absorber being used had a resonance line width of approximately 15 μm/sec. On the scale being used on the velocity transducer, this would correspond to a measured width of approximately 7 channels on the multi-channel scaler.

The calibration procedure above shows that our system was just capable of measuring the ^{73}Ge Mössbauer. However, the parameters used above were for a "best" case scenario. In reality the Mössbauer resonance is some what more difficult to observe.

3.7 Concluding Remarks

The sought for nuclear Borrmann effect was not observed in ^{73}Ge. The effect may still be observable, if a polarizing crystal is used to discriminate against the background noise. Additionally, the activity introduced into the crystal must be increased by a factor of ten. The position of the activity must also be determined through standard Mössbauer techniques. This would entail the use of a Mössbauer spectroscopy system specifically designed for the ^{73}Ge resonance.

A more likely candidate for successful observation of the nuclear Borrmann effect would be some type of Fe crystal. As stated earlier, Fe crystals are generally known to be of poor quality. The move toward Ge crystals was meant to solve the quality issues with Fe crystals. However, if 3% silicon is added to Fe, much of this problem is said to be eliminated[37]. Also, as the Mössbauer effect is an essential criteria for generating a nuclear Borrmann mode, Fe is more attractive than Ge due to its large Mössbauer effect.

Chapter Four

Time Filtering

4.1 Introduction

The time dependence of radiation traveling through a nuclear-resonant material was first described analytically by Hamermesh[38] in 1960. This theory of the so-called "time-filtering effect" treats the absorber as a collection of damped oscillators with a natural frequency of ω_0, and a decay constant of $1/\tau$, where τ is the mean lifetime of the excited state. As the radiation travels through this medium, each Fourier component is phase-shifted and attenuated differently. Upon emergence from the absorber, the radiation has undergone a shift in frequency space. Heuristically, this can be thought of as a Lorentzian line-shape incident upon an absorbing medium. As the radiation propagates through this medium, the line-shape is preferentially absorbed at the center and not at the wings. After leaving the medium, the line-shape is shorter and broader than the original shape. From the time energy uncertainty principle, this broadening of the line width signifies a decrease in the lifetime. Thus, a "speed-up" in the decay will be observed.

4.2 Theoretical Considerations

The quantitative description of time-filtering, now referred to as time-domain Mössbauer spectroscopy is a classical frequency response problem. The treatment considers the source radiation in the frequency domain. A medium response function "operates" on the input signal and produces an output signal in the frequency domain. The medium response function is an exponential function that has both a real and complex exponent to allow for modification of the phase and amplitude of each Fourier component of the input signal[39].

$$a_{output}(\omega) = F(\omega) a_{input}(\omega) \tag{4.1}$$

where F(ω) is the dispersive medium response function. The transmitted intensity as function of time is obtained by taking absolute value squared of the Fourier transform of $a_{output}(\omega)$.

4.3 Mathematical Description

Determining the transmitted intensity in time-domain Mössbauer spectroscopy is a relatively straightforward calculation. The basic method is borrowed from classical dispersion theory by Hamermesh et al.[40] and is outlined below. The incident radiation, which in this case is from a radioactive source, is considered to be a damped oscillator with a natural decay time of τ. Mathematically, this radioactive source term can be written as

$$a(t)=e^{(i\omega_0-\frac{1}{2\tau})t} \tag{4.2}$$

where ω_0 is the natural frequency of the transition. This amplitude can be re-expressed as the Fourier transform of an amplitude that is a function of frequency (Eq. 4.3). This is important because, as stated above, it is the frequency components that are modified as the radiation propagates through the medium.

$$a(t)=\frac{1}{2\pi i}\int_{-\infty}^{+\infty}d\omega\frac{e^{i\omega t}}{\omega-\omega_0-\frac{i}{\tau}}=\int_{-\infty}^{+\infty}d\omega a(\omega)e^{i\omega t} \tag{4.3}$$

The medium is given a dispersive nature by allowing the dielectric constant to be a complex quantity. This can be written as

$$\epsilon(\omega)=1+\frac{r}{(\omega_0^2-\omega^2+i\frac{\omega}{\tau})} \tag{4.4}$$

where ω_0' is the resonant frequency of the absorber (taking into account any possible isomer or second-order Doppler shift), ω is the frequency of the incoming radiation, and τ is the mean lifetime of the excited state.

The propagation vector in the medium can be written as $k=(\omega/c)\epsilon^{1/2}$. If the equation for ϵ from above is inserted in this expression for the propagation vector k, the following expression for the wavevector is obtained

$$k=\frac{\omega}{c}[1+\frac{r}{(\omega_0^2-\omega^2+i\frac{\omega}{\tau})}]^{1/2}. \tag{4.5}$$

For the case of gamma rays, the frequency is on the order of 10^{18} Hz. This allows for an expansion of the above equation. Performing a Taylor series expansion and keeping only the first term, the wavevector can be substituted into the medium equation.

The exponential equation for the medium, including dispersion, can be written as follows:

$$a'(\omega) = a(\omega)e^{ikd} \tag{4.6}$$

Substituting for the wavevector k, this becomes

$$a'(\omega)=a(\omega)\exp\{-2ib\omega[\omega_0^2-\omega^2+i\frac{\omega}{\tau}]^{-1}\} \tag{4.7}$$

where b is the defined as

$$b=\frac{Nf\sigma_0 d}{\lambda}$$

Here, b is related to the nuclear attenuation coefficient. In this equation, N is the number of nuclei per volume, f is the recoilless fraction, λ is the decay constant, σ_0 is the nuclear resonant cross section, and d is the thickness of the absorber.

To determine the time dependent amplitude of the transmitted radiation, the equation for transmitted frequency dependent amplitude is Fourier transformed according to Eq. 4.1.

$$a'(t)=\frac{1}{2\pi i}\int_{-\infty}^{+\infty} d\omega \frac{e^{i\omega t}}{\omega-\omega_0-\frac{i}{2\tau}} \exp[\frac{2ib\omega}{\omega^2-\omega_0^2-i\frac{\omega}{\tau}}] \tag{4.8}$$

This integration is performed most easily in the complex plane. The results include a summation over Bessel functions that converge differently relative to the amount of detuning between the source and the absorber. These results are given below.

$$a'(t)=\exp[i\omega' t-\frac{t}{2\tau}]\sum_{n=0}^{\infty}[\frac{i(\omega_0-\omega_0')}{b}]^n(bt)^{\frac{n}{2}}J_n(2b^{½}t^{½}) \qquad (4.9)$$

or

$$a'(t)=\exp[i\omega' t-\frac{t}{2\tau}]\{-\exp i[\frac{b}{(\omega_0-\omega_0')}+(\omega_0-\omega_0')t]\sum_{n=0}^{\infty}(\frac{ib}{\omega_0-\omega_0'})(bt)^{-n/2}J_n(2b^{½}t^{½})\} \qquad (4.10)$$

The transmitted time dependent intensity is found by computing the absolute value squared of the amplitudes. To further simplify the expressions, it is convenient to write the detuning factor, ω_0-ω_0'=$\Delta\omega$, and the nuclear resonance thickness parameter, β=4b/λ. The results for the two amplitudes are given below.

$$|a'(t)|^2=e^{-T}|\sum_{n=0}^{\infty}[i\frac{4}{\beta}\Delta\omega\tau]^n[\frac{\beta T}{4}]^{n/2}J_n(\beta^{½}T^{½})|^2 \qquad (4.11)$$

$$|a'(T)|^2=e^{-T}|-\exp i[\Delta\omega\tau T+\frac{\beta}{4\Delta\omega\tau}]+\sum_{n=0}^{\infty}[i\frac{\beta}{4\tau\Delta\omega}]^n[\frac{\beta T}{4}]^{-n/2}J_n(\beta^{½}T^{½})|^2 \qquad (4.12)$$

For large values of the detuning factor $\Delta\omega$, Eq. 4.11 converges very slowly. In such cases, the second equation should be used. Mathematically, the convergence criteria can be written as follows. If

$$\frac{2}{\beta}\frac{\Delta\omega}{\lambda}(\beta T)^{1/2} < 1 \tag{4.13}$$

is true, then Eq. 4.11 should be used. If

$$\frac{2}{\beta}\frac{\Delta\omega}{\lambda}(\beta T)^{1/2} > 1 \tag{4.14}$$

is true, then Eq. 4.12 should be used.

4.4 Example Curves

A few examples for different values of the nuclear thickness parameter, β, and the detuning factor, Δω, are shown to illustrate some of the characteristics of the time dependent intensity of the transmitted gamma radiation. For small values of β (approximately = 1), the timing curve departs from the natural decay exponential. Such a case is shown in Fig. 4.1. For large values of β (approximately = 10), the Bessel functions tend to dominate the intensity and cause a "beating" effect in the spectrum. Mathematically, this is due to the Bessel function actually going to zero at some time greater than t=0. Heuristically speaking, as the lineshape propagates through a very thick crystal and gets absorbed at the center, the lineshape can get "eaten out" in the center and form a pseudo-two peak line shape. These two peaks are then coherently added and beat against one another in time. One such curve is shown in Fig. 4.2.

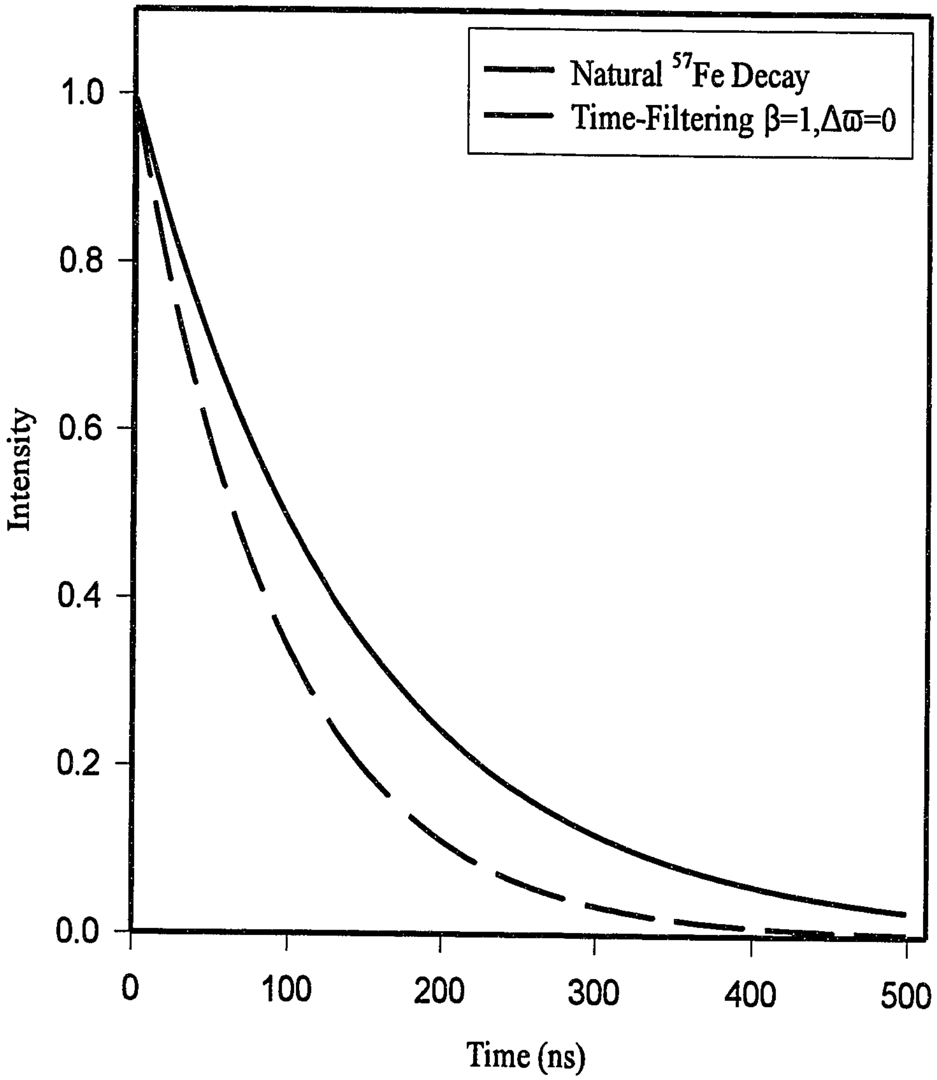

Fig. 4.1 Time-filtering curve for $\beta=1$ and $\Delta\omega=0$. The solid line is the natural ^{57}Fe decay.

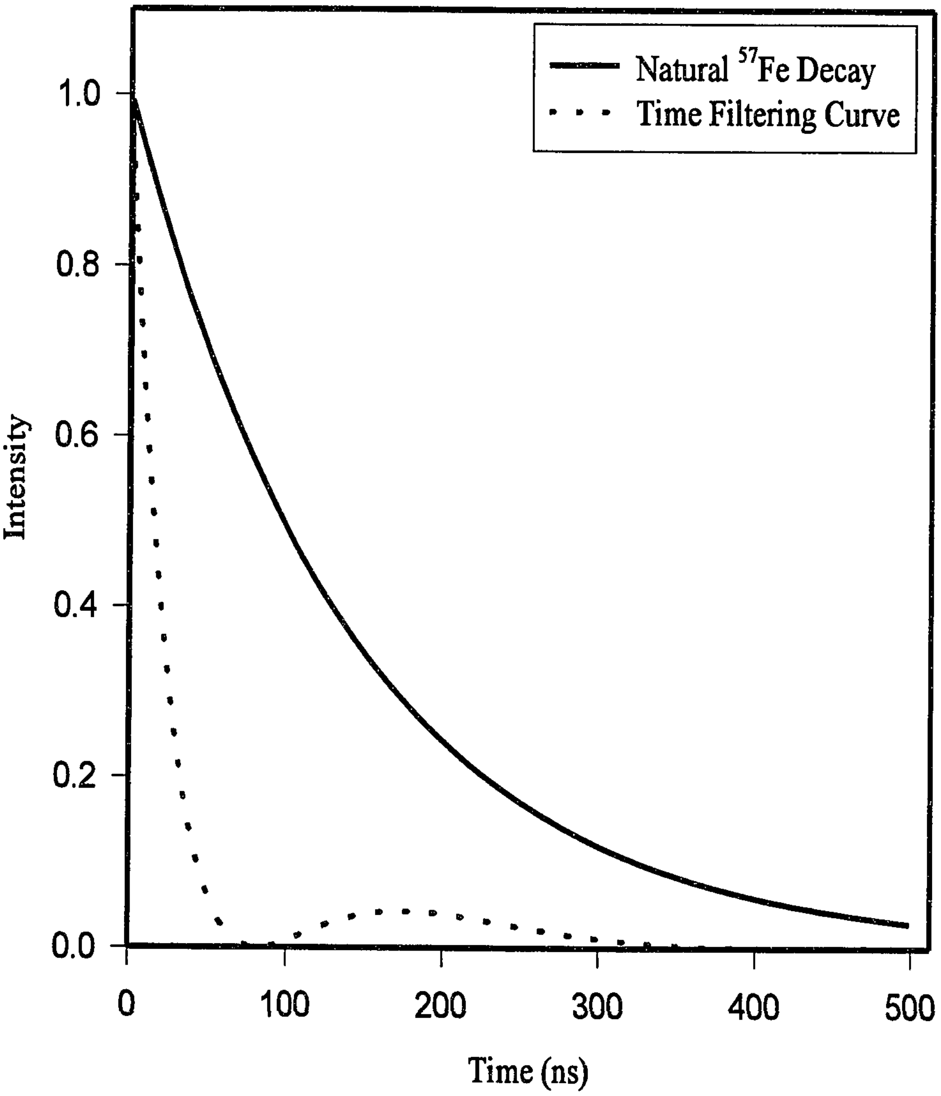

Fig. 4.2 Time-filtering curve for $\beta=10$ and $\Delta\omega=0$. The solid line is the ^{57}Fe natural decay.

Large values of the detuning factor cause the intensity to oscillate about the normal exponential decay (Fig. 4.3). This is a surprising result showing that, at certain times, more radiation exists after traveling through the absorber than would exist if the absorber were not present. As the detuning factor is increased, the time dependent intensity oscillates with shorter and shorter times, so that ultimately this behavior approaches the natural exponential decay.

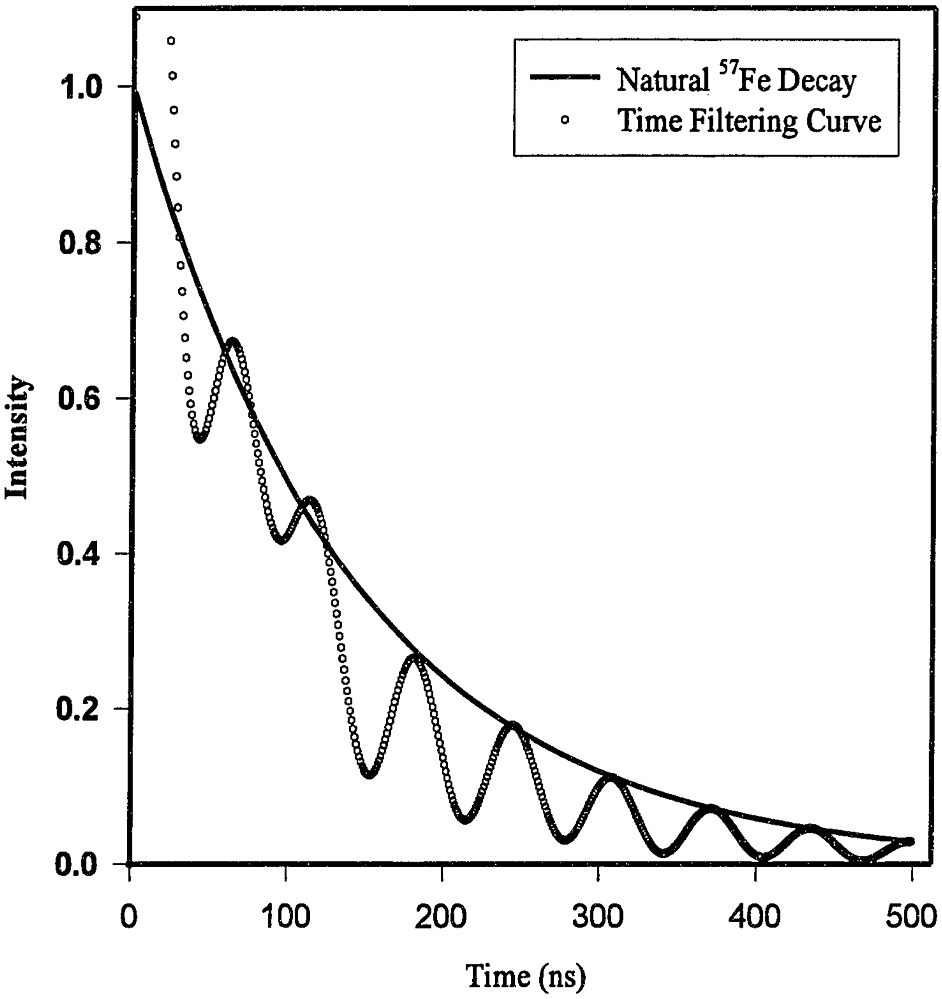

Fig. 4.3 Time-filtering curve for β=10 and $\Delta\omega$=7. The solid line is the ^{57}Fe natural decay. The time-filtering curve oscillates about the exponential curve. Notice that at very early times, more radiation is present when a filter is in place that would be if the filter were not present.

Chapter Five

Experimental Time Filtering

5.1 Introduction

The effort to observe time-filtering of gamma radiation was concentrated on two isotopes, namely ^{73}Ge and ^{57}Fe. The ^{73}Ge was used since this was the focus of the Borrmann effect studies. A positive observation of time-filtering in our samples could be used to distinguish between a Borrmann mode and background noise since any radiation traveling through the thick crystal had to traverse nuclear resonant material, thus undergoing time-filtering effects. The ^{57}Fe was studied because of the large Mössbauer effect this isotope is known to exhibit. By studying time filtering in ^{57}Fe, some basic background knowledge could be gained that could later be applied to the ^{73}Ge case.

In both ^{73}Ge and ^{57}Fe, the parent nuclei can decay through a gamma-gamma cascade. This is very conducive to timing experiments, since in both cases a precursor event allows for the exact determination of the formation of the level of interest. For example, ^{57}Co decays to ^{57}Fe through electron capture leaving ^{57}Fe in the second excited state. This second excited state can decay in one of two possible branches. The first possibility is a transition directly to the ground state through the emission of a 136 keV gamma ray. The isotope will decay through this branch only 10% of the time. The other path of decay is the one of interest. This branch of decay produces a 122 keV photon associated with a transition from the second excited state to the first excited state. The first excited state will then decay to the ground state. This last transition also has two possible modes of decay. The first is by emission of a 14.4 keV gamma-ray. This is the well know ^{57}Fe Mössbauer transition. The second mode of decay is the process of internal conversion. When in the excited state, it is possible for the nucleus to give all of its energy directly to a core electron. The result is an ejected electron with a kinetic energy equal to the energy of the excited nuclear level minus the binding energy of the electron. Additionally, an x-ray will be emitted due to the filling of the hole, created by the internal conversion process, by an outer shell electron. A schematic of the ^{57}Co-^{57}Fe decay is shown in Fig. 5.1.

For the ^{73}As-^{73}Ge case, the situation is much the same. A schematic of the decay is displayed in Fig. 5.2. ^{73}As decays to ^{73}Ge by electron capture. This also leaves ^{73}Ge in the second excited state. The photon emitted when the nucleus makes a transition to the first excited state is 53 keV. Again, as with the ^{57}Fe case, the first excited state has the same two modes of decay: gamma-ray emission or internal conversion. The energy of the first excited state is 13.26 keV. The most dramatic difference between the ^{57}Fe and ^{73}Ge case is the value of the internal conversion coefficient (α) which is the ratio of internal conversion events to gamma-ray emission events. For ^{57}Fe every one out of nine transitions of the first excited state is through gamma emission (α=8). For ^{73}Ge, the ratio is much worse, approximately one out of every 1310 (α=1309). Obviously, observing the gamma ray in the Ge is case

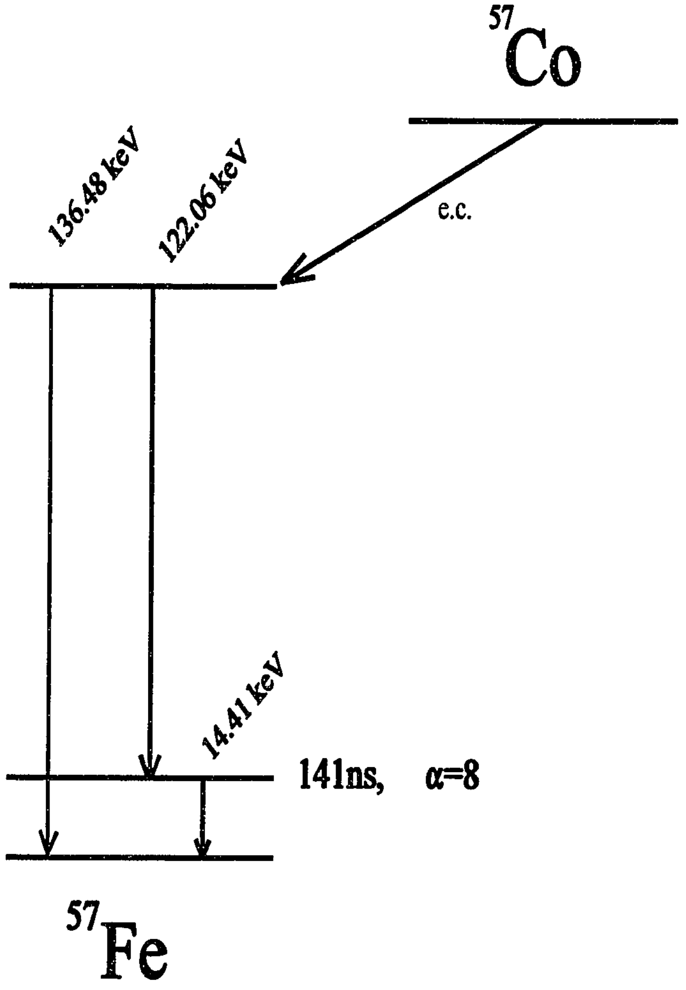

Fig. 5.1 Schematic diagram of the ^{57}Co-^{57}Fe decay.

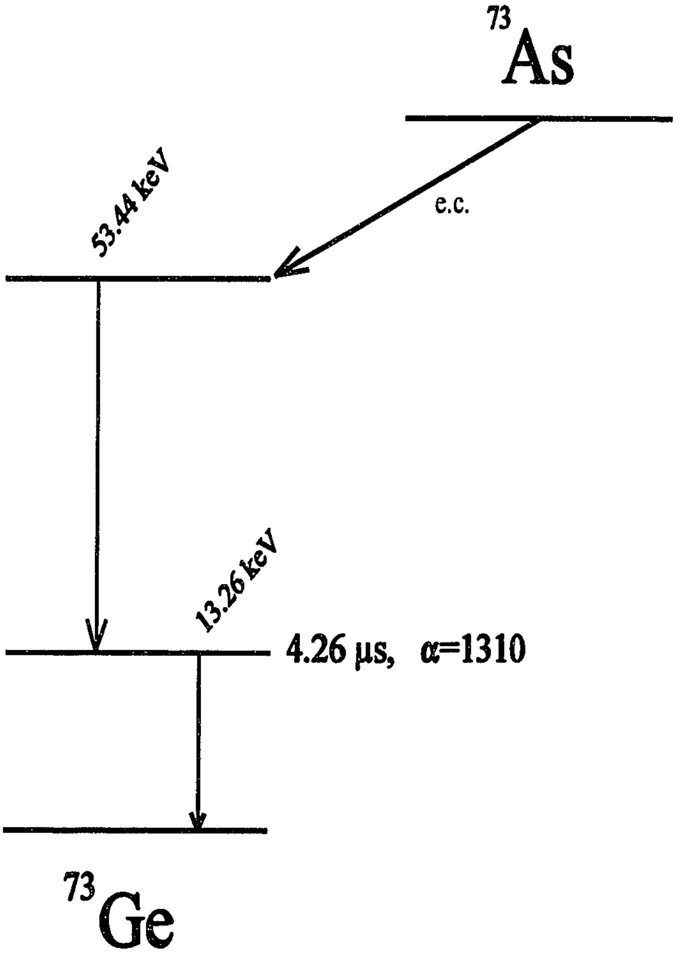

Fig. 5.2 Schematic diagram of the ^{73}As-^{73}Ge decay.

more difficult, purely from a statistical standpoint. An illustration of this point is readily observable in a pulse-height spectrum. Fig. 5.3 shows the K_α and K_β x ray photo peaks at 9.88 keV and 10.98 keV respectively. Only if this same pulse-height spectrum is drastically enlarged (Fig. 5.4), can the 13.26 keV gamma-ray be observed.

5.2 Experimental Setup

In both the ^{73}Ge and ^{57}Fe cases, the first gamma-ray in the cascade signifies the formation of the first excited state. This photon strikes a detector and produces a pulse which is then amplified using a standard spectroscopy amplifier. To discriminate in terms of energy, a timing single channel analyzer (SCA) is used to set an energy window about the desired photo-peak. The output of the SCA, which is a fast negative NIM spike, is used as the start signal for a time-to-amplitude converter (TAC). The subsequent detection of the photon emitted by the first excited state is processed in the same manner, and becomes the stop signal in the TAC. The output of the TAC is a unipolar pulse whose height is proportional to the time difference between the start and the stop pulses. This output is subsequently recorded on a multichannel analyzer (MCA). A diagram of the experimental set-up is shown in Fig. 5.5.

Originally, both detectors were NaI because of the reasonably fast (approximately 1 ns resolution time) timing characteristics associated with these types of detectors. It was found that better energy resolution was required in order to discriminate the photo-peak from the background noise. As a result, one of the detectors (the low-energy side) was replaced

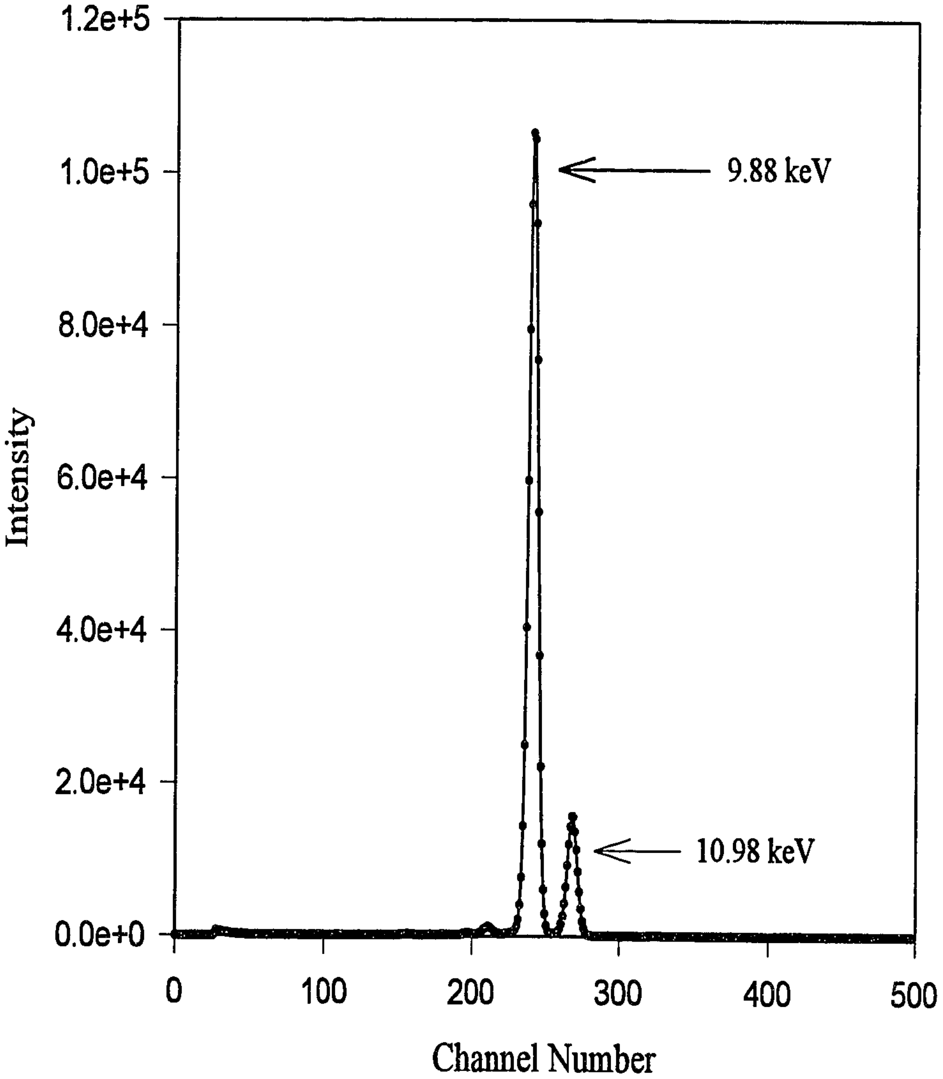

Fig. 5.3 Pulse-height spectrum of ^{73}Ge showing the K_α and K_β x-ray peaks.

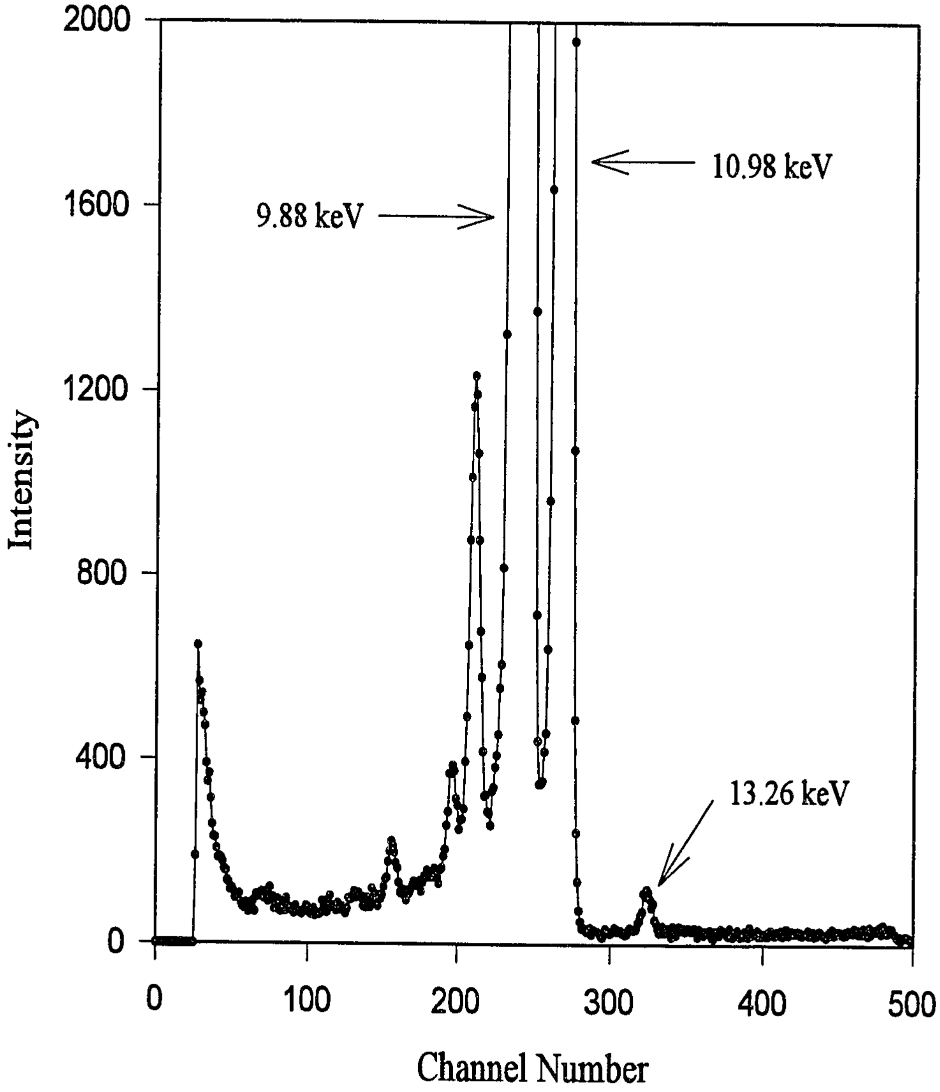

Fig. 5.4 Pulse-height spectrum showing the 13.26 keV ^{73}Ge gamma ray.

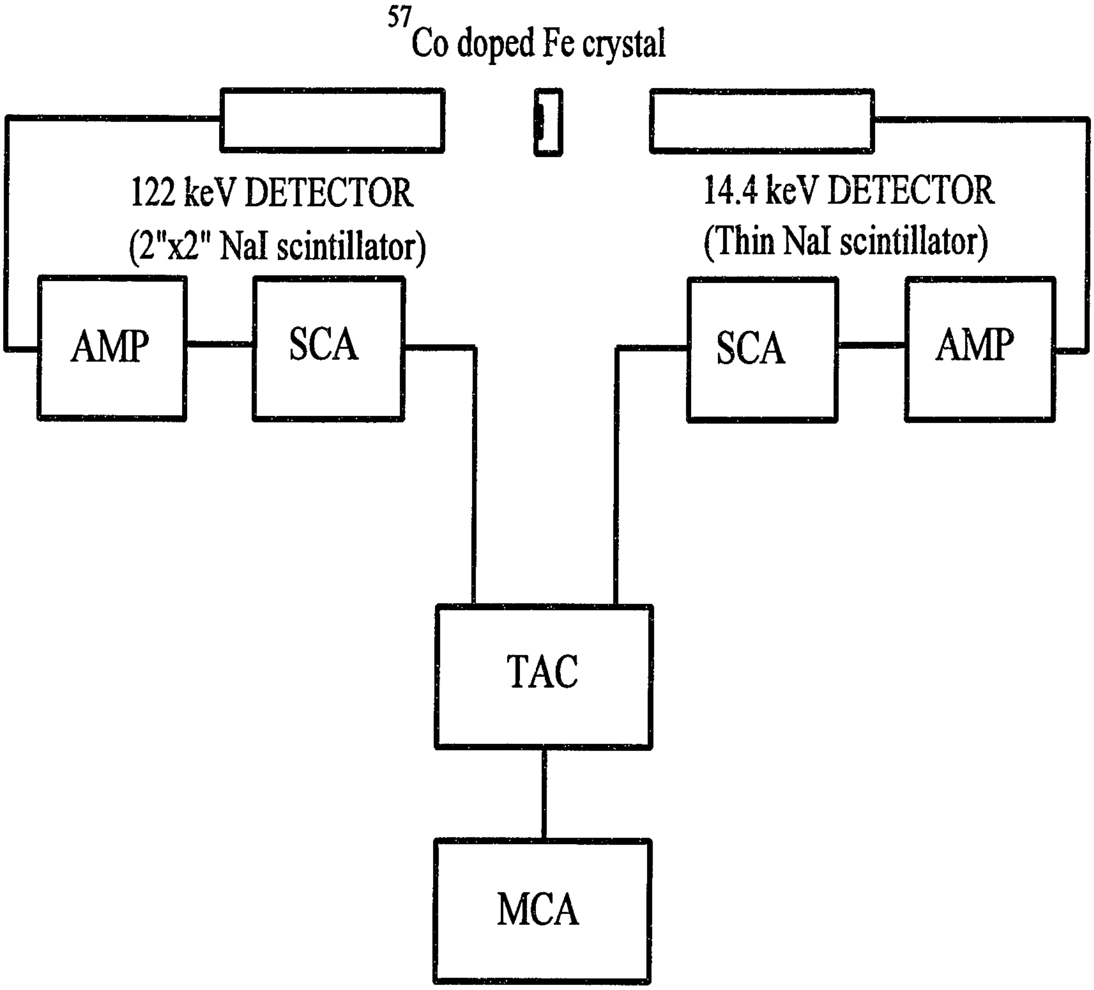

Fig. 5.5 Schematic of the coincidence setup. For some cases, the low energy side of the circuit used a Ge solid state detector instead of a NaI detector.

by a Ge solid state detector. These detectors are known to be slower that NaI because of the longer pulse collection time inherent with solid state detectors.

Adding the Ge solid state detector in one branch of the coincidence circuit would make the timing resolution of the system worse, so special care was taken to reduce the timing characteristics within other parts of the circuit. A series of natural ^{57}Fe lifetime curves were recorded while changing components within the coincidence apparatus. This was done in order to find the slowest component within the circuit. No single component was found to make a significant impact on the timing resolution. Experimentally it was found that the most efficient way to improve the timing resolution and maintain acceptable energy resolution was to simply reduce the shaping time of the amplifiers to their lowest possible setting while using the Ge solid state detectors.

In some cases it was necessary to invert the inputs for the TAC. This is a much more efficient way to run the system when the "normal" stop count rate is much smaller than the start rate. If the input was connected in the normal manner during this situation, the spectroscopy system would miss some coincidence counts. For example, a start may initiate the TAC sweep with no valid stop to follow. In the ^{73}Ge case, if a 53 keV photon starts the TAC sweep, it may run to the end of the time scale before a 13.26 keV photon is detected, as there are far fewer 13.26 keV photons being emitted from the source. During this sweep, a true coincidence gamma-gamma pair may be emitted. Since the TAC was already started by another event, however, the event will either be missed or (if the 13.26 keV photon is collected and stops the system) an uncorrelated coincidence (accidental coincidence) will be generated. This will either increase the dead time of the system (when a valid stop is not generated) or will simply add to the background of the spectrum (when an uncorrelated stop is generated). To reduce this problem, the inputs are reversed[41]. This ensures that the TAC is started on a 13.26 keV photon, which will always be considered a “good” start.

Reversing the inputs in a delayed coincidence system is very simple process. First the system must be run in the "normal" forward setting such that a timing curve can be generated. This involves setting the delays in each branch of the coincidence circuit properly such that the timing curve is correctly displayed on an MCA (i.e. the zero of the timing curve is displayed on the MCA). This process is done to establish a reference point from which to add an artificial delay into the coincidence circuit. Next, a delay must be added into the normal "start" side of the coincidence circuit. The amount of delay corresponds to the full time scale that is set on the TAC. Then reversing the inputs for the TAC (start to stop and stop to start) will produce a spectrum that runs "backwards", such that time t=0 is on the right instead of the left. During set-up, it is best to add a small amount of delay into the start signal when running in the forward mode, or remove a little delay when running in a reverse mode. This allows some of the accidental background to be recorded for time less than t=0, relative to the coincidence event, so that the background count rate parameter can be easily extracted for the fitting process.

5.3 Fitting and Analysis Procedure

The data were fit using a modified form of the Lynch, Holland and Hamermesh treatment described in Chapter 4. In this theoretical treatment, all of the radiation is considered to be emitted and absorbed recoillessly. In reality there are some recoil contributions that must also be included. The fitting equation used in the program was the sum of two separate contributions. First, there is a contribution from the Lynch, Holland, and Hamermesh time-filtering calculation corresponding to the recoilless events. This portion is weighted by the recoilless fraction *f*. Second, there is a contribution from the source that is emitted with recoil *(1-f)*. By emitting with recoil, the photon energy is diminished by the recoil energy and is therefore not on resonance with the absorber. This component will travel through the absorber and be attenuated by ordinary electronic means. The time characteristics of the radiation reaching the detector from this contribution will be the normal natural decaying exponential. The function used to fit the data is given in Eq. 5.1.

$$I=(f)e^{-\frac{t}{\tau}}\left|\sum_{n=0}^{\infty}[i\frac{4}{\beta}\Delta\omega\tau]^{n}[\frac{\beta T}{4}]^{n/2}J_{n}(\beta^{1/2}T^{1/2})\right|^{2} + (1-f)e^{-\frac{t}{\tau}} \qquad (5.1)$$

Once these pieces are added together incoherently, the sum is convoluted with a gaussian function which represents the resolving time of the system. The convolution is performed by taking the Fourier transform of both functions; the time filtering contributions and the gaussian function using the Fatlung theorem. Next the two Fourier transforms are multiplied together, and the inverse Fourier transform of the result is computed. After the convolution, a constant background is added along with a gaussian function that represents any prompt events that have been recorded as a result of Compton scattering events. To give some idea of how close these simulations are to the actual experimental data, a value of χ^2 is calculated. The FORTRAN source code of the fitting program is given in Appendix B.

The fitted data are given in the following sections.

5.4 Gamma Ray Time Filtering for ^{73}Ge

The sources for the ^{73}Ge time-filtering experiments were made in our laboratory as described in Chapter Three. In order to keep the accidental count rate small, the sources were allowed to age through a few half-lives to decrease the relative activity in the crystal sources. Additionally, the count rate in the stop leg of the coincidence circuit was adjusted (through altering the source to detector distance) such that the count rate did not exceed the inverse of the TAC full scale. If the stop rate were higher than this, statistically the TAC would never be allowed to travel to the full scale before some event would produce a stop pulse. This produces a nonlinear background in the timing spectrum that is difficult to model during analysis. An experiment was performed to show this effect. A pulser was used to start the TAC while a strong radioactive source was used to stop it. Having the two source signal independent of each other ensured that all counts would be accidental and would only produce a background shape. The results are given in Fig. 5.6.

The long life time of ^{73}Ge required the use of a long time scale on the TAC. Unfortunately, this made the coincidence count rates worse than would be expected because the stop count rate had to be adjusted to a very small rate to avoid the clipping problem just discussed.

The absorber used in these timing experiments was an enriched ^{73}Ge single crystal of (111) orientation that was the same absorber used by Loren Pfeiffer in his pioneering

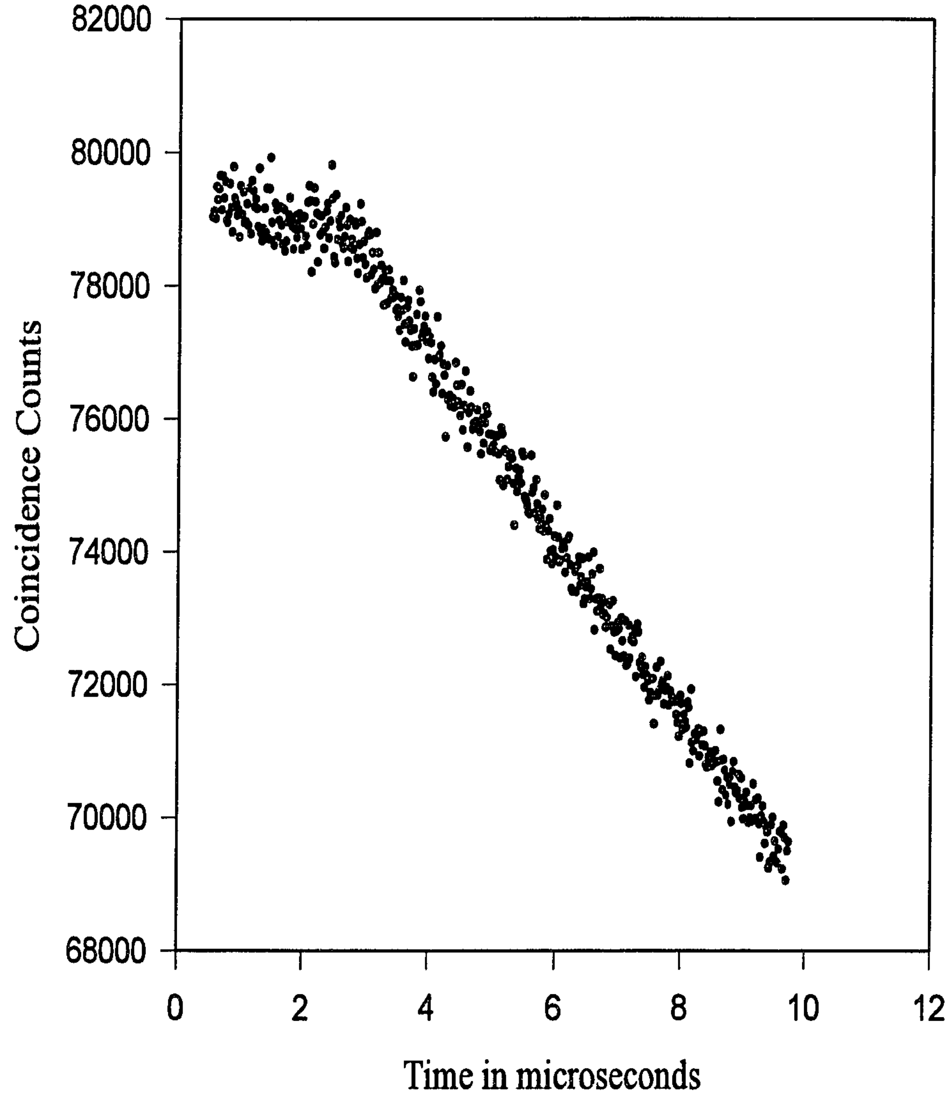

Fig. 5.6 Background shape of coincidence measurements when the stop rate is larger than the inverse of the full scale time range set on the TAC.

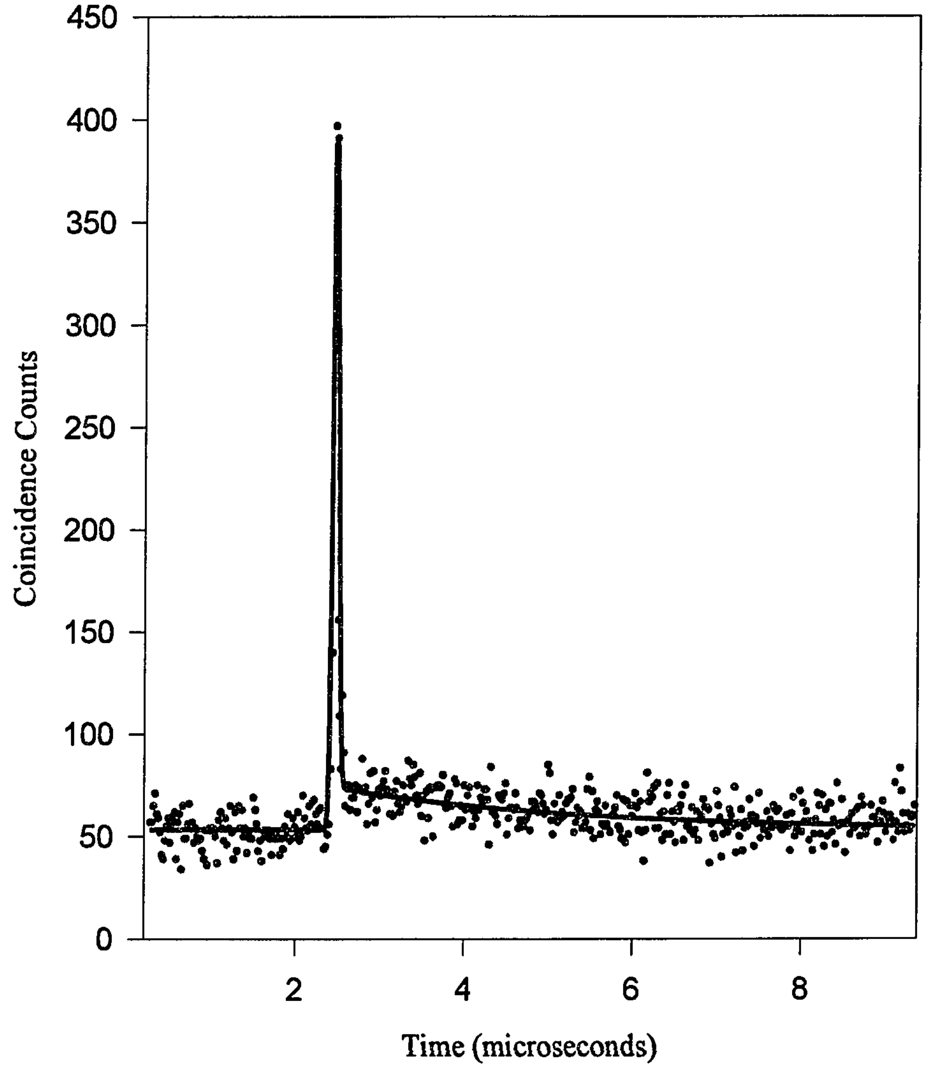

Fig. 5.7 Time-filtering Curve using the 13.26 keV ^{73}Ge gamma ray. The count rate is exceedingly poor partially due to the high internal conversion coefficient.

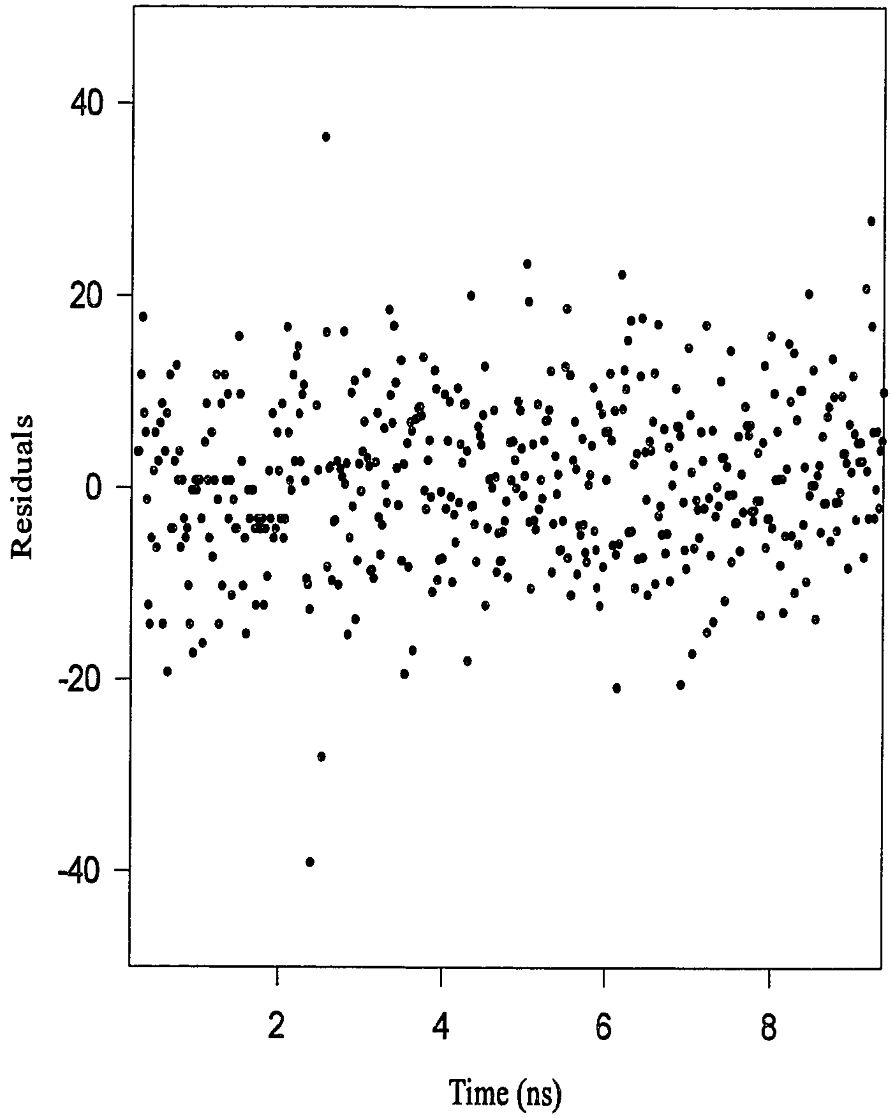

Fig. 5.8 A plot of the residuals from the time-filtering fit for the ^{73}Ge 13.26 keV timing curve.

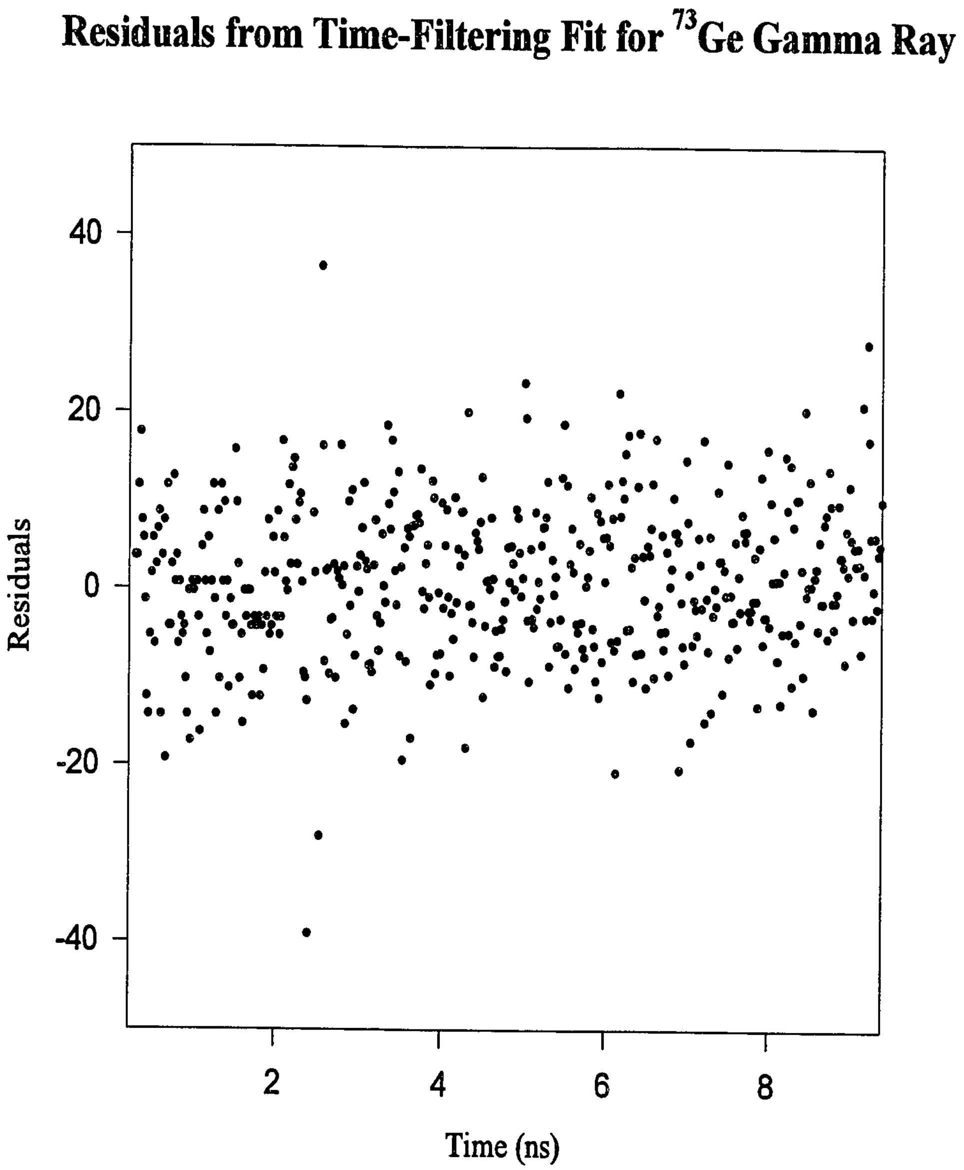
Residuals from Time-Filtering Fit for ^{73}Ge Gamma Ray

Fig. 5.8 A plot of the residuals from the time-filtering fit for the ^{73}Ge 13.26 keV timing curve.

curve above background, Prompt is the amplitude of the prompt curve added to the fit, f is the recoilless fraction, and the isomer shift is the detuning of the emitted line centroid with respect to the absorption line centroid measured in linewidths.

Table 5.1 ^{73}Ge Gamma-Ray Fit Parameters

Parameters	Time Resolution	τ	β	Amp.	Prompt	f	Isomer Shift
Fit Values	33 ns	4.26	1.2	20	340	88	0.0
Calculated	--	4.26	.59	--	--	88	0.0

The statistics of the 13.26 keV gamma ray time filtering spectrum are obviously poor, due to the high internal conversion coefficient for Ge and the adjustments made to the stop rate. The fit parameters given in Table 5.1 have very large errors because of the poor statistics. With the gamma-ray giving such poor results, the inelastic conversion channel was then explored to investigate the presence, if any, of a time filtering effect in this mode of decay. This should at least provide a factor of 1000 improvement to the count rate. If some time filtering information could be found in this inelastic process, this would provide a new method for measuring solid state effects using time domain Mössbauer spectroscopy. Also, Ge is a good candidate for this process due to its high internal conversion coefficient.

5.5 X-Ray Time Filtering for ^{73}Ge

The experimental set-up for this observation was identical to the gamma-ray observation, except that the energy window for the low energy side of the coincidence circuit had to be moved such that it was centered about the 9.88 keV x-ray. The results of the time filtering x-ray curve are displayed in Fig. 5.9 and the residuals from the fit are shown in Fig. 5.10. The data were fit using the same equation as with the gamma ray case. The parameters from the fit are given in Table 5.2. These parameters have the same definitions as the values in Table 5.1.

Table 5.2 **^{73}Ge X-Ray Fit Parameters**

Parameters	Time Resolution	τ	β	Amp.	Prompt	f	isomer shift
Fit Values	33 ns	4.26	0.18	1650	4410	88	0.0
Calculated	--	4.26	0.59	--	--	88	0.0

The count rates did improve significantly (collection time is approximately 10 days) while using the 9.88 keV x ray as the stop event, however, no time filtering information appeared in the Ge x-ray lifetime curve. The small value for β could normally be interpreted as a time filtering effect however, given the poor statistics of the data, this is result can not be trusted, and is therefore inconclusive. This inconclusive result prompted questions about whether the source and absorber were on resonance with respect to one another, or whether there was no time filtering information in the inelastic channel. To investigate this later supposition, ^{57}Fe time filtering experiments were performed, since Fe is known to have a large, and easily observable Mössbauer effect.

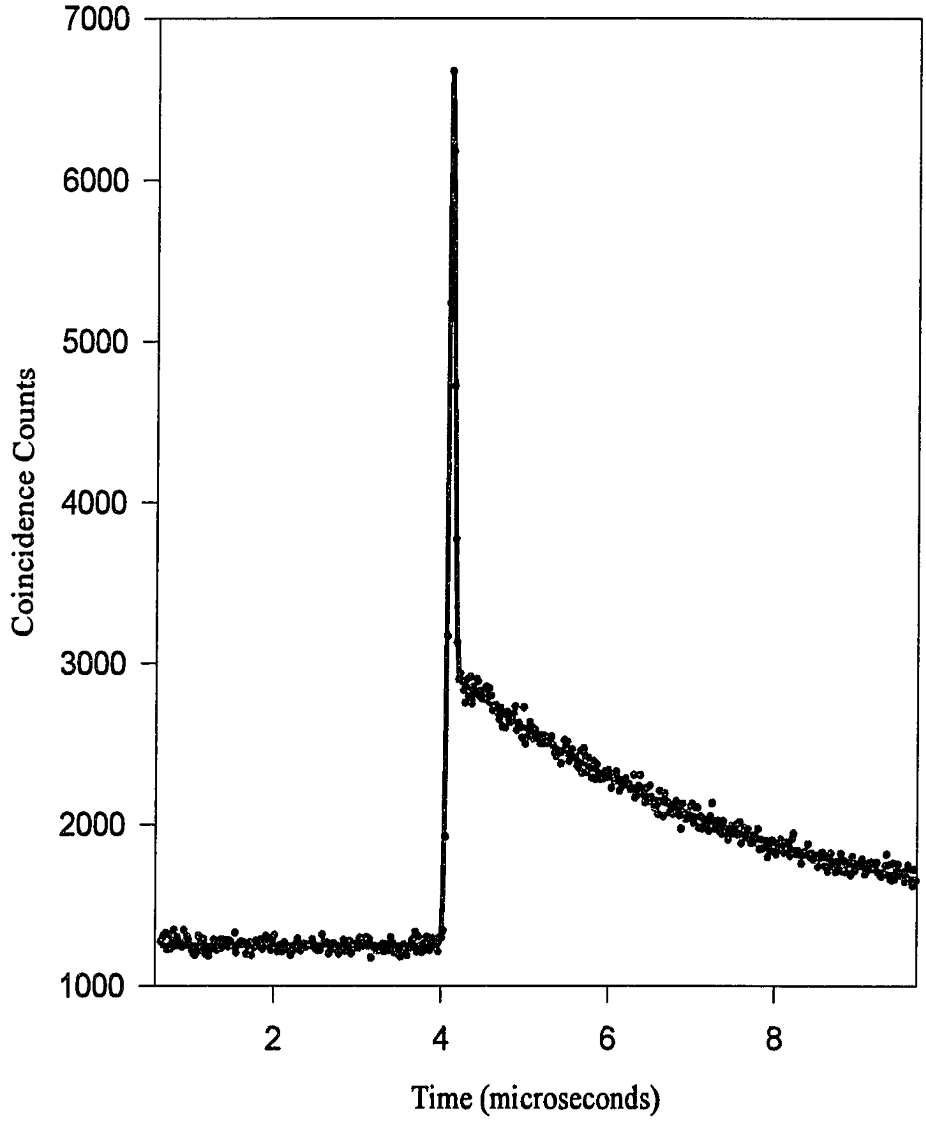

Fig. 5.9 Time-filtering curve using the 9.88 keV ^{73}Ge x-ray.

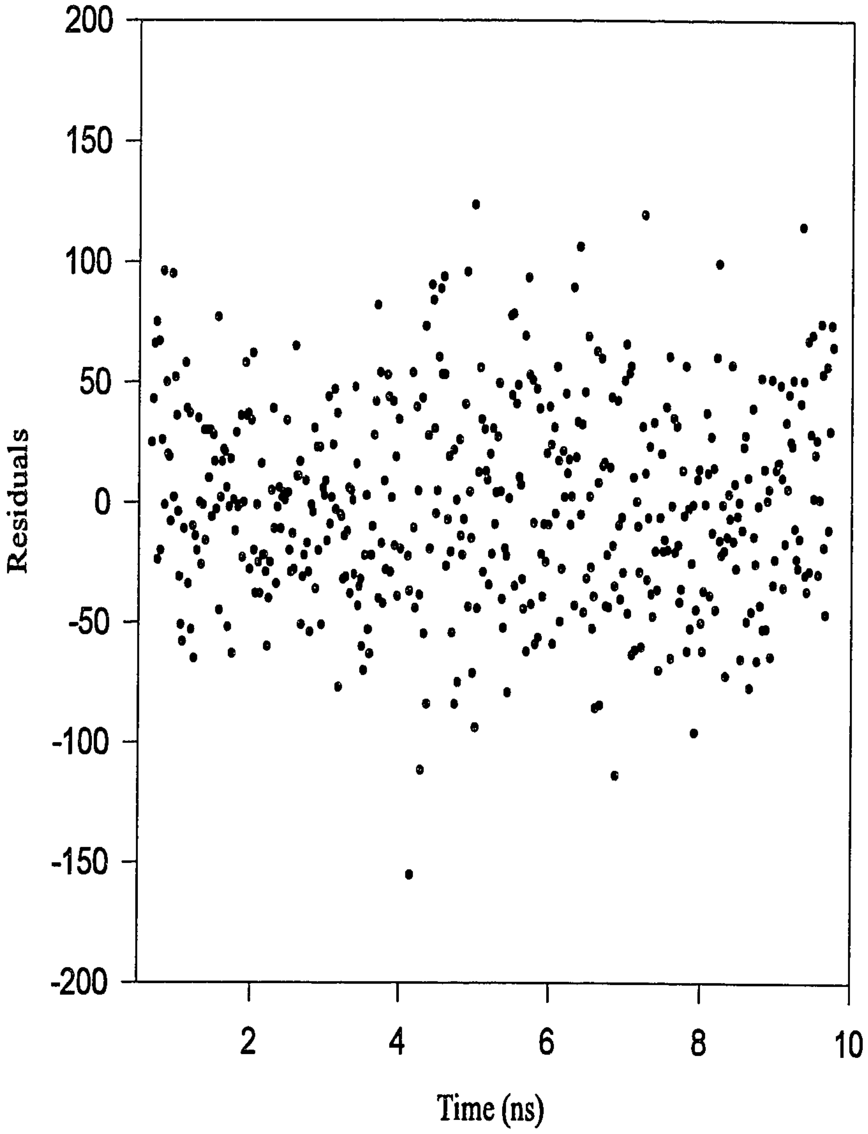

Fig. 5.10 Plot of the residuals from the ^{73}Ge x-ray time-filtering fit.

5.6 Iron Time Filtering: The Gamma Ray Case

As with the Ge case, the experiment was set up to measure the time-filtering effect in ^{57}Fe using the same delayed coincidence system. The first experimental run concentrated efforts to observe time-filtering effects using the elastic or gamma-ray channel. This allowed the determine some experimental parameters such as the nuclear resonant thickness, the added delay in the system, and the timing resolution of the coincidence circuit. The high and low energy windows were reset to 122 keV and 14.4 keV respectively. Additionally, the time scale on the TAC was set to 500 ns (full scale) to coincide with the Fe natural lifetime (141 ns).

The source used in these experiments was ^{57}Co in Rhodium, purchased from Isotope Products. When it was actually used in these experiments, the source strength was approximately 0.008 mCi. Since the source was in a Rhodium matrix, the nuclear levels should have had no hyperfine splitting, as there is no net magnetic field at the nuclear sites. The absorber was 6 μm thick ^{57}Fe in Rh foil. The foil was made of 30% Fe, of which 95% was ^{57}Fe. This foil was also purchased from Isotope Products.

Time filtering curves were collected using two detector setups. One setup used NaI on both the start and the stop side of the TAC setup. In the second setup one of the NaI detectors was replaced with a Ge solid state detector. The results for the two NaI detector set-up are shown in Fig. 5.11 with the residuals from the fit shown in Fig. 5.12. The results from the Ge detector set-up are shown in Fig. 5.13 with the residuals shown in Fig. 5.14. The residuals show features that indicate the Hamermesh time-filtering theory may be

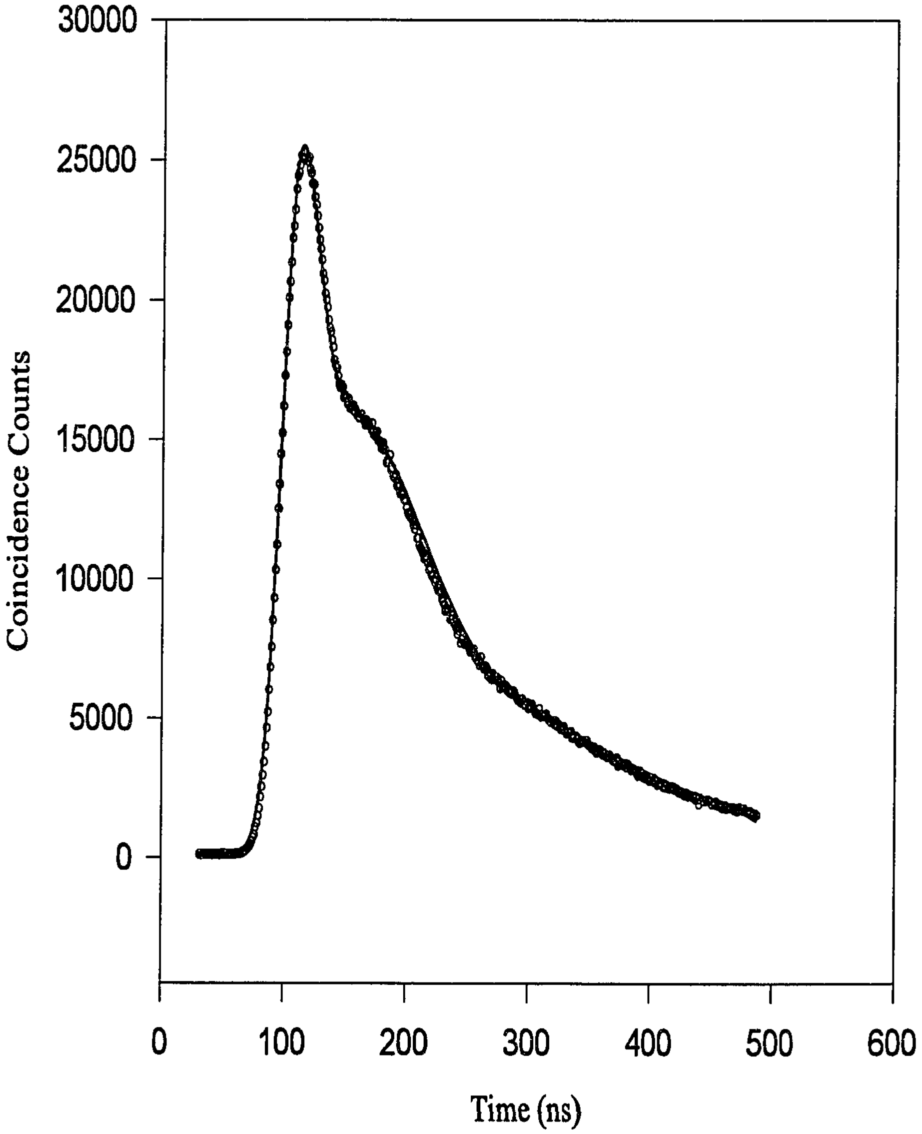

Fig. 5.11 Plot of the ^{57}Fe gamma-ray time-filtering curve using NaI on both branches of the coincidence circuit.

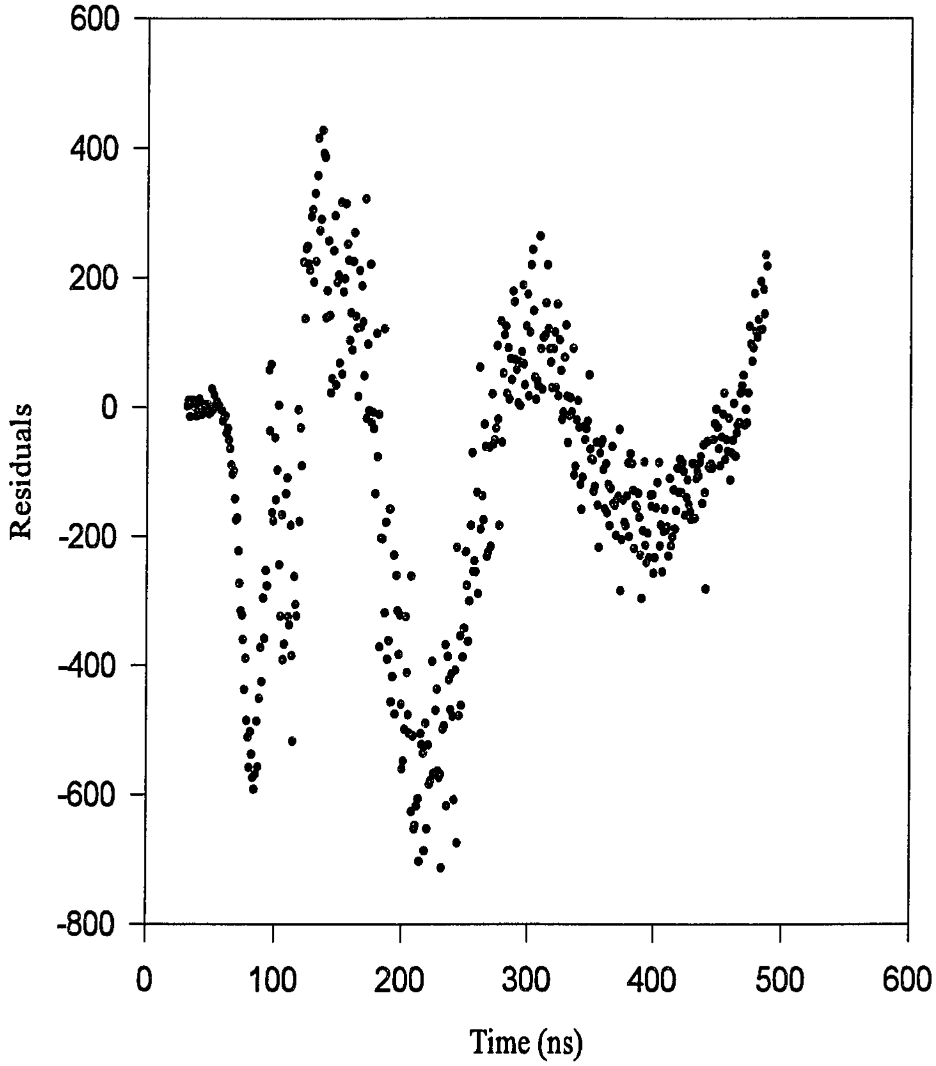

Fig 5.12 Plot of the residuals from the ^{57}Fe time-filtering fit. These data are from the spectrum taken with two NaI detectors in the coincidence circuit.

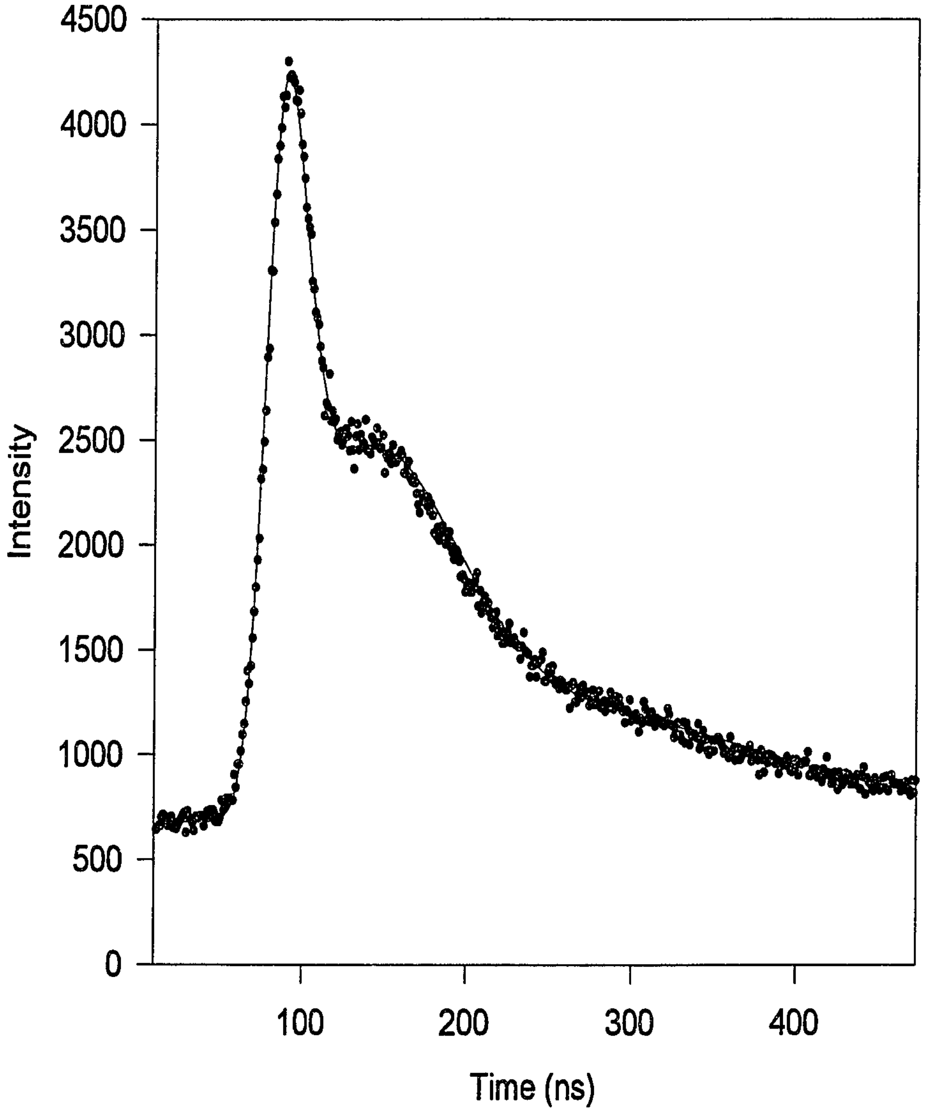

Fig. 5.13 Time-filtering curve for ^{57}Fe using a Ge solid state detector on one side of the coincidence circuit. Special care was taken to reduce the resolution time of the circuit to compensate for the slowness of the Ge detector.

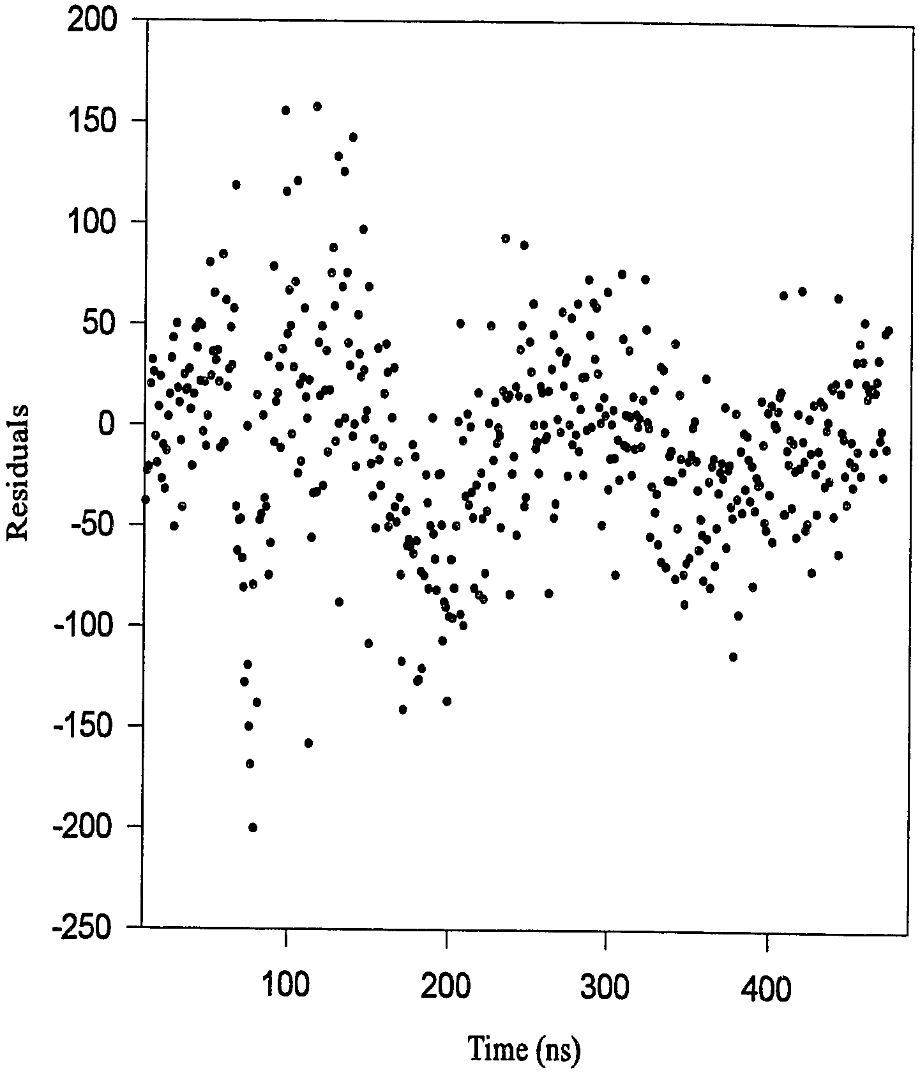

Fig 5.14 Plot of the residuals from the ^{57}Fe time-filtering fit. These data were taken with a Ge detector used in one branch of the coincidence circuit.

incomplete. The fit parameters for the ^{57}Fe spectrum, found using the same fitting routine as for ^{73}Ge, are shown in Table 5.3. Again, the parameters in the table have the same definitions as those in Table 5.1.

Table 5.3 ^{57}Fe Gamma-Ray Fit Parameters

Parameters	Time Resolution	τ(ns)	β	Amp.	Prompt	f	isomer shift
w/Ge det.	11 ns	141	24	3120	600	70	0.4
w/NaI det.	33 ns	141	24	22300	4800	60	0.4

The fit parameters extracted while using the time filtering program were in reasonable agreement with results previously obtained for this source and absorber using standard Doppler shifting Mössbauer absorption spectroscopy. Additionally the parameters were in reasonable agreement when using the two different detector schemes.

5.7 Iron Time Filtering: The X Ray Case

With the parameters for the source and absorber known, and the coincidence system calibrated, the time filtering x-ray measurements could be taken. A large prompt in the timing curve appeared early in the experiment using the NaI detector setup. The amplitude of the prompt was so large that it masked any time structure at times less than one lifetime. In order to see the time structure at earlier times, this problem had to be eliminated (Fig. 5.15).

Elimination of this prompt required determining its origin. The first possibility was

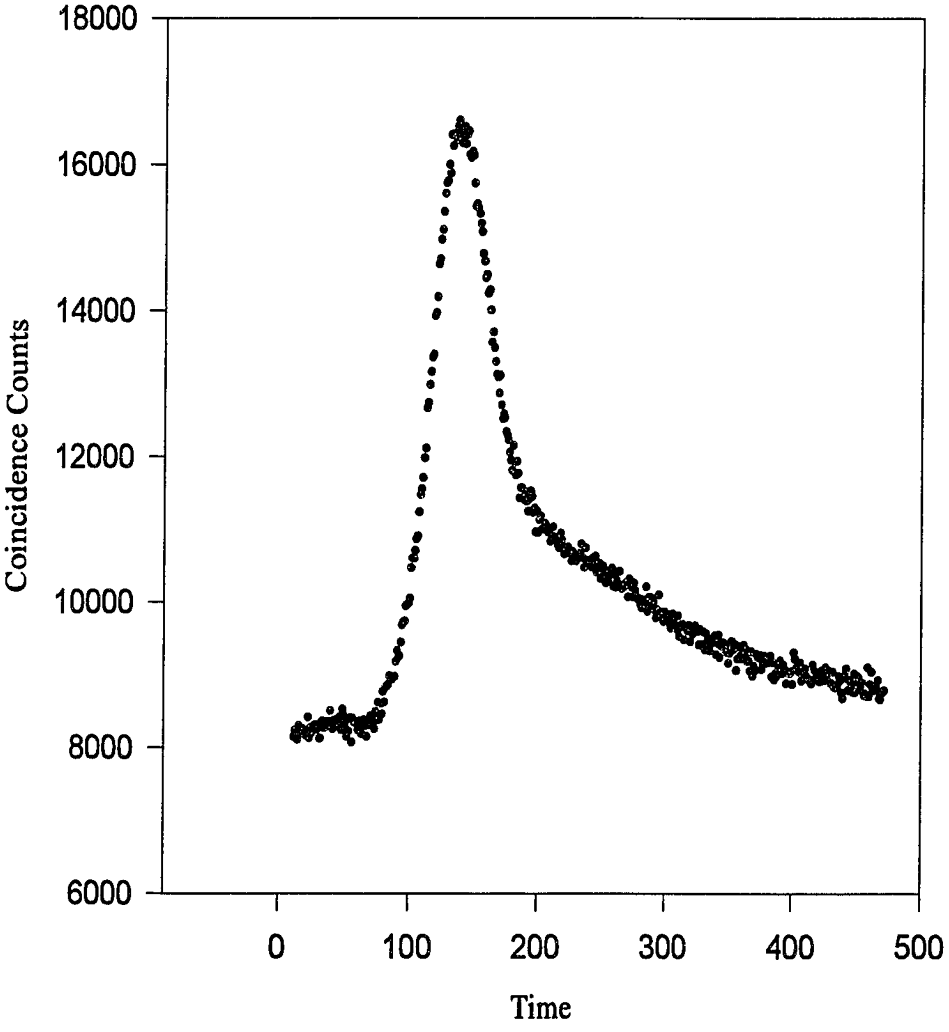

Fig. 5.15 Time-filtering curve using the 6.4 keV of ^{57}Fe. This spectrum was collected with NaI on both sides of the coincidence system. Some effort must be made to eliminate the prompt that is present in the spectrum.

a cross-talk between the detectors. Specifically, a 122 keV photon could Compton scatter from one detector to the other. This seemed feasible because the source and absorber were sandwiched between the two detectors. As a consequence, the detectors subtended a large solid angle with respect to each other. Therefore, the Compton scattered radiation could "slip" around the source and absorber. The first attempt to eliminate this possibility involved embedding the source in a 1/4" thick piece of lead to provide collimation. Testing on the embedded source still produced a prompt in the timing curve. Next, the Ge-detector coincidence set-up was also tested in hopes of providing better energy discrimination against the Compton scattered event. This still did not eliminate the prompt (Fig. 5.16).

An involved process of Compton scattering in the absorber combined with escape peaks within the detectors was finally considered. Specifically, the 122 keV would enter the NaI detector, ionizing an iodine atom. The x-ray from the iodine would then “escape” from the NaI detector and Compton scatter in the absorber foil into the Ge detector. This photon would then produce an escape peak in the Ge detector. These processes would produce approximately a 90 keV photon in the NaI detector and a 14 keV photon in the Ge detector. Since there is still one NaI detector in the system, and it has relatively poor energy discrimination compared to the Ge detector, the 90 keV photon could still satisfy the energy window in this leg of the coincidence circuit.

Experimental evidence was obtained by measuring a pulse-height spectrum with the Ge detector during the collection of the time filtering spectrum. In the pulse-height spectrum (Fig. 5.17), there clearly are photo peaks corresponding to the iodine ionization energies. Considering there were no other sources of iodine in the system, detection of the iodine

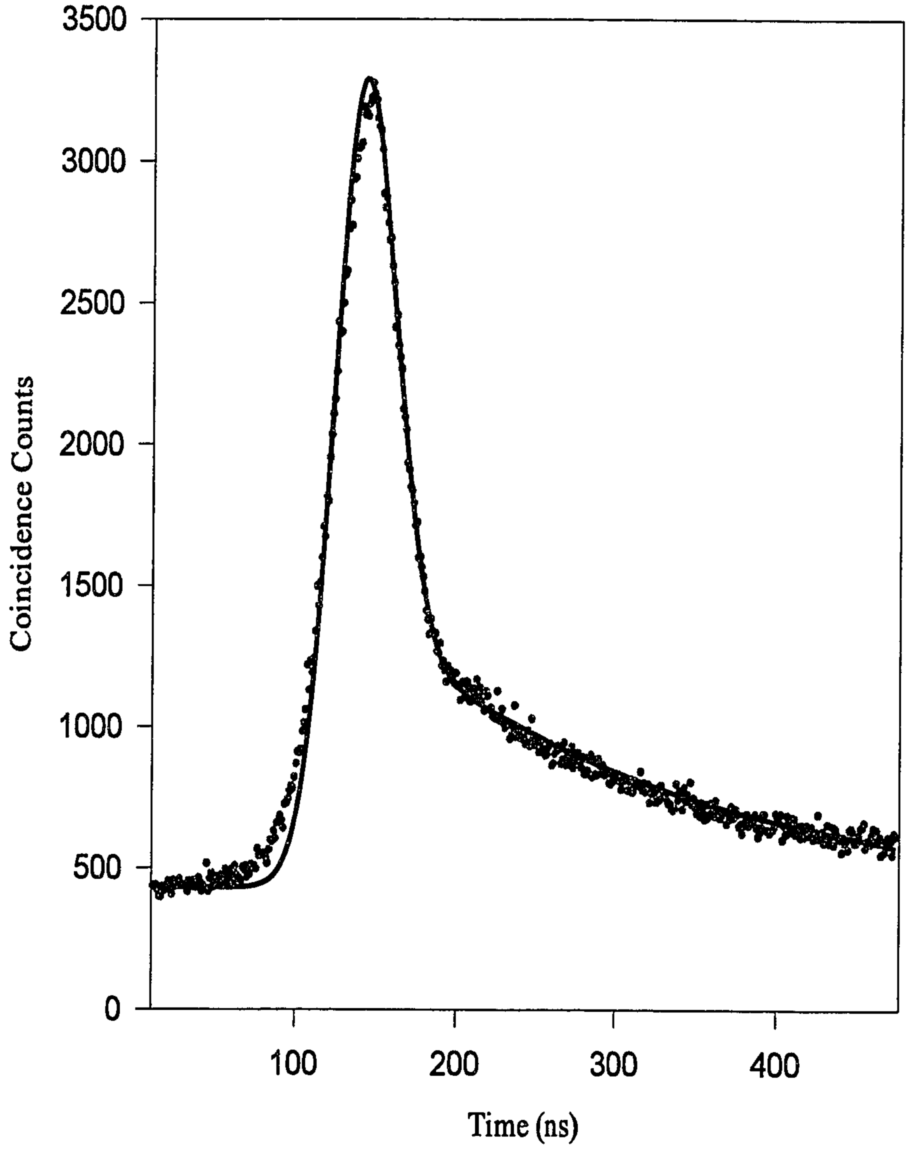

Fig. 5.16 Time-filtering curve for ^{57}Fe using the 6.4 keV x-ray. The solid line is an attempt at fitting by the Hamermesh theory.

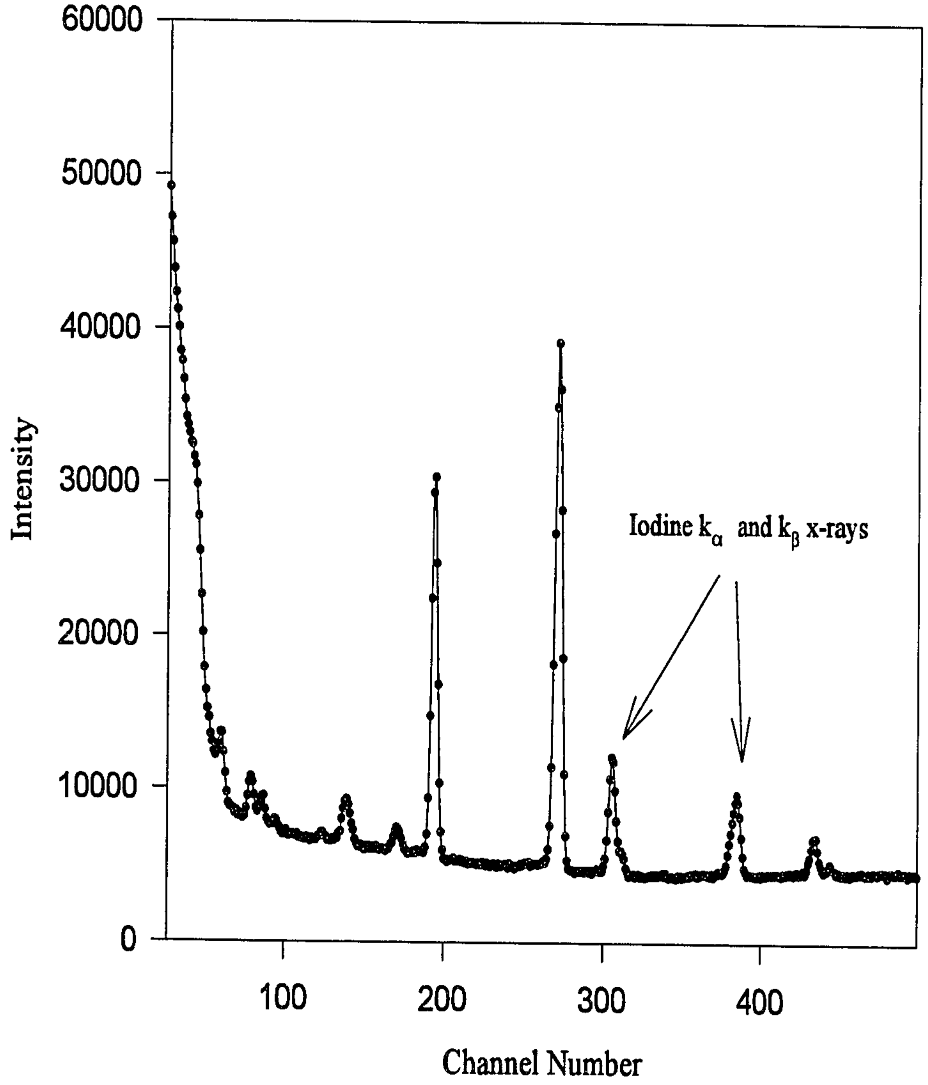

Fig. 5.17 Pulse-height spectrum showing the iodine x-rays that come from ionization of the NaI detector.

peaks signify that the NaI scintillator was being ionized and that this radiation was able to make its way to the Ge detector through the processes described above.

Another feature of the x-ray lifetime curves was a hint of some time-filtering information. When looking at the pulse height spectrum of the radiation that must travel through the absorber, it was clear that the 6.4 keV x-ray peak rides on a very large background. To investigate the origin of this background and to gain some insight into the Compton processes leading to the prompt peak, a timing curve was measured with the low energy window set on the Compton background above the 6 keV Fe x-ray (centered about 8 keV). The surprising result is shown in Fig. 5.18. The strong time filtering characteristics of this spectrum can be attributed to the 14 keV gamma rays Compton scattering in the absorber into this lower energy window. Since this time filtering information is present in the Compton background, it is obvious that this will also appear in the 6 keV x-ray timing curve, as the background extends into the 6 keV photo peak. This contribution caused the hint of the time filtering in the 6 keV spectrum.

The prompt was ultimately eliminated by reversing the Ge and NaI detectors. In this new arrangement, the Ge detector was used to detect the high energy photon while the NaI detector was used to detect the low energy side. With this set-up, it is not physically possible to produce the prompt event by the procedure described above because the energy discrimination on the high energy branch of the coincidence system is very good. Any photon off by more than ± 0.5 keV will not satisfy the energy requirements of the SCA window.

With the prompt eliminated, the fitting of the x-ray spectrum was less complicated.

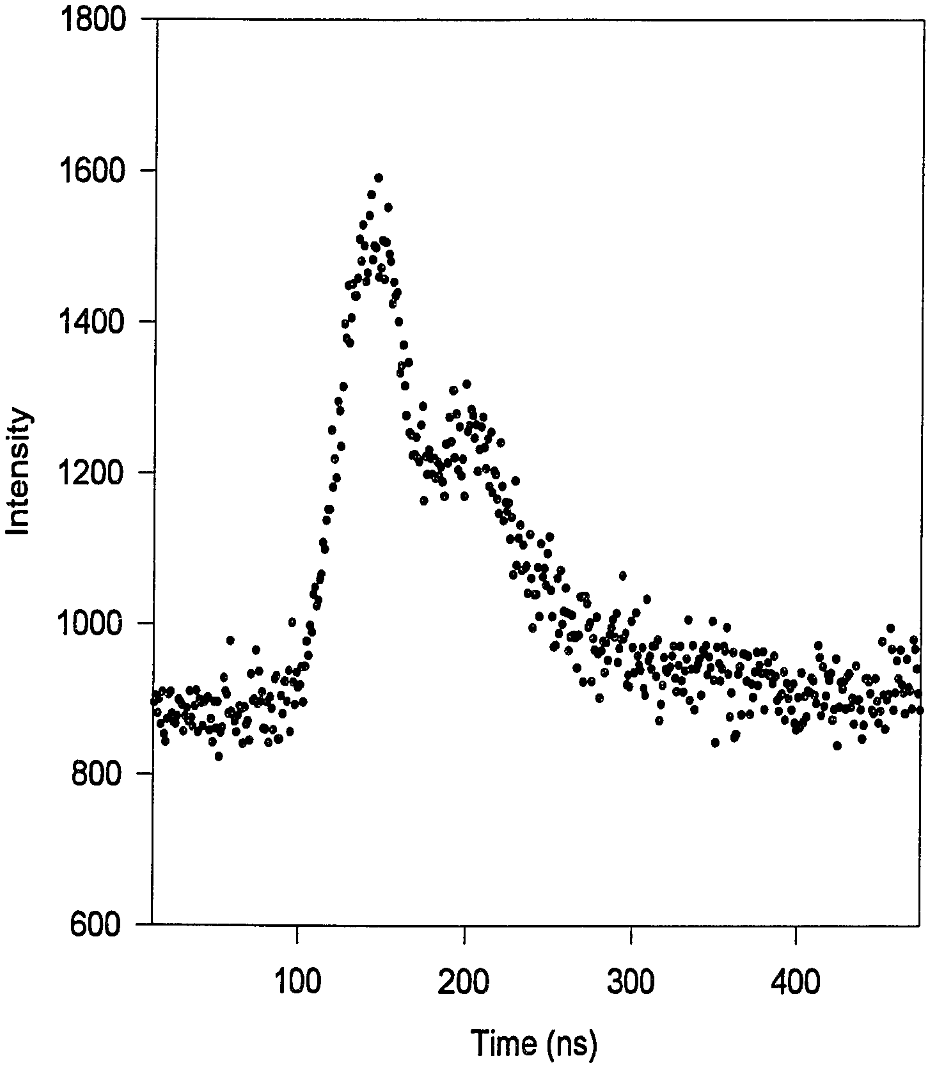

Fig. 5.18 Time-filtering curve collected with the low energy windows set on the Compton background.

However, the spectrum was again complicated by the time-filtering spectrum contained in the Compton background. A fit of the x-ray spectrum using the same theory as for the gamma-ray is shown in Fig. 5.19. Superimposed on the curve is the natural lifetime of 141 ns. It is obvious that the curve does not follow the natural lifetime and that the classical Hamermesh theory is not adequate for describing this process. This implies that a new or modified theoretical approach must be developed.

In 1961 S. Harris[43] was able to show that the quantum mechanical representation of time filtering produced the same Bessel type functions as the classical approach. An advantage to the quantum mechanical theory is that it contains provisions for the inclusion of the internal conversion or inelastic channel. Unfortunately, this part of the theory has not been completed. Due to these experimental results, current work is being concentrated on developing the remaining part of this theory[44]. At the time of this writing, the theory is still not complete; however, preliminary results seem very promising.

The idea behind the quantum mechanical calculations is that the source would emit a gamma-ray which is allowed to interact with the absorber to some degree. However, at some point in the absorber, the gamma-ray is absorbed by a nucleus and internally converted. The resulting released photon is no longer coherent with the incident radiation. Provided this holds true, not only will this contribution be able to describe the inelastic channel, but will also have a significant impact on the elastic, gamma-ray channel. Consider the same process shown above, but rather than allowing the nucleus to internally convert, the excited state emits a photon and the nucleus recoils. After recoil, the photon would no longer resonant with the absorber. Additionally, the photon would no longer be coherent

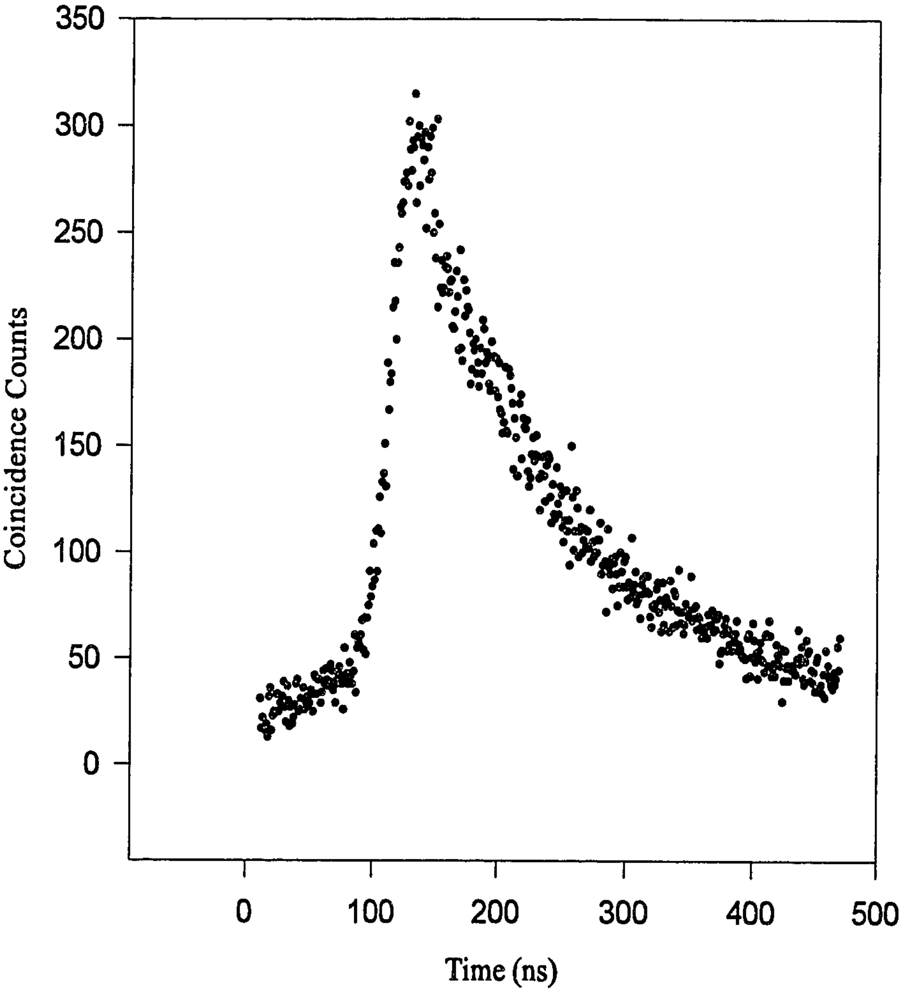

Fig. 5.19 Time-filtering curve using the 6.4 keV x-ray of ^{57}Fe. The prompt has been eliminated by switching the Ge solid state detector and the NaI detector.

with the incident photon which is the essence of the classical optical calculation. In this picture, the recoil gamma-ray time filtering spectrum should behave in the same manner as the x-ray equivalent. This process is currently not included in any analysis involving time filtering.

This modification to existing theory will have a large impact on the synchrotron community currently using time-filtering with a synchrotron source. Most of the synchrotron configurations consist of detectors with fast recoveries, and hence little or no energy resolution. The recorded spectrum consists of any delayed photons that happen to find their way into the detector. As has been shown in this research, there is a difference between the elastic and inelastic timing channels which has not been taken into account in the analysis of the synchrotron nuclear forward scattering experiments.

Chapter Six

Summary, Conclusions and Future Directions

6.1 The Nuclear Borrmann Effect

In our experiments, the nuclear Borrmann effect was not observed in ^{73}Ge. The probable cause in this case was the sample preparation process, which did not allow for the source nuclei to be placed in a "good" environment (i.e. no isomer shift due to a non-identical chemical environment). Such an environment could be achieved by definitively placing all of the radioactive nuclei inside the lattice of the crystal. This could be accomplished by ion implantation and subsequent growth of the host crystal over the active area. This would help in two ways: 1) the activity would be placed deep within the crystal, and 2) the crystal growth over top of the implanted nuclei would effectively seal the nuclei in the lattice of the crystal. Both improvements would ensure a minimum isomer shift environment.

Another possible explaination for the unobserved nuclear Borrmann effect is that the effect actually is occurring in our samples, and is simply masked by background radiation.

If this is the case, polarization selection would help increase the signal to noise, since the Borrmann mode is highly polarized. The polarization selection could be achieved through the use of a silicon monochromator designed to reflect the 13.26 keV gamma rays at a 45° Bragg angle. This monochromator could then be used on the radiation emitted from the crystal to select a particular polarization.

Even though the nuclear Borrmann effect was not definitively observed, the criteria and method for such an observation was established. Additionally, the sample preparation and testing procedures were developed to aid in working with new and different samples in the future.

In the future, focus should return to ^{57}Fe; specifically, some form of Fe-Si crystal. These crystals are found to be of relatively high crystallographic quality which would address the problem of the poor quality natural Fe single crystals. Also, ^{57}Fe has the large, well known, Mössbauer transition which is vital to a successful observation of this effect.

6.2 Time-Filtering Effect

The time-filtering effect does appear to be present in the inelastic conversion electron channel. This surprising result could have a profound impact on nuclear forward scattering using synchrotron radiation. Currently, most of the detection systems used in these types of studies have little to no energy resolution. This implies that the detector cannot distinguish between an Fe x-ray and a ^{57}Fe gamma ray, both of which are present in nuclear forward scattering. Preliminary theoretical work involving the conversion electron channel suggest, that these two modes of decay possess different time structures. If this is not accounted for in time-domain Mössbauer spectroscopy, information obtained from the fitting of the timing curves will be in error.

6.3 General Remarks

Gamma-ray optics is a field still in its infancy. The theoretical effort greatly outweighs the experimental effort. If a gamma ray laser is to be developed, there are many experiments to be performed. Specifically, many of the phenomena already observed in atomic systems should be attempted with nuclear decaying systems, beginning with such experiments as two photon excitation and level crossing experiments in order to development a knowledge base of gamma-ray optical systems. These experiments would provide some insight to potential problems and successes with other gamma-ray optical studies. A drawback to these type of experiments is that they are not guaranteed successes. However, the possible technological applications of a gamma-ray laser merit further experimentation and study.

REFERENCES

[1] G.C. Baldwin, J.C. Solem and V.I. Gol'danski, Rev. Mod. Phys. **53**, 687 (1981)

[2] J.P. Hannon and G.T. Trammell, Phys. Rev. **169**, 315 (1968)

[3] J.P. Hannon and G.T. Trammell, Phys. Rev. **186**, 306 (1969)

[4] J.P. Hannon, N.J. Carron, and G.T. Trammell, Phys. Rev. **B 9**, 2810 (1974)

[5] J.P. Hannon, N.J. Carron, and G.T. Trammell, Phys. Rev. **B 9**, 2791 (1974)

[6] J. Timothy Hutton, Ph. D. thesis, Rice University, (1988)

[7] J. Timothy Hutton, J.P. Hannon and G.T. Trammell, Phys. Rev. **A37**, 4269 (1988)

[8] G.T. Trammell, J. Timothy Hutton, and J.P. Hannon in *Proc. of the IST/IDA Gamma-Ray Laser Workshop,*"(IDA Memorandum Report M-162), Institute for Defense Analyses 1801 N. Beauregard, Alexandria, VA 22311 (1986)

[9] G. Borrmann, Zeit. f. Physik, **127**, 297 (1950)

[10] J. D. Jackson, Classical Electrodynamics, 2nd ed. (Wiley, New York, 1975) p. 354

[11] R.L. Mössbauer, Zeit. Phys. **151**, 124 (1958)

[12] G.R. Hoy, Encyclopedia of Physical Science and Technology, Vol. 10, (Academic Press, Inc., 1992) p. 469

[13] T.C. Gibb, Priciples of Mössbauer Spectroscopy, (Wiley, New York, 1976)

[14] W. Kuhn, Phil Mag., **8** 625 (1929)

[15] T.C. Gibb, p.2

[16] F.R. Metzger and W.B. Todd, Phys. Rev. **95**, 853 (1954)

[17] Shokrollah Rezaie-Serej, “Search for the Mössbauer Effect in ^{109}Ag” Diss. Old Dominion University 1992, p.10

[18] T.C. Gibb, p.5

[19] Shokrollah Rezaie-Serej, p. 16

[20] G.R. Hoy, p. 470

[21] G.R. Hoy, p.470

[22] F. J. Lynch, R. E. Holland, and M. Hamermesh, Phys. Rev., **120**, 513 (1960)

[23] G. Borrmann, Zeit. f. Physik, **127**, 297 (1950)

[24] B. W. Batterman and H. Cole, Rev. Mod. Phys. **36**, 681 (1964)

[25] W.H. Zachariasen, Theory of X-ray Diffraction in Crystals, (Dover Publications, 1945) p.111

[26] P. P. Ewald, Ann Physik, **49**, 1, 117 (1916); **54**, 519 (1917)

[27] B.E. Warren, X-Ray Diffraction, (Dover Publications, 1957) p. 9

[28] H. Hönl, Zeitschr. f. Phys., **84**, 1 (1933); Ann. der Phys., [5], **18**, 625 (1933)

[29] M. von Laue, Acta Cryst., **2**, 106 (1949)

[30] C. G. Darwin, Phil Mag., **27**, 315, 675 (1914)

[31] B.E. Warren, p. 315-323

[32] J. D. Jackson, Classical Electrodynamics, 2nd ed. (Wiley, New York, 1975) p. 354

[33] B.E. Warren, p. 329

[34] Dr. M. Dudley, SUNY Stoney Brook, private communications

[35] W.L. Bond J. Sci. Instr. **88**, 63 (1961)

[36] L. Pfeiffer, R. S. Raghavan, C. P. Lichtenwalner, and A. G. Cullis, Phys. Rev. B, **12**, 4793 (1975)

[37] Dr. R.D. Taylor, Los Alamos National Laboratory, private communications

[38] F. J. Lynch, R. E. Holland, and M. Hamermesh, p. 513

[39] J.R. Reitz, F.J. Milford, R.W. Cristy, Foundations of Electromagnetic Theory, (Addison Weslet, Publishing Company, 1979) p. 428

[40] F. J. Lynch, R. E. Holland, and M. Hamermesh, p. 513

[41] G.F. Knoll, Radiation Detection and Measurement, (John Wiley & Sons, 1989) p. 631

[42] L. Pfeiffer, R. S. Raghavan, C. P. Lichtenwalner, and A. G. Cullis, Phys. Rev. B, **12**, 4793 (1975)

[43] S. Harris, Phys. Rev., **124**, 1178 (1961)

[44] G. R. Hoy, Old Dominion Univeristy, (private communications)

Appendix A

The Two-Beam Borrmann Mode

Consider a wave incident on a plane of atoms as depicted in Fig A.1. As stated above, a Fresnel zone will be constructed such that the path lengths of a wave traveling along AOP will be λ/2 longer than the path ABP. This condition will produce a Fresnel zone that will be elliptical in shape. The differential electric field at the point P is then given by

$$dE_p=\left(\frac{e^2}{mc^2 r_{\epsilon\eta}}\right)f(2\theta)e^{(2\pi i/\lambda)[ct-(R_{\epsilon\eta}+r_{\epsilon\eta})]}Md\epsilon d\eta \qquad \text{(A.1)}$$

In this equation, (e2/mc2) is the classical electron radius, f(2θ) is the angle dependent atomic scattering factor for the atoms comprising the crystal, λ is the wavelength of the radiation, $R_{\epsilon\eta}$ and $r_{\epsilon\eta}$ are the source to scatterer and scatter to observation point radii repsectively, and M is the number of atoms per area. This construction is generally used when calculating the intensity from a perfect crystal that is oriented for a Bragg reflection. Since we are interested in a Laue transmission experiment, we will use a

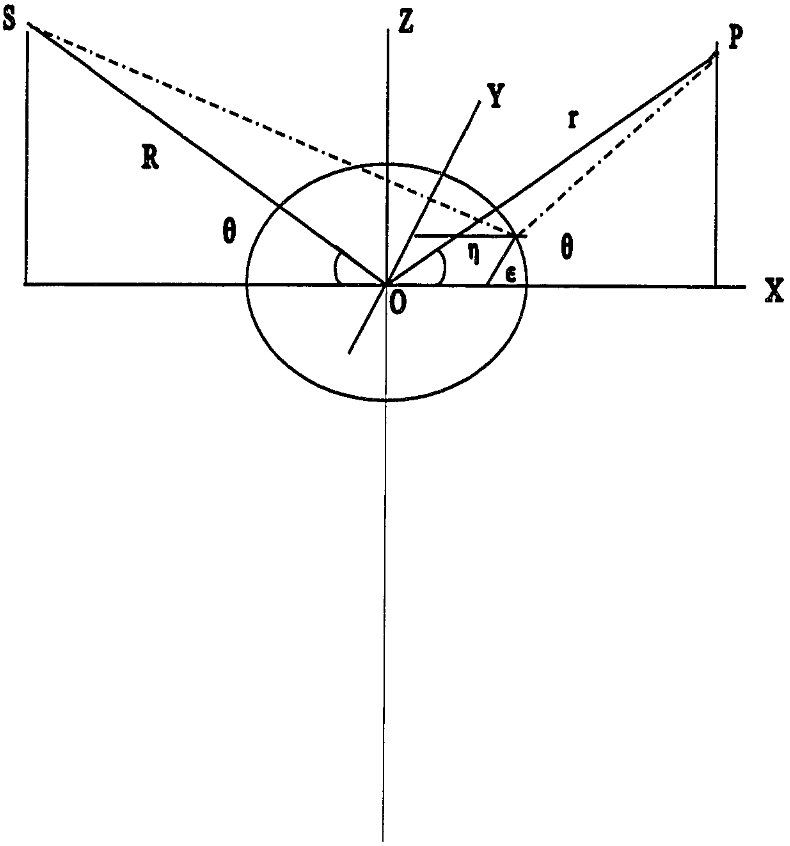

Fig. A.1 The reflection of x rays from a plane can be described in terms of a Fresnel zone. In this figure, the Fresnel zone in a horizontal plane.

modified approach that was first described by Borie. Borie's extension to Laue's treatment of the dynamical theory considers the Fresnel zone to be lying in the vertical plane, perpendicular to the plane defined by the incident and diffracted plane, as opposed to the horizontal plane. This is depicted in Fig A.2.

From Fig. A.2, the lengths of $R_{\epsilon\eta}$ and $r_{\epsilon\eta}$ can be expressed in terms of ϵ and η by the following equation

$$R_{\epsilon\eta}=R-\epsilon\sin\theta+\frac{\epsilon^2\cos^2\theta+\eta^2}{2R} \qquad \text{(A.2)}$$

and

$$r_{\epsilon\eta}=r-\epsilon\sin\theta+\frac{\epsilon^2\cos^2\theta+\eta^2}{2r}. \qquad \text{(A.3)}$$

By adding $R_{\epsilon\eta}$ and $r_{\epsilon\eta}$ together and assuming R>>r we get,

$$R_{\epsilon\eta}+r_{\epsilon\eta}=R+r-\epsilon(\sin\theta_1+\sin\theta_2)+\frac{\epsilon^2\cos^2\theta_2+\eta^2}{2r} \qquad \text{(A.4)}$$

In the vertical planes, the atoms are located at the positions ϵ=nd and to nearly satisfy Bragg's law, the condition must exist such that

$$d(\sin\theta_1+\sin\theta_2)=\lambda \qquad \text{(A.5)}$$

Using these relationships in the equation for the sun of $R_{\epsilon\eta}$ and $r_{\epsilon\eta}$, the sum can be

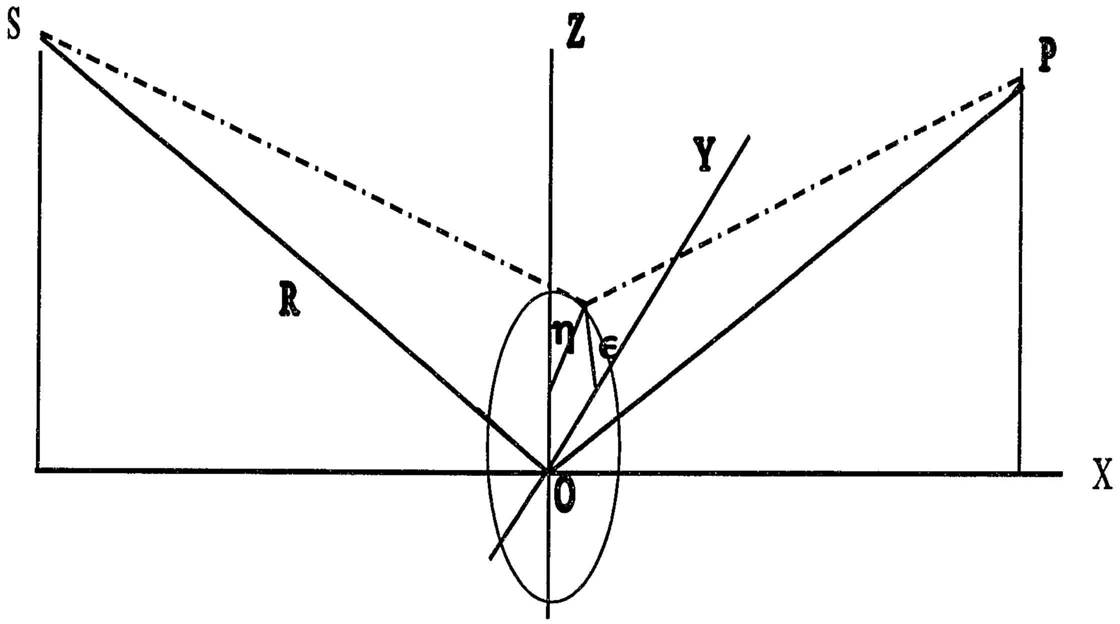

Fig. A.2 Fresnel zone in the vertical planes. This was Borie's extension to Laue's construction.

substituted into the equation for the differential electric field. This is desirable because it allow the differential to be expressed in terms of R and r and the integration variables ϵ and η.

$$dE_p=(\frac{e^2}{mc^2 r_{\epsilon\eta}})f(2\theta)e^{(2\pi i/\lambda)[ct-(R+r-n\lambda+\frac{\epsilon^2\cos^2\theta_2+\eta^2}{2r})]}Md\epsilon d\eta \qquad (A.6)$$

Integrating this expression gives the value of the electric field, at a point P, scattered by a single vertical Fresnel zone.

$$E_p=E_0(ig)e^{i[\omega t-k(R+r)]} \qquad (A.7)$$

where the g is given by

$$g=(\frac{e^2}{mc^2})\frac{M\lambda f(2\theta)}{\cos\theta} \qquad (A.8)$$

The imaginary component comes from the integration over the contributions from the different nuclei in the Fresnel zone. These contributions effectively add up to give a total phase shift in the electric field of $\pi/2$ relative to an electric field generated by a scattering at the point O.

It is now necessary to determine a recursion relationship for both the forward diffracted and the diffracted waves so that the wavefields inside the crystal may be summed. The phases of the forward diffracted and the diffracted waves may be written, respectively, as

$$\phi_1=\frac{2\pi a\cos\theta_1}{\lambda}\ ,\ \phi_2=\frac{2\pi a\cos\theta_2}{\lambda} \tag{A.9}$$

The diffracted wave S_r as depicted in Fig. A.3 can be written as a superposition of a reflection beam T_r and a transmission of S_{r-1} provided the correct phase and scattering factors are introduced. This is as follows

$$S_r=T_r(ig)+S_{r-1}(1+ig_0)e^{-i\phi_2} \tag{A.10}$$

In a similar manner, the forward diffracted wave T_{r+1} can be written as a superposition of the forward diffracted wave T_r and the diffracted wave S_{r-1}.

$$T_{r+1}=T_r(1+ig_0)e^{-i\phi_1}+S_{r-1}(ig)e^{-i(\phi_1+\phi_2)} \tag{A.11}$$

Solving these equations for S_{r-1}, rewriting the indexing subscript r as r+1, and performing these substitutions, we may obtain an expression that is just in terms of T_r.

$$S_{r-1}=\frac{T_{r+1}-T_r(1+ig_0)e^{-i\phi_1}}{(ig)e^{-i(\phi_1+\phi_2)}}\qquad S_r=\frac{T_{r+2}-T_{r+1}(1+ig_0)e^{-i\phi_1}}{(ig)e^{-i(\phi_1+\phi_2)}} \tag{A.12}$$

$$T_{r+2}+T_re^{-i(\phi_1+\phi_2)}[g^2+(1+ig_0)^2]=T_{r+1}(1+ig_0)(e^{-i\phi_1}+e^{-i\phi_2}) \tag{A.13}$$

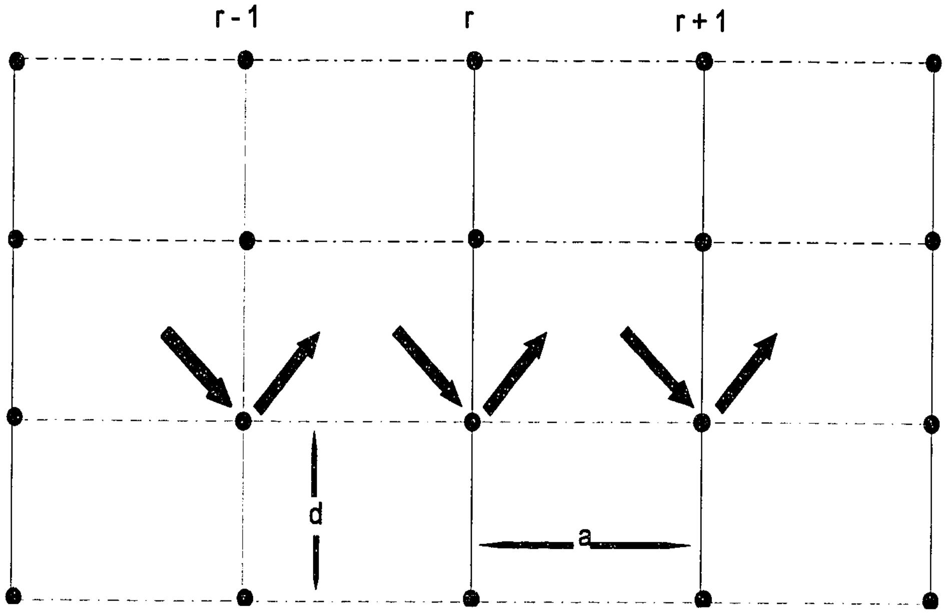

Fig. A.3 Schematic representation of the diffracted and forward diffracted wavefields inside the crystal. This construction is useful for finding recursion relationships for the forward diffracted and diffracted waves.

Assuming the solution

$$T_r = T_0 x^r, \tag{A.14}$$

this can be substituted into the equation for T. After substituting, the equation reduces to a quadratic equation in x.

$$x^2 + [g^2 + (1 + ig_0)^2] e^{-i(\phi_1 + \phi_2)} = x(1 + ig_0)(e^{-i\phi_1} + e^{-i\phi_2}) \tag{A.15}$$

If we make the following abbreviations,

$$\phi_1 = \phi + \Delta\phi, \quad \phi_2 = \phi - \Delta\phi, \quad \phi_1 + \phi_2 = 2\phi \tag{A.16}$$

and

$$e^{-i\phi_1} + e^{-i\phi_2} = e^{-i\phi} 2 \cos\Delta\phi \tag{A.17}$$

The quadratic equation can be simplified to

$$x^2 - xe^{-i\phi}(1 + ig_0) 2 \cos\Delta\phi + [g^2 + (1 + ig_0)^2] e^{-i2\phi} = 0 \tag{A.18}$$

If we define the following relationship,

$$u = [g^2 + (1 + ig_0)^2 \sin^2\Delta\phi]^{1/2} \tag{A.19}$$

the equation can be solved for x by completing the square. This will give two solutions for x,

$$x_1 = e^{-i\phi}[(1+ig_0)\cos\Delta\phi + iu] \tag{A.20}$$

$$x_2 = e^{-i\phi}[(1+ig_0)\cos\Delta\phi - iu] \tag{A.21}$$

The most general solution for T_r will be a sum of x_1. and x_2. This summation is expressed as follows:

$$T_r = T_0(C_1x_1^r + C_2x_2^r) \tag{A.22}$$

Now it is necessary to use some initial condition in order to solve for the coefficients C_1 and C_2. At r=0, $T_0 = T_0(C_1+C_2)$ and there for $C_1+C_2=1$. Also, since $S_{r-1}=0$ it follows $T_1= T_0(1+ig0)e^{-i\phi}$. Substituting these into the above equation we get a second equational relationship for the coefficients.

$$C_1x_1 + C_2x_2 = (1+ig_0)e^{-i\phi_1} \tag{A.23}$$

Using these two constraints on C_1 and C_2, we solve for C_1 and C_2 and substitute these into the expression for T_r. A general expression for T_r in terms of the incident amplitude T_0 is then obtained.

$$T_r = \frac{T_0}{2}([1 - \sin\Delta\phi(1+ig_0)/u]x_1^r + [1+\sin\Delta\phi(1+ig_0)/u]x_2^r) \tag{A.24}$$

And likewise for an equational form for S_{r-1} in terms of x_1 and x_2.

$$S_{r-1}e^{-i\phi}=\frac{T_0 g}{2u}(x_1^r-x_2^r) \qquad \text{(A.25)}$$

These two equations (Tr and Sr-1) give the amplitudes of the two wavefield components inside the crystal for the most general case. Since we are interested in the case where the Bragg condition is exactly satisfied, we can set $\Delta\phi=0$ and $\theta_1=\theta_2=\theta$. The equations for T_r and S_{r-1} then reduce to

$$T_r=\frac{T_0}{2}e^{-i\phi r}[(1+ig_0+ig)^r+(1+ig_0-ig)^r] \qquad \text{(A.26)}$$

$$S_{r-1}e^{-i\phi}=\frac{T_0}{2}e^{-i\phi r}[(1+ig_0+ig)^r-(1+ig_0-ig)^r] \qquad \text{(A.27)}$$

which can be re-expressed in exponential form as

$$T_r=\frac{T_0}{2}e^{-i\phi r}[e^{i(g_o+g)r}+e^{i(g_0-g)r}] \qquad \text{(A.28)}$$

$$S_{r-1}e^{-i\phi}=\frac{T_0}{2}e^{-i\phi r}[e^{i(g_o+g)r}-e^{i(g_0-g)r}]\,. \qquad \text{(A.29)}$$

To allow for absorption we permit the scattering factors g and g_0 to be complex. To a very good approximation, the imaginary part of the atomic scattering factor is angle independent. Therefore, the imaginary part of the forward diffracted wave $\Delta f(0)$ is equal to the imaginary part of the diffracted wave Δf(2θ).

$$g=g'+ig'' \qquad g_0=g_0'+ig_0'' \tag{A.30}$$

The wave fields inside the crystal can be a superposition of two possible configurations. This arises from considering the polarization of the each wave. The π polarization is defined by an electric field vector which lies in the scattering plane where the scattering plane is defined by the diffracted and forward diffracted wavevector. A wave is considered σ polarized when the electric fields are perpendicular to scattering plane. By considering each case seperately, it is possible to determine a relationship between the imaginary parts of the scattering amplitudes g and g_0.

For the π polarization case,

$$g=(\frac{e^2}{mc^2})\frac{Na\lambda f(2\theta)\cos 2\theta}{\cos\theta} \tag{A.31}$$

$$g_0=(\frac{e^2}{mc^2})\frac{Na\lambda f(0)}{\cos\theta} \tag{A.32}$$

This implies that $g_0''=g''\cos 2\theta$.

For the σ polarization case,

$$g=(\frac{e^2}{mc^2})\frac{Na\lambda f(2\theta)}{\cos\theta} \tag{A.33}$$

$$g_0=(\frac{e^2}{mc^2})\frac{Na\lambda f(0)}{\cos\theta} \tag{A.34}$$

Which implies, for the σ polarization case, $g''=g_0''$.

Substituting these relationships into the exponential expressions in the equations for the wavefields, we get for the π polarization,

$$e^{i(g_0+g)r}=e^{i(g_0'+g')r}e^{-g_0''(1+\cos2\theta)r} \tag{A.35}$$

$$e^{i(g_0-g)r}=e^{i(g_0'-g')r}e^{-g_0''(1-\cos2\theta)r} \tag{A.36}$$

and for the σ polarization case,

$$e^{i(g_0+g)r}=e^{i(g_0'+g')r}e^{-g_0''2r} \tag{A.37}$$

$$e^{i(g_0-g)r}=e^{i(g_0'-g')r}e^{-g_0''(1-1)r} \tag{A.38}$$

If we allow for the crystal to become very thick such that the radiation has to traverse through many layers r, all of the exponential factors above vanish except the last one. This is the Borrmann mode. Since each of these factors can be considered as a different polarization, the **surviving Borrmann mode is highly polarized in the σ polarization state**. Substituting this surviving exponential factor into the equations for the forward diffracted and diffracted electric field we get and expression for the forward diffracted and diffracted wave field amplitudes.

Appendix B

The FORTRAN Fitting Program SIMULATE

The FORTRAN fitting program SIMULATE, used to calculate the time dependent intensity of the time filtering curves, took advantage of specialized subroutines in several commercial packages. Specifically, Integrated Mathmatical and Statistic Library (IMSL) was used for calculating the Bessel functions that are required when calculating the Hamermesh theory. The equivalent subroutine in Numerical Recipes was also used as a test of the IMSL routines. Both packages calculated the same results for the Bessel functions to within 5%. To perform the convolution, another Numerical Recipes subroutine was used. This subroutine calculated the convolution of two numerical arrays by taking the Fourier transform of each data array (time-filtering contribution and a gaussian function), multiplying the two Fourier transforms together, and then the inverse Fourier transform is taken. After this, a prompt is added to the spectrum at a time equal to the added delay of the coincidence system then followed by a back ground level. The results are written to a file.

SIMULATE is a generic FORTRAN program that will run on many platforms. The majority of the runtime for this research was a IBM clone 486 machine.

```
      program simulate
       real*8  tau,width,res(1024),e data(1024),back
       real*8 ans1(1024),displace,d amp,xdata(1024),ydata(1024),f
       real*8 chi,prom ampl,scale,beta,dw,data2(1024),scale2
       integer veclen,ndata
       character*2 isotope

C;;;;;;;;;;;;;;;;;;;;;;;;;;;;;;;;;;;;;;;;;;;;;;;;;;;;;;;;;;;;
C     Call the initialization subroutine
C;;;;;;;;;;;;;;;;;;;;;;;;;;;;;;;;;;;;;;;;;;;;;;;;;;;;;;;;;;;;

 10   call init(tau,beta,width,back,displace,d amp,xdata,ydata,ndata,
     1        prom ampl,f,dw,isotope)

C;;;;;;;;;;;;;;;;;;;;;;;;;;;;;;;;;;;;;;;;;;;;;;;;;;;;;;;;;;;;
C     Call the gaussian subroutine
C;;;;;;;;;;;;;;;;;;;;;;;;;;;;;;;;;;;;;;;;;;;;;;;;;;;;;;;;;;;;

      call gaussian(width,veclen,res,xdata)

C;;;;;;;;;;;;;;;;;;;;;;;;;;;;;;;;;;;;;;;;;;;;;;;;;;;;;;;;;;;;
C     Call the timefiltering subroutine
C;;;;;;;;;;;;;;;;;;;;;;;;;;;;;;;;;;;;;;;;;;;;;;;;;;;;;;;;;;;;

       call timefilt(xdata,e data,beta,tau,displace,dw,isotope)

C;;;;;;;;;;;;;;;;;;;;;;;;;;;;;;;;;;;;;;;;;;;;;;;;;;;;;;;;;;;;
C     Call the decay function
C;;;;;;;;;;;;;;;;;;;;;;;;;;;;;;;;;;;;;;;;;;;;;;;;;;;;;;;;;;;;

       call decay(data2,tau,displace,1.0,xdata)

C;;;;;;;;;;;;;;;;;;;;;;;;;;;;;;;;;;;;;;;;;;;;;;;;;;;;;;;;;;;;
C     Add and normalize these two functions
C;;;;;;;;;;;;;;;;;;;;;;;;;;;;;;;;;;;;;;;;;;;;;;;;;;;;;;;;;;;;

      do 88 hh=1,512
      e data(hh)=(f*e data(hh)/100.0)+((1.0-(f/100.0))*data2(hh))
 88   continue

C;;;;;;;;;;;;;;;;;;;;;;;;;;;;;;;;;;;;;;;;;;;;;;;;;;;;;;;;;;;;
C     Set data points beyond 513 to zero for FFT
C;;;;;;;;;;;;;;;;;;;;;;;;;;;;;;;;;;;;;;;;;;;;;;;;;;;;;;;;;;;;
```

```
      do i = 513,1024
      e  data(i)=0.
      end do

C;;;;;;;;;;;;;;;;;;;;;;;;;;;;;;;;;;;;;;;;;;;;;;;;;;;;;;;;;;;;;;;;;;
C     Call Convolution function (Numerical Recipes)
C;;;;;;;;;;;;;;;;;;;;;;;;;;;;;;;;;;;;;;;;;;;;;;;;;;;;;;;;;;;;;;;;;;

      call convlv(e  data,1024,res,veclen,1,ans1)

C;;;;;;;;;;;;;;;;;;;;;;;;;;;;;;;;;;;;;;;;;;;;;;;;;;;;;;;;;;;;;;;;
C     Rescale the output from the convolution to 1.0
C;;;;;;;;;;;;;;;;;;;;;;;;;;;;;;;;;;;;;;;;;;;;;;;;;;;;;;;;;;;;;;;;

       scale=0.
      do 13 ii=1,512
      if(ans1(ii).gt.scale)scale=ans1(ii)
  13  continue
C
      do 14 jj=1,512
      ans1(jj)=ans1(jj)*d  amp/scale
 14   continue

C;;;;;;;;;;;;;;;;;;;;;;;;;;;;;;;;;;;;;;;;;;;;;;;;;;;;;;;;;;
C     Add prompt into spectrum
C;;;;;;;;;;;;;;;;;;;;;;;;;;;;;;;;;;;;;;;;;;;;;;;;;;;;;;;;;;

      call prompt(ans1,displace,prom  ampl,width,xdata)

C;;;;;;;;;;;;;;;;;;;;;;;;;;;;;;;;;;;;;;;;;;;;;;;;;;;;;;;;;;
C     Add Background to the spectrum
C;;;;;;;;;;;;;;;;;;;;;;;;;;;;;;;;;;;;;;;;;;;;;;;;;;;;;;;;;;

      call backgrnd(ans1,back)

C;;;;;;;;;;;;;;;;;;;;;;;;;;;;;;;;;;;;;;;;;;;;;;;;;;;;;;;;;;
C     Write out results and calculate Chi squared
C;;;;;;;;;;;;;;;;;;;;;;;;;;;;;;;;;;;;;;;;;;;;;;;;;;;;;;;;;;

      open(unit=21,file='sim4.out',status='old')
      chi = 0
      do l=1,512
      write(21,*)xdata(l),ans1(l)
```

```
      end do
      close(21)
C
      do 60 nn=29,499
      chi=chi+(ans1(nn)-ydata(nn))**2
 60   continue
C
      write(*,*)'CHI SQUARED =',chi
 100  format(a1)
      stop
      end
C
C***************************************************************************
C
     subroutine gaussian(width,veclen,res,xdata)
      real*8 width,res(1024),temp,pi,xdata(1024)
      integer j,veclen,i,t
      pi = 3.2425927
      t=1
      j=1

C;;;;;;;;;;;;;;;;;;;;;;;;;;;;;;;;;;;;;;;;;;;;;;;;;;;;;;;;;;;;;;;;;
C     The gaussian function must be structured such
C      that it is a periodic function.  This is required
C      by the FFT subroutine to prevent a “wrap around”
C      effect
C;;;;;;;;;;;;;;;;;;;;;;;;;;;;;;;;;;;;;;;;;;;;;;;;;;;;;;;;;;;;;;;;;

10   arg=0.5*(xdata(t)/width)**2
      if(arg.lt.10) then
         res(j) = dexp(-arg)
         j = j + 1
      else if((arg.ge.10).and.(xdata(t).gt.0)) then
         goto 20
      end if
      t = t + 1.
      goto 10
20   jmax = j
      do I =1,jmax-1
         res(jmax+i) = res(jmax-i+1)
      end do
      veclen = 2*jmax-1
      return
      end
```

```
C
C************************************************************
C

    subroutine decay(e  data,tau,displace,ampl,xdata)
     real*8 e  data(1024),t,tau,displace,ampl,xdata(1024)
     integer I
     do 10 i=1,512
     t = xdata(i)
     if(t.le.displace) then
     e  data (i)=0.
     else
     e  data(i) = (dexp(-(t-displace)/tau))
     end if
10   continue
     return
     end

C
C************************************************************
C

     subroutine prompt(p  data,displace,amp  p,p  width,xdata)
     real*8 p  data(1024),displace,amp  p,p  width,t,xdata(1024)
     do i=1,512
     t = xdata(i)
     p  data(i)=p  data(i)+amp  p*exp(-0.5*((t-displace)/p  width)**2)
     end do
     close(23)
     return
     end
C
C************************************************************
C

     subroutine init(tau,beta,width,back,displace,ampl,xdata,ydata,
    1            ndata,p  ampl,f,dw,isotope)

C;;;;;;;;;;;;;;;;;;;;;;;;;;;;;;;;;;;;;;;;;;;;;;;;;;;;;;;;;;;;;;;;
C     Input parameters are read from a data file.
C;;;;;;;;;;;;;;;;;;;;;;;;;;;;;;;;;;;;;;;;;;;;;;;;;;;;;;;;;;;;;;;;

     real*8 tau,width,back,displace,ampl,p  ampl,xdata(1024),ydata(1024)
     real*8 beta,f,dw
```

```
      integer ndata
      character*12 filename
      character*2 isotope
      open(unit=32,file='prompt4.dat',status='old')
      read(32,*)width
      read(32,*)tau
      read(32,*)beta
      read(32,*)ampl
      read(32,*)displace
      read(32,*)back
      read(32,*)p  ampl
      read(32,*)f
      read(32,*)ndata
      read(32,100)filename
  100 format(a12)
      read(32,*)dw
      read(32,101)isotope
  101 format(a2)
      open(unit=56,file=filename,status='old')
      do 10 i=1,ndata
      read(56,*) xdata(i),ydata(i)
  10  continue
      close(32)
      close(56)
      return
      end
C
C*************************************************************
C
      subroutine backgrnd(dat1,bkgrnd)
      real*8 dat1(1024),bkgrnd
      do i=1,512
      dat1(i) = dat1(i)+bkgrnd
      end do
      return
      end
C
C***************************************************************
C
      subroutine timefilt(xdata,e  data,beta,tau,disp,line,isotope)
      real*8 xdata(1024),e  data(1024),tau,disp,beta,shift
      real*8 line,dw,hbar,gamma,arg,power,part1,part4
      real*8 bs(100),xnu
      integer n
```

```
      complex*16  sum,z1,part2,part3
      character*2 isotope,ge,fe
      parameter (z1=(0,1))

C;;;;;;;;;;;;;;;;;;;;;;;;;;;;;;;;;;;;;;;;;;;;;;;;;;;;;;;;;;;;;;;;;;;;;;;
C    set up some constants
C;;;;;;;;;;;;;;;;;;;;;;;;;;;;;;;;;;;;;;;;;;;;;;;;;;;;;;;;;;;;;;;;;;;;;;;
      ge='ge'
      fe='fe'
      if(isotope.eq.ge) dw= line*1.545e-10/6.582173e-10
      if(isotope.eq.fe) dw = line*4.665e-9/6.582173e-7
      n = 10000

C;;;;;;;;;;;;;;;;;;;;;;;;;;;;;;;;;;;;;;;;;;;;;;;;;;;;;;;;;;;;;;;;;;;;;;;
C  start do loop
C;;;;;;;;;;;;;;;;;;;;;;;;;;;;;;;;;;;;;;;;;;;;;;;;;;;;;;;;;;;;;;;;;;;;;;;

      do 10 I=1,512

C;;;;;;;;;;;;;;;;;;;;;;;;;;;;;;;;;;;;;;;;;;;;;;;;;;;;;;;;;;;;;;;;;;;;;;;
C   calculate some things used in all possiblilities
C;;;;;;;;;;;;;;;;;;;;;;;;;;;;;;;;;;;;;;;;;;;;;;;;;;;;;;;;;;;;;;;;;;;;;;;

      sum = z1*0.

C;;;;;;;;;;;;;;;;;;;;;;;;;;;;;;;;;;;;;;;;;;;;;;;;;;;;;;;;;;;;;;;;;;;;;;;
C  if the time is less than the "added delay" skip the calculation
C  and set the intensity to zero  else do the calculation
C;;;;;;;;;;;;;;;;;;;;;;;;;;;;;;;;;;;;;;;;;;;;;;;;;;;;;;;;;;;;;;;;;;;;;;;

     if(xdata(i).le.disp) then
          e  data(i) = 0.0
      else
C;;;;;;;;;;;;;;;;;;;;;;;;;;;;;;;;;;;;;;;;;;;;;;;;;;;;;;;;;;;;;;;;;;;;;;;
C   determine whether there is a shift
C;;;;;;;;;;;;;;;;;;;;;;;;;;;;;;;;;;;;;;;;;;;;;;;;;;;;;;;;;;;;;;;;;;;;;;;

      power = (xdata(i)-disp)/tau
      part1 = dexp(-power)
      arg = ((xdata(i)-disp)*beta/tau)**0.5

C;;;;;;;;;;;;;;;;;;;;;;;;;;;;;;;;;;;;;;;;;;;;;;;;;;;;;;;;;;;;;;;;;;;;;;;
C    first get bessel functions
C;;;;;;;;;;;;;;;;;;;;;;;;;;;;;;;;;;;;;;;;;;;;;;;;;;;;;;;;;;;;;;;;;;;;;;;
```

```
          xnu = 0.0
          call dbsjs(xnu,arg,75,bs)
         shift = dabs(2*dw*arg*tau/beta)

C;;;;;;;;;;;;;;;;;;;;;;;;;;;;;;;;;;;;;;;;;;;;;;;;;;;;;;;;;;;;;;;;;;;;;;;;;;
C    determine whether there is an isomer shift
C;;;;;;;;;;;;;;;;;;;;;;;;;;;;;;;;;;;;;;;;;;;;;;;;;;;;;;;;;;;;;;;;;;;;;;;;;;

      if(shift.eq.0.0) then
          e  data(i) = part1  * (bs(1))**2
      else
           do 34 l = 1,74
             part2 = (z1*4*dw*tau/beta)**(l-1)
             part3 = (beta*(xdata(i)-disp)/(4*tau))**((l-1)/2)
             sum = sum + part2*part3*bs(l)
 34       continue
             e  data(i) = part1  * cdabs(sum)**2
       endif
      endif
 10   continue
      return
      end
```

Vita

Walter Carlton McDermott III
Old Dominion University
Department of Physics
Norfolk, VA. 23529

Education

OLD DOMINION UNIVERSITY *Ph.D. Physics May 1996*
Dissertation Title "Gamma-Ray Optics using ^{57}Fe and ^{73}Ge." Advisor Dr. G.R.Hoy.

OLD DOMINION UNIVERSITY *M.S. Physics May 1991*

OLD DOMINION UNIVERSITY *B.S. Secondary Education May 1988*

Professional Experience

HARVARD-SMITHSONIAN CENTER FOR ASTROPHYSICS *Astrophysicist*
1995-current Member of the Calibration Mission Support Team for NASA's AXAF project.

OLD DOMINION UNIVERSITY *Virginia Department of Education GAANN Fellow*
1994-1995 Doctoral research and teaching undergraduate recitation sessions.

OLD DOMINION UNIVERSITY *Special Doctoral Research Fellow*
1991-1994 Doctoral research.

OLD DOMINION UNIVERSITY *Assistant Adjunct Instructor Department of Education*
1990-1995 Astronomy Instructor for the Community Outreach Elderhostel Program.

INTERNATIONAL BUSINESS MACHINES *Consultant in Scientific Vector Processing*
1990 Consultant to Old Dominion University in Fortran Vector Processing.

Publications

W.C. McDermott III, D.E. Johnson, G.R. Hoy, Hyperfine Interactions 92 (1994) 1077
"Gamma-Ray Optics using ^{57}Co-Doped Iron Single Crystals"

G.R. Hoy, S.R. Serej, W.C. McDermott III, D.E. Johnson, Proc. of the Inter. Conference on Lasers (1992) 81 "Recent Progress and Speculations in Gamma-Ray Optics"

To Be Published

W.C. McDermott III, G.R. Hoy, International Conference on the Applications of the Mössbauer Effect (1995) "Time-Domain Mössbauer Spectroscopy: The Inelastic Channel"